Design and Scanning Electrochemical Microscopy Transport Study of Immobilized Liposome: Towards the Investigation of a Membrane Bound Electroactive Reaction

Debby Correia Ledo

A Thesis

in

The Department

of

Chemistry and Biochemistry

Presented in Partial Fulfillment of the Requirements

for the Degree of Doctor of Philosophy at

Concordia University

Montreal, Quebec, Canada

July 2010

Your file Votre référence
ISBN: 978-0-494-71144-6
Our file Notre référence
ISBN: 978-0-494-71144-6

Abstract

Design and Scanning Electrochemical Microscopy Transport Study of Immobilized Liposome: Towards the Investigation of a Membrane Bound Electroactive Reaction

Debby Correia Ledo

Concordia University, 2010

Chemotherapy treatment and its secondary effects are devastating for patients and it is due to cellular resistance. So there is a scientific and medical interest in understanding cellular transport mechanisms of anti-cancer drugs. As part of this thesis, biomimetic models, in particular liposomes have been specially designed to study some of the transport mechanisms. While maintaining their simplicity, liposomes have been preferred over other models because their membranes are similar (structure and behaviour) to that of cell membranes. Thus, a bare liposome, a liposome with electroactive units encapsulated within its internal void and surface-modified redox liposomes were designed.

In order to obtain the surface-modified redox liposome, the phospholipid headgroup of 1,2-distearoyl-*sn*-glycero-3-phosphocholine (DSPC) was first modified with an electroactive ferrocene derivative. The modification of the phospholipid headgroup with ferrocenemethanol led to the synthesis of an unstable redox phospholipid. Thus ferrocene-ethanol was preferred. Since the latter is a primary alcohol and DSPC is a

choline bearing phospholipid, Phospholipase D-assisted transphosphatidylation was performed. To our knowledge, it is the first time an organometallic redox phospholipid was synthesised. The ferrocene group was attached covalently to the phospholipid headgroup and this was mostly verified by infrared studies. Mass spectrometry and 31-phosphorus NMR spectroscopy were also used to quantify the reaction mixture. Cyclic voltammetry analysis confirmed that the functionalized phospholipid is indeed redox active.

The ethylferrocene phospholipid was then used to produce surface-modified redox liposomes by the double emulsion technique. The liposome was immobilised by sedimentation by encapsulating sucrose within the liposome. Scanning electrochemical microscopy studies were performed on this redox active liposome, which mimicked a surface bound reaction. It was demonstrated, by chronoamperometry experiments, that its surface was not only electroactive, but its electrochemical response could be modulated upon the use of a specific sacrificial mediator. This preliminary investigation was only the beginning of a much larger SECM study on surface bound reactions at membranes.

Finally, the design of a new ring microelectrode is presented. The fabrication steps of this microelectrode are simpler than what is already presented in the literature. Moreover, the use of pure platinum (and not an alloy) and the isolation of the micropipet by a silicon oxide coating make this distinct from others. However, cyclic voltammetry analysis combined with numerical simulations showed that during the ring exposure by focused ion beam the insulating properties of the silicon oxide layer are weakened. A small modification of this step would lead to the fabrication of a ring microelectrode suitable for SECM local probe.

What if I didn't believe in myself?

Inspired by NHL, History will be made© slogan

2010 Stanley Cup Playoffs

Acknowledgements

My greatest thanks to my supervisor, Pr. Janine Mauzeroll. With your help, not only did I become a better chemist, but also a better person. You taught me patient and tolerance towards my peers.

I would also like to acknowledge Pr. Christine DeWolf, my co-supervisor. We did not start this incredible adventure together, but I am sure glad you were with me for the end. Thank you for your support, help and advice.

Thank you to my wonderful family. À maman et papa, pour tous les petits soins que vous avez eu pour moi durant ces quatre années de Doctorat, «um grande obrigado»! Un merci special à Diane et Jean-Mo pour les nombreux soupers, les multiples discussions scientifiques et votre soutien qui m'est si précieux. Merci /galement à Nelson et Gaby pour votre support moral. Finalement, merci à Marianne, Mariline, Philippe et à tous mes amis qui ne m'ont jamais abandonnés.

J'aimerais exprimer toute ma gratitude et mon amour à Mathieu, la personne qui compte le plus pour moi. Merci pour les nombreux conseils, les discussions interminables sur la science, les fous-rires, ton amour et toutes les petites attentions qui font que je craque pour toi. Love you!

I would also like to acknowledge my colleagues from both labs. You guys were great with me. Good luck in your studies! Un merci particulier à Dr. Renaud Cornut de m'avoir appris à penser un peu plus comme une théoricienne et un peu moins comme une chimiste expérimentale. A special thank you to Pr. Sylvain Canesi (UQAM) and Dr.

Alexandre Arnold (UQAM) for sharing with me a little of their knowledge in organic synthesis and in NMR spectroscopy. Many thanks to Pr. Louis Cuccia and Pr. Cameron Skinner, my committee advisor members, for their help and greatly appreciated advice. Finally, I would like to acknowledge Marie-Hélène Bernier (LMF, Polytechnique), the UQAM technical staff, and the Concordia University administrative staff for their support.

Thank you guys! I couldn't have done it without you!

Table of content

Abbreviations

α	Transfer coefficient
A	Ampere
C_O or C_R	Concentration of the oxidized or reduced species
CV	Cyclic voltammetry
D	Diffusion coefficient (cm^2/s)
DSPC	1,2-distearoyl-*sn*-glycero-3-phosphocholine
DSPG	1,2-distearoyl-*sn*-glycero-3-phospho-(1'-*rac*-glycerol) (sodium salt)
DSP-OMeFc or DSP-OCH_2Fc	1,2-distearoyl-*sn*-glycero-3-phospho-methylferrocene
DSP-OEtFc or DSP-OCH_2CH_2Fc	1,2-distearoyl-*sn*-glycero-3-phospho-ethylferrocene
E	Open circuit potential
E_a	Activation energy
$E^{0'}$	Formal potential
F	Faraday constant (96485 C/mole)
FcMeOH or $FcCH_2OH$	Ferrocenemethanol
FcEtOH or $FcCH_2CH_2OH$	Ferrocene-ethanol
FIB	Focused ion beam
i	Current

i_{ss} or $i_{T,\infty}$	Steady-state current
IR	Infrared
$[IrCl_6]^{2-}$ and $[IrCl_6]^{3-}$	Iridium chloride oxidized and reduced species
KCl	Potassium chloride
MAS	Magic angle spinning
MDR	Multidrug resistance
MS	Mass spectrometry
n	Number of electrons involved in a reaction
O	Oxidized species
PLD	Phospholipase D
^{1}H NMR	Proton nuclear magnetic resonance spectroscopy
^{31}P NMR	Phosphorus nuclear magnetic resonance spectroscopy
R	Reduced species or gas constant (8.3145 J/K.mole or 0.0821 L.atm/K.mole)
SAM	Self-assembled monolayer
SECM	Scanning electrochemical microscopy
SEM	Scanning electron microscopy
T	Temperature
UME	Ultramicroelectrode
V	Volt

List of figures

List of tables

Chapter 1. Introduction

1.1 Generalities

All cellular tissues and organs of the human body can be affected by cancer, without discrimination. Cancer cells present abnormal characteristics such as frequent and anarchic mitoses and abnormally large nuclei. The neoplastic cells of a tissue or an organ alter their structure such that it no longer resembles the healthy tissue or organ. Regardless of the type of cancer, it has an insidious nature and if left untreated or undetected, it can easily spread throughout the human body through blood or lymphatic transportation. There are several treatments to cure, counteract or slow cancer progression. Surgery, radiotherapy, chemotherapy and immunotherapy treatments are the most commonly used ones.

Chemotherapy is routinely used for metastatic cancer treatments. Massive doses of anti-cancer drugs are systematically given regardless of the patient specific metabolism.[1] Thus, anti-cancer drugs can fail to kill cancer cells and may lead to severe side effects such as nausea, hair loss and muscle and bone pain. With prolonged drug exposure, cancer cells become resistant towards the majority of anti-cancer drugs. This phenomenon is known as Multidrug Resistance (MDR) and its response can be affected by cell kinetics, pharmacokinetics and cellular drug resistance mechanisms.[2] Research in the field indicates that cellular resistance is usually due to either the specific nature and genetic background of cancer cells or the genetic changes due to chemotherapy toxicity.[1] Increasing drug efflux, decreasing drug uptake, drug sequestration, change in targeting

and activation of the detoxification system are some examples of mechanisms of cellular drug resistance.[2] The action mechanism of most interest here is related to the ATP-binding cassette (ABC) transporters. These transporters, such as P-glycoproteins (PGPs) and Multidrug Resistant Proteins (MRPs), belong to a family of energy-dependant transporters. Selective inhibition of key ABC transporters could reduce MDR and limit undesirable side effects. Inhibitors, such as cyclosporine, VX-710 or Biricodar, V-104 and tricyclic isoxazoles, have been identified.[1] However, specificity and selectivity problems, affect ABC transporters expressed in healthy cells as well.

These cellular resistance mechanisms have particularly attracted our attention since it is possible to study and quantify the inherent transport of drugs by electrochemical measurements. Such electrochemical studies have been previously performed on living cells. It was shown that scanning electrochemical microscopy (SECM) could be used to quantify the rate of uptake of menadione and the rate of release of thiodione (menadione-gluthatione conjugate), a cellular metabolite.[3-5] However, the theoretical treatment developed in these studies was limited by the complexity of living cells. As such, there is an interest in developing simpler models that mimic properly living cells, especially cell membranes. Therefore, some studies were performed on biomimetic models such as self-assembled monolayers (SAMs), chromatophores and liposomes with imbedded proteins (ion flux channels, gramicidin channels, membrane-bound reaction centers, etc.).[6-9] Particularly, ferrocene terminated monolayers on electrodes was thoroughly studied. For example, Cannes and co-workers[10] studied quantitatively the kinetics of the heterogeneous electron transfer at mono- and bilayers modified gold electrodes. Cyclic voltammetry, scanning electrochemical microscopy

measurements and numerical simulations lead to the conclusion that the surface coverage was high and depended on the thickness of the layer. As a consequence, it was demonstrated that ferrocenemethanol can permeate into the monolayer and that the electron transfer at the bilayer is governed by diffusion of the mediator through pinholes with electron transfer occurring at the free sites on the electrode. Moreover, the complexity of tethered ferrocene electrochemistry in SAMs on gold electrodes was also studied.[11] These SAMs were either prepared from single component (FcRS-) or from a mixture (FcRS-/CH_3RS-). As a result, ferrocenylalkylthiolates in binary SAMs presented a lower- and higher-potential voltammetric peaks, which can be assigned to ferrocene moieties in isolated and clustered states. It would be exhaustive to report here every study concerning ferrocene-modified-self-assembled monolayers. Those are some examples that demonstrate the importance of the use of ferrocene derivatives in electron transfer studies using biomimetic models.

The general purpose of the research work presented here is to create a biomimetic model that can decouple surface reactivity from ATP-assisted response from MDR proteins present in cancer cells. Liposomes have been selected because their double lipidic membrane is remarkably similar to that of living cells. In addition, the 3D aspect of this model facilitates the study of diffusion-limited molecular transport such as diffusion process. One transport mechanism was particularly studied in this research project, the surface bound reaction at a membrane modified with ferrocene units (Figure 1.1).

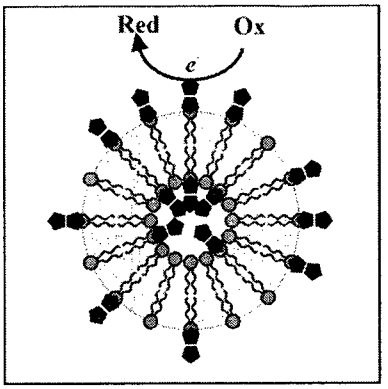

Figure 1.1. Schematic representation of a surface bound reaction at a membrane.

1.2. Presentation of the biomimetic models

Two types of liposomes were prepared and studied by scanning electrochemical microscopy. Bare liposome was designed (Figure 1.2a) and served as a control model during the electrochemical measurements. An ethyl-ferrocene surface-modified redox liposome was used in this study (Figure 1.2b) as the main membrane bound reaction model.

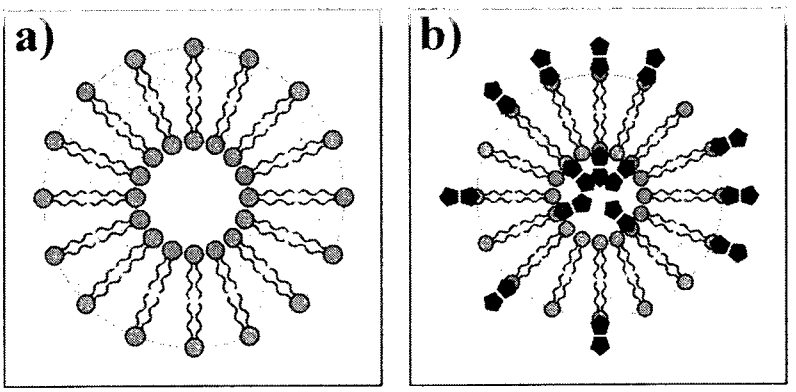

Figure 1.2. Schematic representation of the two types of liposomes used in this study: a) bare liposomes and b) surface-modified redox liposomes.

1.2.1. Lipids and liposomes

Lipids can be generally defined as amphiphilic molecules with a hydrophilic head and a hydrophobic tail. Some phospholipids such as phosphatidylcholine (PC) and phosphatidylethanolamine (PE) are neutral (zwitterionic), while others like phosphatidylserine (PS), phosphatidylglycerol (PG) and phosphatidylinositol (PI) are electrically charged. This difference is important for the lipid capacity to incorporate or bind proteins and drugs into the lipid membrane.[12]

Naturally and spontaneously, phospholipids assemble in aggregates to form lipid monolayers, lipid bilayers, multilamellar lipid bilayers, micelles, unilamellar and multilamellar vesicles and liposomes.[12] In particular, liposomes, which are of interest here, are divided into multilamellar (MLV), small size unilamellar (SUV), large size unilamellar (LUV) and giant (GUV) liposomes.[13] The phospholipid reorganization tends to minimize the interactions between the hydrophobic components and the water molecules. This usually corresponds to a lipid bilayer with the non-polar tails found inside and the polar headgroups exposed to the aqueous phase.[13]

Liposomes are not static models. The lipid membrane presents a fluidity that originates from lateral expansion and flip movement within the lipid bilayer. Lateral expansion results from the rotation of the hydrocarbon chains of the non-polar tails around the C-C bound. The three configurations of the C-C bound, trans, «gauche +» and «gauche -», are responsible for altering the thickness of the bilayer.[13] The flip motion occurs because the hydrocarbon chains are flexible. It is therefore possible to observe a lipid rotation around the axis perpendicular to the membrane surface and a lateral

diffusion, that is to say that two lipids can exchange positions.[13] Finally, diffusion of small molecules across the lipid bilayer provides also a degree of mobility in the liposome. This fluidity is one of the most important properties of liposomes (or any lipid bilayer). It modifies the mobility of the lipids within the membrane at a specific temperature. Here, the lipids used in this research study have a transition temperature above room temperature, thus insuring a stability of the generated biomimetic model.

Liposomes are biomimetic models that can be used for different applications (therapeutic, cosmetic, biochemical and biophysical applications). As such, liposomes have seen used for targeting and drug delivery purposes. If the drug to be delivered is water soluble, it is usually encapsulated within the liposome internal void, while a hydrophobic drug would be dissolved within the lipidic phase. For either case, liposomes are introduced in the body by simple injection.[13] In cosmetics, the active substances are usually applied topically in the form of an emulsion, which can damage the skin upon prolonged use. The encapsulation of these ingredients into liposomes can overcome this problem.[13] Finally, study of membrane properties are often performed using liposomes. They are ideal models for such studies because they are able to reproduce many of the structures and properties of biological membranes.[13]

1.2.2. Liposome formation: double emulsion technique

As mentioned previously, vesicles and liposomes are spontaneously formed in nature. However, for research purposes, it is advantageous to control the type and the size of liposomes during their formation. In 1965, Bangham and co-workers were the first to

propose a simple method of preparing liposomes.[13-14] It consists of evaporating the organic phase of an emulsion obtained by dissolving the lipids into an organic solvent, which is then mixed with an aqueous phase. Since then, several other techniques of liposome design were developed. For example, unilamellar liposomes can be prepared from a suspension of multilamellar vesicles and a series of freezing/drying steps.[13, 15-16]

Another liposome preparation technique, commonly used, is the reverse-phase evaporation method, also known as the double-emulsion technique.[17-19] For our research purposes, the double-emulsion method has proven to be the most promising method because it leads to the preparation of large diameter liposomes required for SECM electrochemical measurements. Szoka and Papahadjopoulos[17] described the different steps involved in the preparation of liposomes through double-emulsion technique, which is schematically presented on Figure 1.3.

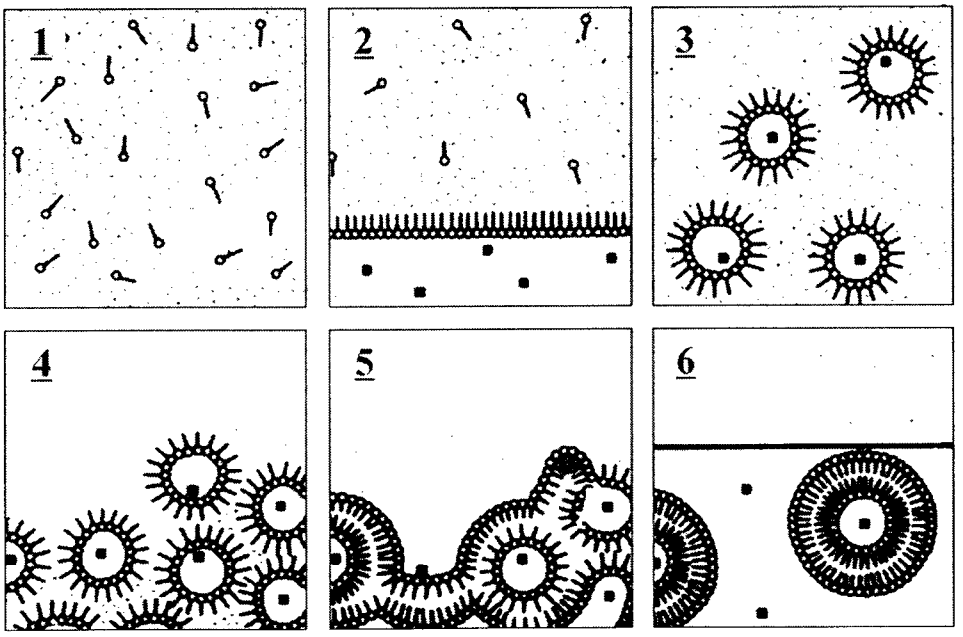

Figure 1.3. Schematic representation of the different steps involved in the double-emulsion technique as described by Szoka and Papahadjopoulos.[17]

First, lipids are dissolved in an organic phase (1). Then, an aqueous buffer solution is added (2) followed by the formation of «inverted micelles» by sonication or vortex (3). The organic solvent is evaporated is then evaporated to reach a «viscous gel-like state» (4), which collapse to form a gel state (5) and thus, the liposome (6).

Here, the phospholipids used for the double-emulsion method are 1,2-distearoyl-*sn*-glycero-3-phosphocholine (DSPC), and 1,2-distearoyl-*sn*-glycero-3-phospho-(1'-*rac*-glycerol) (sodium salt) (DSPG), both saturated phospholipids. Their chemical structures are presented in Figure 1.4. These phospholipids were chosen because they are the most commonly used lipids, and therefore the best known in the literature. They are also part of the lipid family that constitute the cell membrane. Note that 1,2-dibutyryl-*sn*-glycero-3-phosphocholine structure is also presented because it is used later in some organic synthesis. However, it was not used for liposome formation.

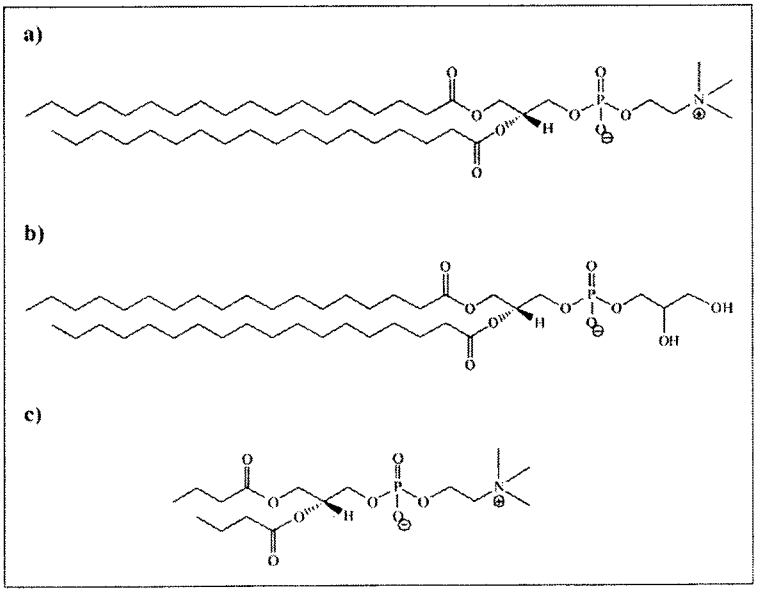

Figure 1.4. Chemical structures of the phospholipids used in this work: a) 1,2-distearoyl-*sn*-glycero-3-phosphocholine (DSPC), b) 1,2-distearoyl-*sn*-glycero-3-phospho-(1'-*rac*-glycerol) (sodium salt) (DSPG) and c) 1,2-dibutyryl-*sn*-glycero-3-phosphocholine.

Finally, the electroformation of liposomes is an interesting alternative to the other liposome formation techniques. Large diameter liposomes of about 5 to 60 μm diameter can be reproducibly obtained, with high efficiency (95%), good size distribution and optimal encapsulation efficiency. It consists of the "hydration of dried lipid films above the phase transition temperature in the presence of an AC electric field[20-22] For the liposome electroformation, the choice of phospholipids can be justified by the fact that the lipid charge must not be too high and they must behave as negatively charged lipids. It has been proven that negatively charged lipids swell faster and reach greater extent of swelling on the negative electrode than on the positive one.[21]

1.3. Synthetic and characterisation techniques

The first two models presented in Figure 1.2 were obtained directly through double emulsion technique from the appropriate phospholipid mixture. Their size and the nature of the analytes encapsulated within their internal void are controlled and modulated during their formation. However, the surface-modified redox liposome, required the modification of the phospholipid headgroup prior to its use in liposome formation. The redox active phospholipid synthesis was realised through enzymatic catalysis and the resulting product was characterised by mass spectrometry and solid-state 31-phosphorus nuclear magnetic resonance, infrared and cyclic voltammetry. A brief overview of these techniques and synthetic routes is presented here to better understand the results presented in the following chapters.

1.3.1. Enzymatic-catalyzed synthesis

To obtain the desired surface-modified redox liposome, phospholipids headgroups were modified prior to their assembly into liposomes rather than directly modifying the surface thereof. Moreover, research groups using liposomes as biomimetic models are not necessarily specialized in organic synthesis. It is therefore important to find synthetic routes that will modify phospholipid headgroups with electroactive tethers in a simple, clean and accessible to all way. An enzymatically-catalyzed synthesis is the ideal pathway considering the characteristics sought.

Enzymes are defined as proteins that increase the rates of biological and chemical reactions. Just like any other catalyst, enzymes lower the activation energy (E_a) of a reaction, thus increasing its reaction rate up to 10^5 to 10^8 times.[23] Also, in principle, it is not consumed during the reaction and does not modify the equilibrium of the system. Enzymes have unique advantages that distinguish them from other conventional chemical catalysts. The fact that enzymes function is not restricted to their natural aqueous medium, they have a high sensitivity and selectivity, they can work under mild conditions and may work in organic solvents, they are recyclable, biocompatible and thus environmentally friendly.[24] The use of enzymes as catalysts in organic and organometallic syntheses is ever increasing. Some examples are given in Table 1.1, which summarises the type of enzymes currently used in organic syntheses as well as the type of reaction it catalyzes.

Table 1.1. Commonly used enzymes in different organic syntheses and type of reaction catalyzed by those enzymes.[23]

Enzymes	Reaction the enzyme catalyzes
Esterase, lipase	Ester hydrolysis and formation
Amidase	Amide hydrolysis and formation
Dehydrogenase	Oxidoreduction of alcohols and ketones
Oxidase	Oxidation
Peroxidase	Oxidation
Kinase	ATP-dependent phosphorylation
Aldolase	Aldol reaction
Glycosidase	Glycosidic bond formation
Phosphorylase, phosphotase	Phosphate hydrolysis and formation
Sulphotransferase	Sulphate formation
Transaminase	Synthesis of amino acid
Hydrolase	Hydrolysis
Isomerase	Isomerisation

If one wants to use enzymes as catalysts for an organic or organometallic synthesis, special attention must be paid to the enzyme specific activity (k_{cat}), specificity (k_{cat}/K_m), stability and its degree of inhibition.[23] The reagents structure, the nature of the organic solvent,[25] if any is used, and the enzyme immobilization must also be considered in the development of a synthetic route.

Enzymes are commonly used in well known organic synthesis such as polymer chemistry (polycondensation, ring opening, oxidative polymerization), enantioselective catalyzed transesterification and hydrolysis and usual reduction and oxidation syntheses.[24] In the present work, the transphosphatidylation reaction caught our attention

because it is catalyzed by phospholipases, which are enzymes that hydrolyse phospholipids. Phospholipases can be separated into five types: phospholipase A1 (PLA1), phospholipase A2 (PLA2), phospholipase B (PLB), phospholipase C (PLC) and phospholipase D (PLD). They can be distinguished from one another by their action site as presented in the following figure.[26]

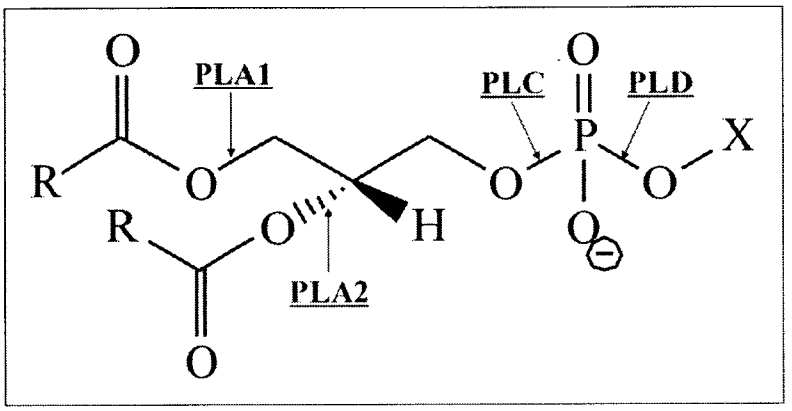

Figure 1.5. Cleavage sites of the different phospholipase types.

Here, only the modification of the phospholipid headgroup is necessary. The phospholipid skeleton must remain unchanged in order to use the modified phospholipid in the liposome formation. Thus, PLD was preferred over the other phospholipases because it can cleave the ester function between the acid function of the phosphate and the alcohol, therefore releasing an alcohol and phosphatidic acid.

Over the years, phospholipase D has been extensively studied.[27-34] Phospholipase D activity will vary depending in the enzyme source. The most common sources of PLD are bacterial sources such as *Streptomyces sp.*,[31] the peanut source (*Arachis hypogaea*)[30, 35-36] and the cabbage source. In aqueous medium, PLD catalyzes the hydrolysis of the phosphodiester bond of phosphatidylcholines to generate, as mentioned already,

phosphatidic acid and an alcohol (Rx. 1.1). Also, in the presence of a primary alcohol, PLD is able to catalyze a transesterification reaction, known as transphosphatidylation. The latter leads to the formation of a modified phospholipid and a choline (Rx. 1.2). Transphosphatidylation is usually performed either in anhydrous organic solvent or in a two-phase system (biphasic system), such as organic/buffer mixture. Various studies have demonstrated that the nature of the organic solvent and the enzyme source play an important role on the synthesis yield.[25, 37]

$$\text{Phosphatidylcholine} + H_2O \xrightarrow{\text{PLD}} \text{Phosphatidic acid} + \text{Choline} \qquad \text{(Rx. 1.1)}$$

$$\text{Phosphatidylcholine} + \text{ROH} \xrightarrow{\text{PLD}} \text{Phosphatidyl-OR} + \text{Choline} \qquad \text{(Rx. 1.2)}$$

1.3.2. Mass spectrometry

During the transphosphatidylation reaction, it is important to follow up the progress of the reaction in a simple and fast way. Thin layer chromatography (TLC) is the usual way to follow the evolution of an organic synthesis. However, the presence of a polar headgroup and a nonpolar tail on the phospholipids complicates the analysis of the reaction mixture by TLC. Of course, a reverse-phase TLC could allow such analysis, but it was more appropriate here to follow the reaction by mass spectrometry. In addition to being fast and available, this approach requires no special handling or preparation of the sample and allows the verification of the efficiency of the purification step, while identifying the reaction products.

Mass spectrometry (MS) collects information on the nature, structure and composition of a given sample. It is based on the determination of the masses of individual species present in the sample. Its versatility and high sensitivity makes the MS one of the analytical techniques with the largest scope.[38] The MS principle lies in the ionisation of a very small amount of the sample. The charged species are subject to the action of an electric or magnetic field and the study of their pathway determines the nature of the generated ions. In detail, the sample analysis follows four steps: (i) sample vaporisation and ionisation by the apparatus source, (ii) acceleration of the ions to increase their kinetic energy, (iii) ion separation according to their mass/charge ratio through an analyser and (iv) detection of the separated ions using a detector that amplifies the low ionic current.[38-39] The results are presented graphically as the ions abundance as a function of the mass/charge ratio.

Analysis of a sample includes several steps and the device itself is made from several parts (ioniser, analyser and detector). There are two ways to introduce the sample into the MS, by direct injection or by separation on a chromatographic column prior to the ionisation.[38-39] Direct injection, preferred here, consists in the introduction of the sample directly into the ionisation chamber. Otherwise, the sample is separated by chromatography prior to its ionisation. Pure components, and not the mixture, reach the ionisation chamber.

Sample ionisation, one of the most important steps in MS analysis, is done using different methods that are divided into two large families. Electronic impact (EI) ionisation, positive chemical ionisation (CI), fast atom bombardment (FAB) and assisted laser desorption ionisation are high vacuum ionisation methods, while argon plasma

ionisation and intermediate sprays ionisation (electrospray ionisation (ESI) and atmospheric pressure chemical ionisation (APCI)) are realised at atmospheric pressure.[38-39] A detailed discussion of all ionisation methods is beyond the scope of this thesis. Only the ESI will be discussed, since it was mainly used in this work. The ESI principle, schematically presented in Figure 1.6, consists of forming droplets at the end of a very fine capillary, which is biased, *e.g.* a positive or negative potential is applied depending on the type of ions to be studied. The droplets charge density increases in contact with an intense electric field. Under gas flux, they are evaporated and the solvent molecules are lost following very complex mechanisms of desolvation. The charge density becomes very high, which leads to the droplets explosion. Protonated unfragmented ions carrying the charges are thus released and detected.[38-39]

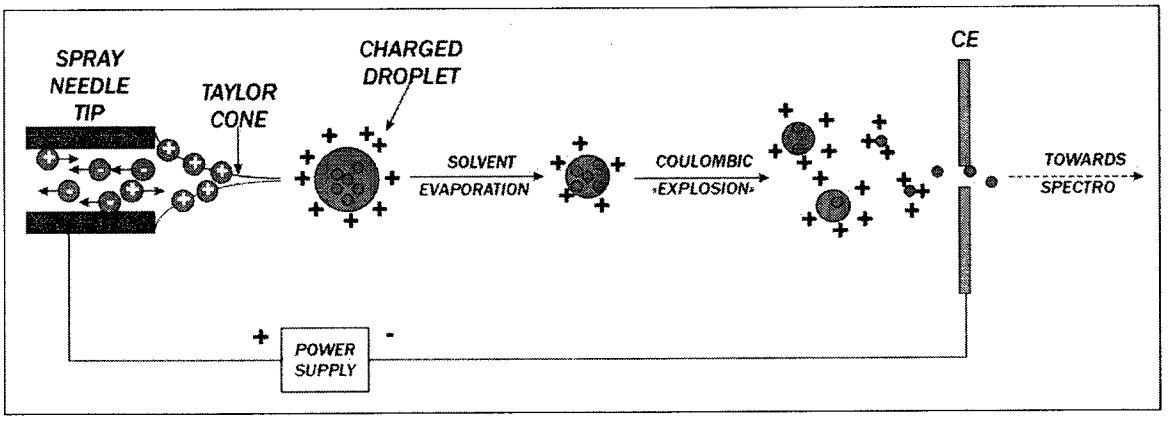

Figure 1.6. Schematic representation of the electrospray ionisation process.

There are as many types of analysers as there is types of ionisers, if not more. Among others, one can use electromagnetic EB type, Fourier transformation (FTMS), time-of-flight (TOF), quadrupole filter and electric ion trap analysers.[38-39] The choice of

the analyser depends more on the type of information sought than the nature of the sample.

Finally, ion detection is based on the measurement of the charges present on the ions. Detectors can amplify the ion signals in such way that many can detect the impact of a single ion. The detectors are separated into three classes: (i) electron multipliers with separated dynodes where the ions hit a cathode thereby releasing electrons that are multiplied by fifteen dynodes, (ii) electron multipliers with continuous dynodes where released electrons following the ion collection by a collector doped with lead (cathode) are multiplied by successive collisions with positively charged electrodes and (iii) microchannels detectors where the electrons are collected by many microchanneltrons coated with a semiconductor material arranged in a honeycomb structure.[38]

1.3.3. Solid state 31-phosphorus nuclear magnetic resonance spectroscopy

Considering that the PLD-assisted reaction product is a phospholipid, 31-phosphorous nuclear magnetic resonance (^{31}P NMR) was chosen over proton nuclear magnetic resonance (^{1}H NMR) for this study because phospholipids have only one phosphorous atom in their structure. Therefore, the ^{31}P NMR spectrum is simpler than the proton spectrum. In addition, solid-state NMR allows, unlike liquid NMR, the analysis and characterisation of the sample without using solvents that could modify, or worse, partly degrade the phospholipids under study. It also presents some special characteristics that are worth to be mentioned and put in the context of the phospholipid studies.

The broader NMR spectrum obtained from solids is distinct from the well known liquid NMR spectrum. This is due to the fact that the nuclei in the solid state are subject to static anisotropic interactions.[40] In liquids, the natural rapid isotropic motion of the nuclei eliminates the anisotropic interactions. Thus, high-resolution NMR spectra are observed for liquids. For solids, where nuclei motion is very slow, the natural motion observed in liquid is mimic by rotating the sample at an angle of 54.44o, which is known as the magic angle spinning (MAS) (Figure 1.7). As a result, the anisotropic interactions in solid-state NMR analyses are average.

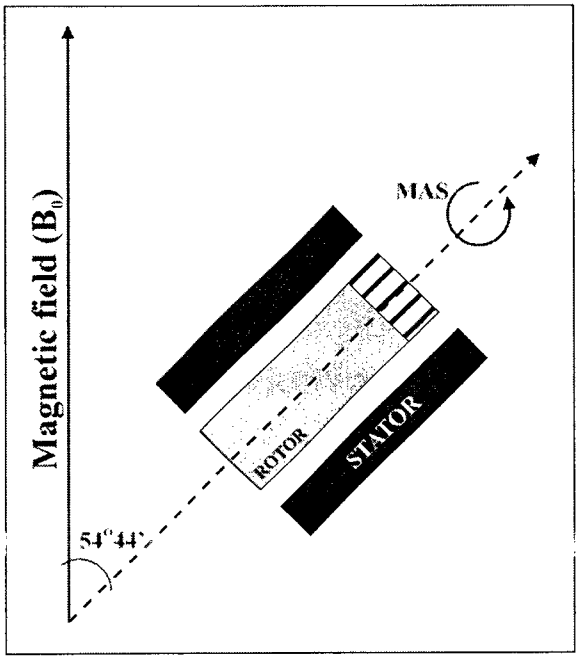

Figure 1.7. Schematic representation of magic angle spinning (MAS).

The anisotropic nuclear interactions that are mostly affected by magic angle spinning method are the direct magnetic dipolar interactions (homonuclear and heteronuclear), indirect electron-coupled interactions (homonuclear and heteronuclear),

electric quadrupolar interactions and electron shielding interactions (chemical shift and Knight shift).[40]

^{31}P NMR is an ideal tool to study and characterise the motion and average orientation of the phosphate group in phospholipids. The chemical shift anisotropy of the phosphate group is the most predominant interaction when studying phospholipids.[41-42] Thus, not only is the chemical shift influenced by the chemical environment of the phosphorus atom present on each phospholipid, but the peak shape also gives valuable information. The peak will be more or less broadened depending if hydrated phospholipids are vesicles or micelles.

1.4. Electrochemical studies

Scanning electrochemical microscopy (SECM) is the technique used to study the biomimetic models designed during this research project. It can measure readily the active and passive transport of redox active molecules. Scanning electrochemical microscopy was also chosen because it is a non-invasive technique that allows the measurement of the kinetics of homogeneous reactions coupled to heterogeneous electron transfer. Figure 1.8 presents a schematic representation on how the electrochemical measurements were conducted on these biomimetic models.

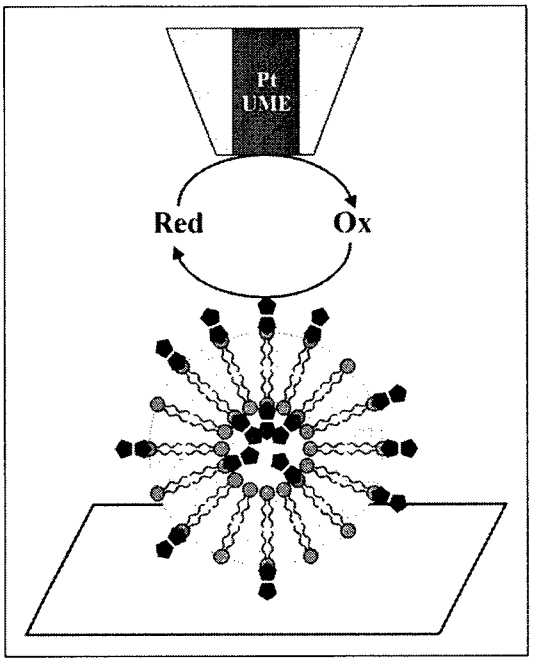

Figure 1.8. Schematic representation of a scanning electrochemical microscopy measurement on a liposome as a biomimetic model.

The SECM measurements were carried out using specially designed ultramicroelectrodes (UMEs) immersed in a solution containing a sacrificial redox mediator. It is biased such that a mass transfer limited electrochemical reaction occurs with the sacrificial redox mediator. The UME current is monitored as it approaches to a single immobilized liposome. The measured approach curves (current versus tip-to-substrate distance curve) or the chronoamperometric curves (current over time curve at a constant and near tip-to-substrate distance) are characteristic of the interaction of the sacrificial redox mediator with the immobilized liposome. Thus, the interaction with a bare liposome or with a liposome containing redox active units within its internal void or a surface-modified redox liposome will yield to different cyclic voltammetry, chronoamperometry and approach curve responses, each representative and characteristic of the biomimetic model studied.

1.4.1. Electrochemical fundamentals

The interfacial nature of electrochemistry is explained by the fact that material is dissolved in a 3D volume, the electrochemical cell, and reaction occurs at a 2D surface, the electrode surface.[43] For a reaction to occur, material has to physically move from one part of the solution to another, in this case the electrode surface. This movement is defined has the mass transfer, which arises from migration, convection and/or diffusion. Migration originates from the movement of a charged species placed in an electrical field. Migration is usually suppressed by adding a large amount of supporting electrolyte (dissociated inert salt) into the solution.[43-44] Convection results from mechanical stirring of the solution or from hydrodynamic transport due to density gradients. Usually, convection prevails at large distances from the electrode surface. However, very near the electrode surface, where the reaction occurs, convection is suppressed because the presence of the insulating sheath affects the fluid velocity.[43-44] Therefore, mass transfer is usually governed only by diffusion. It is defined as the movement of material due to a gradient of chemical potential, also known as the concentration gradient.[44]

When an electrode is immersed in a solution, an electrical double layer is instantly formed. It is characteristic of the capacitive current observed in the absence of reaction at the electrode surface (faradic current). The Stern model was proposed to explain the electrical double layer (Figure 1.9). This model combines the Helmholtz and Gouy-Chapman models. It states that the species near the electrode surface are necessarily located in the rigid Helmholtz plane and that the species located outside of this plane follow the distribution proposed by Gouy-Chapman. The Gouy-Chapman distribution depends, among other, on the concentration of the species in solution, in the presence of

charged molecules, the temperature of the solution, etc. Moreover, it is assumed by this model that specific adsorption of species is possible and that the external Helmholtz plane passes through the center of the species having lost their sphere of solvation.

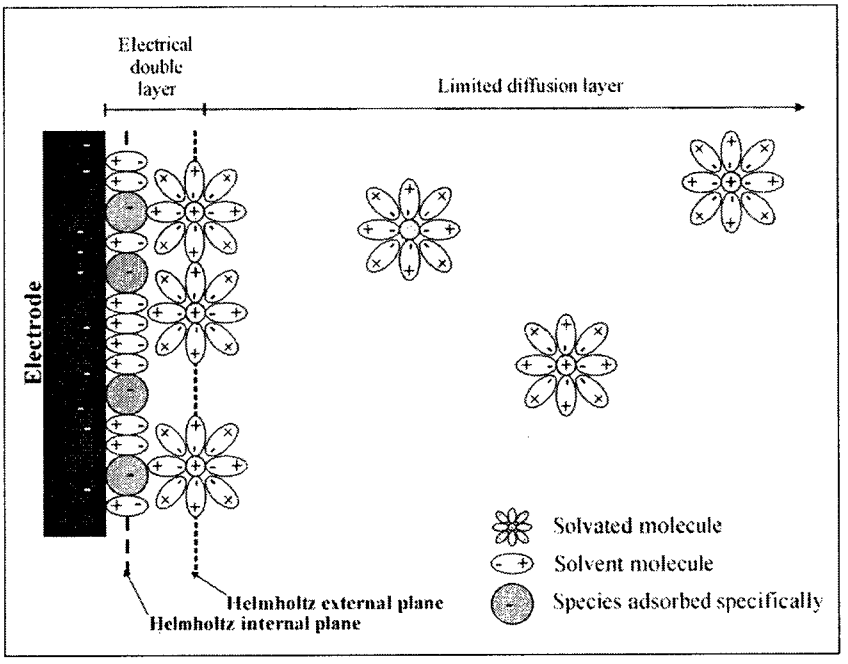

Figure 1.9. Schematic representation of the electrical double layer described by the Stern model, which includes Helmholtz and Gouy-Chapman models.

Figure 1.9 makes it possible to distinguish between the diffusion layer and the electrical double layer. When a potential is applied at the electrode, a reaction can occur. This creates a concentration gradient that generates a flux of reactants towards the electrode surface and a flux of product away. Let's consider an infinitesimal element of solution connecting two points, x and $x+dx$, where the electrochemical potential of x, $\overline{\mu}(x)$ is different than the electrochemical potential of $x+dx$, $\overline{\mu}(x+dx)$ (Figure 1.10).[44] The difference of $\overline{\mu}$ (gradient of potential) over the distance can occur because there is a

difference in the species concentration (gradient of concentration). To ease the $\overline{\mu}$ difference, a flux, J, occurs and follows Fick's law of diffusion.[44]

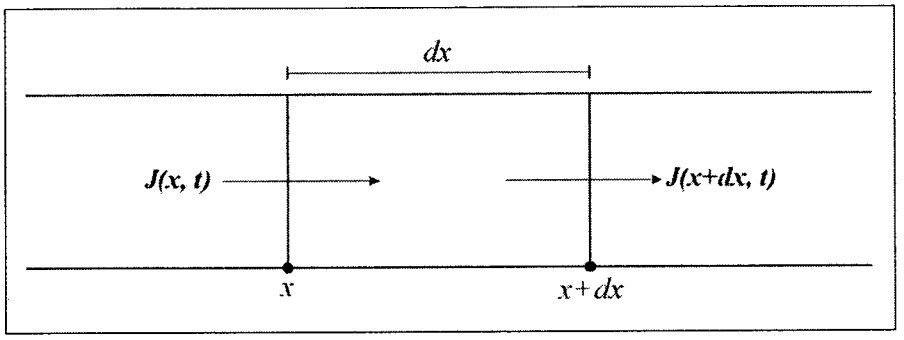

Figure 1.10. Fluxes into and out of an infinitesimal element of solution connecting two points, x and $x+dx$.[44]

Fick's first law describes the flux of species for a given time and position ($J(x, t)$) and it is proportional to a gradient of concentration, $\partial C/\partial x$:

$$-J(x,t) = D\frac{\partial C(x,t)}{\partial x} \qquad \text{(Eq. 1.1)}$$

where D is the diffusion coefficient of the species.

This relation describes the flux of species in solution at a given position, x. From it Fick's second law can be derived:[44]

$$\frac{\partial C(x,t)}{\partial t} = \frac{J(x,t) - J(x+dx)}{dx} \qquad \text{(Eq. 1.2)}$$

$$J(x+dx,t) = J(x,t) + \frac{\partial J(x,t)}{\partial x}dx \qquad \text{Flux at } x+dx \qquad \text{(Eq. 1.3)}$$

$$-\frac{\partial J(x,t)}{\partial x} = \frac{\partial}{\partial x} D\frac{\partial C(x,t)}{\partial x} \qquad \text{(Eq. 1.4)}$$

$$\frac{\partial C(x,t)}{\partial t} = \left(\frac{\partial}{\partial x}\right)\left[D\left(\frac{\partial C(x,t)}{\partial x}\right)\right] = D\left(\frac{\partial^2 C(x,t)}{\partial x^2}\right) \quad \text{(Eq. 1.5)}$$

Fick's second law (Eq. 1.5) is related to the change in concentration of the species with time. Finally, the changes in solution composition due to reaction at the electrode, is usually small enough that the variation of diffusion with x is neglected. Therefore, Fick's laws can apply to the majority of electrochemical systems, except for those with high concentration of electroactive units.[44]

The expression of the current is often given or related to Fick's law. The Nernst equation is usually used to express the potential of a system at equilibrium:[44]

$$E = E^{0\prime} + \frac{RT}{nF} ln\frac{C_O^*}{C_R^*} \quad \text{(Eq. 1.6)}$$

where E and $E^{0\prime}$ are respectively the potential and the formal potential of an electrode, C_O^* and C_R^* are the bulk solution concentration of the oxidized and reduced species, R is the gas constant, T is the temperature, n et is the number of electron exchanged and F is Faraday's constant. The equilibrium is thus characterised by Nernst equation, which relates the electrode potential to the bulk concentration, assuming the unity value of the activity coefficient. Considering a one step, one electron reversible reaction:

$$O + e^- \underset{k_b}{\overset{k_f}{\rightleftarrows}} R \quad \text{(Rx. 1.3)}$$

The forward reaction rate is proportional to the species concentration at a position x and time t, $C(x, t)$ and k_f expresses the proportionality constant between both parameters. Likewise for the backward reaction and k_b.[44] The kinetics of a system are greatly affected

by the potential applied at the electrode. The way the potential affects the k_f and k_b can be predicted by the Butler-Volmer expression.

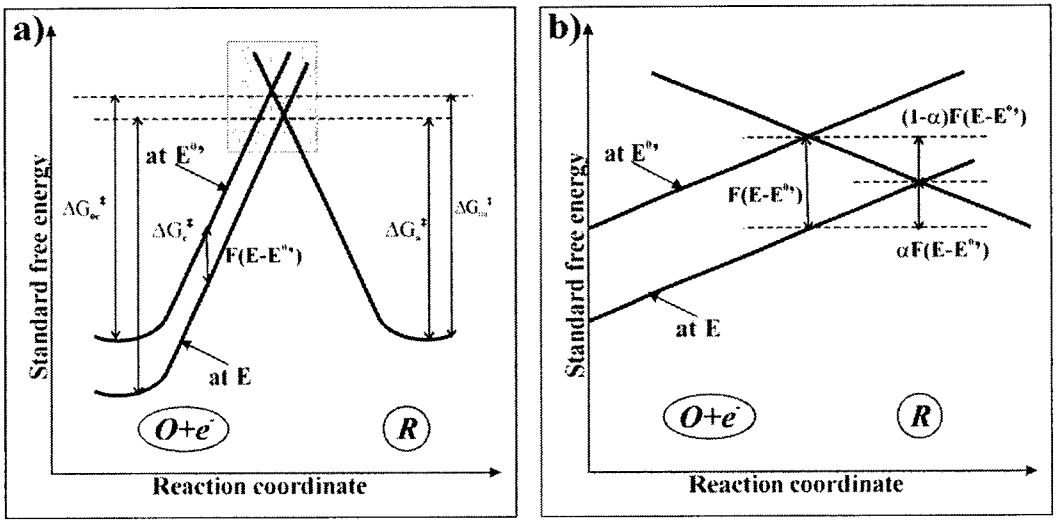

Figure 1.11. a) Standard free energy profiles along the reaction coordinate presenting the effects of a potential change. b) Magnified grey section.[44]

In Figure 1.11, $O + e^-$ curve (upper one) is obtained when the applied potential equals the formal potential ($E = E^{0'}$). If this potential is change (ΔE), the $O + e^-$ curve increases by a $-F\Delta E$ (or $-F(E-E^{0'})$) amount, which corresponds to the relative energy of the electron resident on the electrode charges.[44] Thus, the oxidation barrier, $\Delta G_a^{\ddagger}$, decreases to a value lower then $\Delta G_{0a}^{\ddagger}$ by a factor of 1-α, where α is the transfer coefficient.

$$\Delta G_a^{\ddagger} = \Delta G_{0a}^{\ddagger} - (1-\alpha)F(E-E^{0\prime}) \qquad \text{(Eq. 1.7)}$$

where $\Delta G_{0a}^{\ddagger}$ and $\Delta G_a^{\ddagger}$ are the initial free energy of transfer during oxidation process.

Also the reduction barrier, $\Delta G_c^{\ddagger}$, is higher than $\Delta G_{0c}^{\ddagger}$ by a factor of $\alpha F \Delta E$ when the potential is changed once more.[44]

$$\Delta G_c^{\ddagger} = \Delta G_{0c}^{\ddagger} + \alpha F(E - E^{0\prime}) \quad \text{(Eq. 1.8)}$$

where $\Delta G_{0c}^{\ddagger}$ and $\Delta G_c^{\ddagger}$ are the initial free energy of transfer during reduction process.

Knowing that rate constants k_f and k_b can be expressed as:

$$k_f = A_f exp\left(-\frac{\Delta G_c^{\ddagger}}{RT}\right) \quad \text{(Eq. 1.9)}$$

$$k_b = A_b exp\left(-\frac{\Delta G_a^{\ddagger}}{RT}\right) \quad \text{(Eq. 1.10)}$$

and that at equilibrium $C_O^* = C_R^*$, $E = E^{0\prime}$, $k_f C_O^* = k_b C_R^*$ and $k_f = k_b$, Butler-Volmer equation of electrode kinetics can be expressed as follow:

$$k_f = k^0 exp[-\alpha f(E - E^{0\prime})] \quad \text{(Eq. 1.11)}$$

$$k_b = k^0 exp[(1 - \alpha) f(E - E^{0\prime})] \quad \text{(Eq. 1.12)}$$

where k^0 is the standard rate constant, which represents the formal potential value when the forward and backward rate constants have the same value.[44] Finally, Butler-Volmer expressions (Eq. 1.11 and 1.12) are important when studying any problems requiring a heterogeneous kinetics treatment, just as it is presented in Chapter 4.

The above theory and equations are based on macroscopic concepts and are very useful to study electrochemical reaction mechanisms. However, to predict the effect on reaction kinetics of the nature and structure of the reacting species, the solvent and the

electrode material, a microscopic approach can also be used. The Marcus model is commonly used to explain and predict structural effects on kinetics. First, one must distinguish between the inner-sphere and the outer-sphere electron transfer reactions at electrodes.[44] In an inner-sphere electrode reaction there is a strong interaction between the active species and the electrode (specific adsorption of the species at the electrode surface). Likewise, in an outer-sphere electrode reaction, the active species are separated from the electrode surface by a solvent layer distance. There is a weak interaction between both.[44]

The heterogeneous rate constant, k_0, of an outer-sphere electron transfer can be expressed as follow:[44-45]

$$k_0 = \kappa_{el} K_P \nu_n \, exp\left(-\frac{\Delta G^{\ddagger}}{RT}\right) \qquad \text{(Eq. 1.13)}$$

where $\Delta G^{\ddagger}$ is the activation energy, K_P is a precursor equilibrium constant representing the ratio of the reactant concentration in the reactive position at the electrode to the concentration in bulk solution, ν_n (s^{-1}) is the nuclear frequency factor representing the frequency of attempts on the energy barrier and κ_{el} is the electronic transmission coefficient representing the probability of electron tunnelling in the transition state. κ_{el} is often considered as unity for a reaction with a strong interaction between the active species and the electrode. Equation 1.13 can apply to either a heterogeneous reaction at an electrode or a homogeneous electron transfer reaction.

The activation energy can also be expressed as a function of λ, the reorganisation energy, which is the sum of a solvational component (λ_0) and a vibrational one (λ_i):[44, 46]

$$\Delta G^{\ddagger} = \frac{\lambda}{4}\left(1 + \frac{\Delta G^0}{RT}\right)^2 \qquad \text{(Eq. 1.14)}$$

where ΔG^0 is the standard Gibbs free energy of a reaction. Specifically, for an electron transfer reaction at an electrode, Equation 1.14 can be written as follow:[44, 46]

$$\Delta G^{\ddagger} = \frac{\lambda}{4}\left(1 + \frac{F(E - E^0)}{RT}\right)^2 \qquad \text{(Eq. 1.15)}$$

For a predominant outer-sphere transfer process, λ_0 can be expressed assuming that the solvent is a dielectric continuum and the active species is a sphere of radius r.[44-45]

$$\lambda_0 = \frac{e^2}{8\pi\varepsilon_0}\left(\frac{1}{r} - \frac{1}{2d}\right)\left(\frac{1}{\varepsilon_{op}} - \frac{1}{\varepsilon_s}\right) \qquad \text{(Eq. 1.16)}$$

where e is the electronic charge, d is the distance from the active species to the electrode surface, ε_{op} and ε_s are the optical and dielectric constant and r is the radius of the active species. The latter can be determined by either crystallographic measurements or by calculations using ellipsoidal or mean spherical approximations. The radius r can also be considered as a hydrodynamic radius and thus, it can be estimated using the Stokes-Einstein equation.[45] Thus, $\Delta G^{\ddagger}$ can be given as follow:

$$\Delta G^{\ddagger} = \frac{N_A e^2}{32\pi\varepsilon_0}\left(\frac{1}{r} - \frac{1}{2d}\right)\left(\frac{1}{\varepsilon_{op}} - \frac{1}{\varepsilon_s}\right) \qquad \text{(Eq. 1.17)}$$

Finally, as presented above, Marcus theory can be used to treat electron transfer reactions at electrodes. However, in the context of this work, the Marcus theory does not apply to the studied system, because the rate limiting process remains the diffusion of the

active species to the electrode surface, which is best described by Fick's law presented previously.

1.4.2. Scanning electrochemical microscopy

Scanning electrochemical microscopy (SECM) principle lies in the measurement of a current through an ultramicroelectrode (UME) immersed in a redox mediator solution when held or moved near a substrate. Substrates can be solid (glass, metal, etc.), liquid (mercury, oil, etc.), polymeric and even biological materials.[47] When positioned within a few tip radii of the substrate, the nature and geometry of the UME and the kinetics of the electron transfer reaction at the substrate influence directly the measured current.[48] Ultramicroelectrodes are moved using motors based on piezoelectric elements, such as those found in scanning tunnelling microscopy (STM). Over larger distances, inchworm motors are usually used, as where piezoelectric motors are preferred when higher resolution is needed.[47]

The significance of SECM is observed from the increasing number of manuscripts applying the technique to a wide variety of applications.[48] Being a very versatile tool, SECM is used to study different processes such as metal corrosion, membrane transport, electrocatalysis and surface patterning.[48] Therefore, several SECM modes of operation have been developed. The tip generation-substrate collection mode (TG/SC) is usually used to generate a reaction at the UME that is then detected at the substrate electrode.[47-48] A second mode is the substrate generator/tip collector mode (SG/TC), where reactions generated at the substrate surface are studied.[47-48] Penetration experiments consist of

using a specially designed UME to penetrate microstructures, such as a polymer film, imbedded with redox mediator. Concentration, kinetic and mass transport parameters are extracted from solid-state voltammetry.[48] Electron-transfer and ion-transfer feedback modes at a liquid/liquid interface are important modes for biological and technological systems. They consist of studying heterogeneous charge-transfer reactions at an interface between two immiscible electrolyte solutions or at a liquid-membrane interface.[48] However, the most important mode and the most frequently used mode is the positive and negative feedback mode.

To define the positive and negative feedback mode, let's consider the following situation:

$Ox + ne^- \longrightarrow Red$ Reduction reaction occurring at the biased UME (Rx. 1.4)

$Red \longrightarrow Ox + ne^-$ Oxidation reaction occurring at the substrate (Rx. 1.5)

By approaching the UME tip near a conducting substrate (tip-to-substrate distance (d) ≈ few tip radii) a positive feedback response is observed. Oxidized species (*Ox*) generated at the tip diffuse to the substrate where they are reduced back to *Red* (Figure 1.12a). An additional flux of *Red* is thus generated, which leads to an increase of the current relative to the steady-state current, $i_{T,\infty}$ ($i_T \rightarrow \infty$ when $d \rightarrow 0$). If the UME tip is brought near an insulating substrate, a negative feedback is observed. Once again, *Ox*, produced at the tip, will diffuse to the substrate, but won't react with it (Figure 1.12b). As the tip-to-substrate distance decreases, the diffusion of *Red* species in solution to the tip surface is hindered. This yields a smaller current than $i_{T,\infty}$ ($i_T \rightarrow 0$ when $d \rightarrow 0$).[47-49]

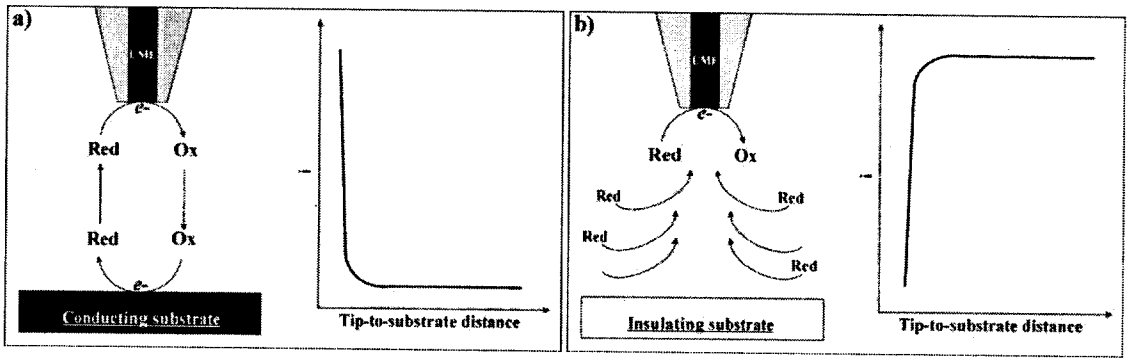

Figure 1.12. Approach curves for a a) positive and b) negative feedback response.

1.4.3. Microelectrode design

Ultramicroelectrodes (UMEs) are characterised by micrometer and sub-micrometer dimensions and nA to pA current range. The ohmic drop reduction, the high rates of mass-transfer and the fast charging of the double layer are some advantages sought when using UMEs.[50] Their unique electrochemical properties allow monitoring of a wide range of chemical species with high spatial resolution. Therefore, UMEs are well adapted for studying biological or biomimetic systems and specifically designed for close approaches to surfaces.

Theoretical treatment for a UME is different from that of a macroelectrodes. The former reaches a steady state current when biased at a potential far exceeding the standard potential of the studied redox mediator. Its cyclic voltammetry (CV) and amperometric response is distinct from that of a macroelectrode (Figure 1.13a and b).

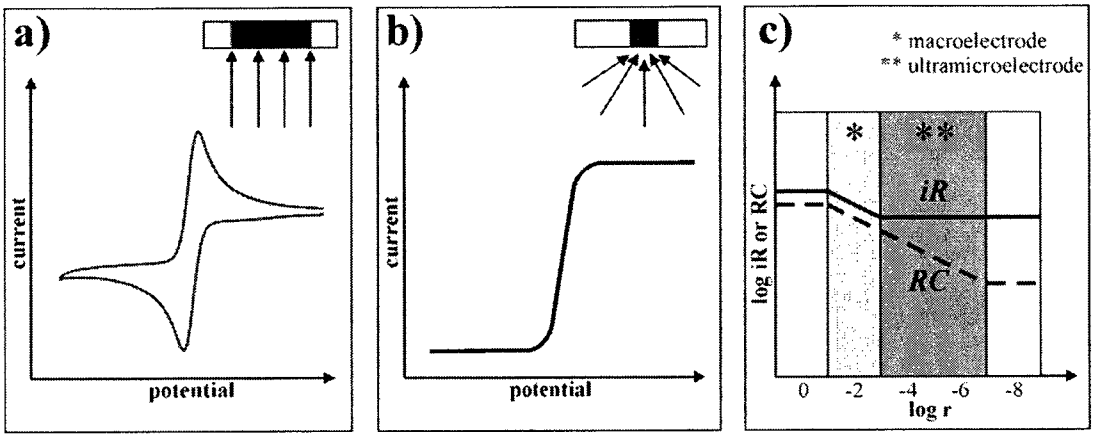

Figure 1.13. Diffusion layer (inserts) and cyclic voltammetry response at a) a macroelectrode and b) an ultramicroelectrode. c) Schematic representation of the ohmic drop (IR, —) and time constant (RC, - - -) as a function of the electrode radius.[43]

In the case of a UME, the transport of molecules is controlled by edge effects and nonplanar diffusion. Therefore, the steady-state current is a function of the dimension of the electrode, *e.g.* the radius (r) of the electrode rather than its surface area (r^2), as is the case for a macroelectrode. Also, the electrode capacitance varies with the electrode surface because it is not affected by the edge effects if the electrode dimensions are greater than the double layer thickness. As for the ohmic drop (IR) and the time constant (RC), they are respectively independent of the electrode surface and proportional to the electrode dimensions (Figure 1.13c).[43] In the case of a macroelectrode, one must first consider that its surface is smaller than the counter electrode surface. Thus, the current is force to flow through a conical volume between the working and counter electrodes and is proportional to the electrode surface (r^2). This means that the electrode capacitance is proportional to the electrode surface and that the iR and RC both vary with the electrode dimension (Figure 1.13c).[43] The different analytical solutions of the diffusion equations for UMEs and macroelectrodes are a direct consequence of the previous properties.

Ultimately, the current versus time curve for a UME reaches a steady state current at longer times rather than fitting to the well known Cottrell equation[44, 51] derived for macroelectrodes.

Even though the most commonly used SECM tip geometry is the disk, ring, spherical, hemispherical, cylindrical and band electrodes are also presented in the literature.[43, 47-48, 51-52] Several steps are involved in the fabrication of disk-UMEs and are summarized in Figure 1.14 (note that the fabrication of ring-UMEs is presented in detail in Chapter 5).[53-56]

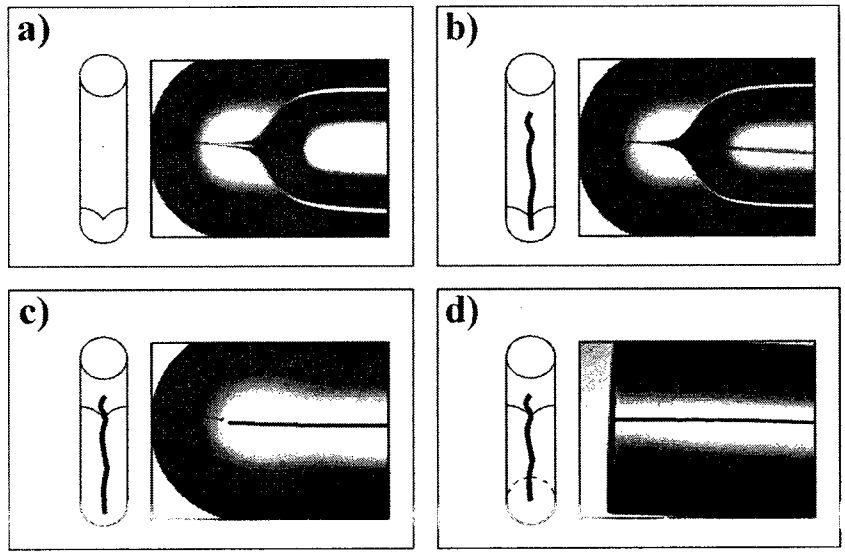

Figure 1.14. Presentation of the steps involved in the fabrication of a disk-ultramicroelectrode. (a) Sealing of one end of a glass capillary, (b) insertion of the wire, (c) sealing of the wire within the glass capillary and (d) exposure of the disk surface.

First, one end of a clean borosilicate capillary (ID/OD=1mm/2mm) is sealed in such way that a V-shape groove is formed (Figure 1.14a). A straight metal wire (Pt, Au or C) is then wedged into the groove (Figure 1.14b). The capillary and wire assembly is placed under vacuum and sealed using a nichrome resistor coil (Figure 1.14c). Finally, the

electrical connection is made and the metal surface is exposed by removing/polishing the excess glass from the tip (Figure 1.14d).[56] A variety of disk-UMEs have been produced (25μm diameter Pt and Au, 10μm diameter Pt, 7μm diameter C) using a custom-built machine. Rapid and reproducible UME fabrication was obtained from careful optimization of the software parameters (fusion height, applied heating periods, number of heating cycles and motor speed between two fusion heights). The glass capillary is put under vacuum prior to and during the sealing process to prevent air bubble formation. The capillary is initially heated for 20 minutes to eliminate moisture and other contaminants (dust, impurities due to handling with the fingers, etc). Optimized sealing parameters are presented in Table 1.2 for different wire diameters and materials.

Table 1.2. Setup parameters for disk-UME sealing processes.

Parameters	**25μm Pt**	**10μm Pt**	**25μm Au**	**7μm C**
Fusion Height (mm)	6	6	6	6
Time Step (s)	300	300	300	180
Distance Step (mm)	1.001	1.001	1.001	1.001
Number of Steps	6	6	6	6
Step Speed (mm/s)	0.1	0.1	0.1	0.2
Beginning Height (mm)	~17	~17	~17	~17
Temperature (°C)	800	800	750	820
Vacuum Time (min)	30	45	30	45

Cyclic voltammetry is used to assess the quality of the seal and the electrical connection and SECM approach curve measurements are necessary to characterise the disk-UME RG value. RG is defined as the ratio of the radius of the electroactive and insulating material (rg) over the radius of the electroactive material (a) and it should

ideally be equal to or smaller than 5 (Figure 1.15a).[47] A sharpened UME is required for approach curve measurements (Figure 1.15b). Thus, the quantity of glass surrounding the metal wire must be minimized in order to prevent the hindering that can happen during close approach of the UME. Usually, the RG is determined by optical microscopy imaging and by fitting the experimental approach curve to the analytical equations[47] of positive and negative approach curves.

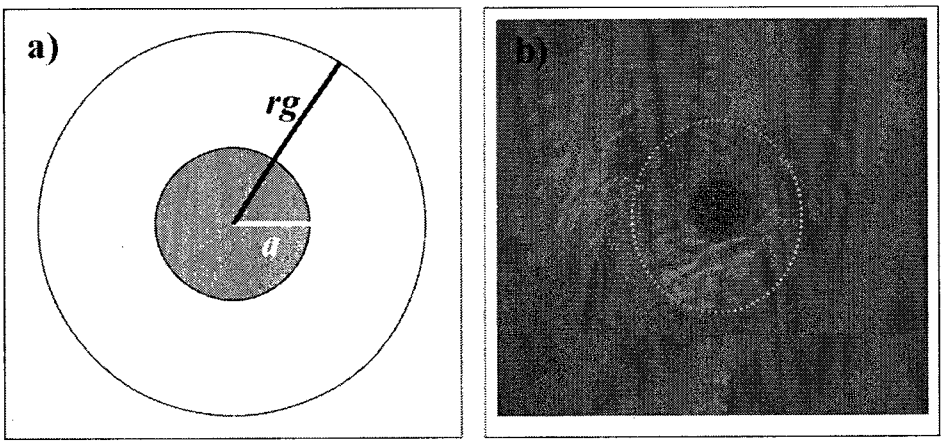

Figure 1.15. a) Schematic representation of the RG defined as rg/a and b) optical image of a sharpened 25 µm diameter platinum ultramicroelectrode tip.

1.4.4. Chronoamperometry measurements

Chronoamperometry, a pulsed technique, is a useful technique that, when combined with cyclic voltammetry measurements, allows differentiation between various electrochemical mechanisms. The chronoamperometry principle lies in the measurement of the faradic current as a function of the time when a constant potential is applied at the working electrode. It is therefore a technique that is especially useful under conditions of

semi-infinite linear diffusion and not in the case of a stationary state system.[44] Here, this technique was used to assess the surface reaction occurring at a biomimetic model surface. Specifically, it involves applying a potential step that generates the species that will diffuse to the redox liposome surface and react with the electroactive tethers. If the generated species react with the redox liposome surface, an additional flux is created, which leads to an increase in the measured current with time. This is only true because measurements are performed with a tip-to-substrate distance that enables feedback effects to be detected. It can also occur at larger distances if the electrolysis time is sufficiently long, but, at long distances and short electrolysis time, the current measured would not be affected by the substrate. However, if the liposome surface is not electroactive, the measured current will decrease because the species will not be regenerated by the liposome surface. An analogy can be made with the positive and negative feedback theory presented above. During the positive feedback mode, the species consumed at the microelectrode are regenerated at the substrate surface, as for the redox liposome. In both cases, an additional current flow is created when species diffuse back to the microelectrode. The surface of the redox liposome can thus be considered as a conducting substrate even though its conductive character is necessarily limited compared to a pure conductive substrate. It is the same for the negative feedback and its analogy with the surface of the bare liposome. As a non-conductive or insulating surface, the bare liposome surface hinders species diffusion. However, the comparison stops there because the insulating properties of the bare liposome cannot be compared to those of a purely insulating surface.

1.5. Objectives

The main focus of this thesis was the scanning electrochemical microscopy study of transport mechanisms using specially designed liposomes as biomimetic models. Particularly, a surface bound reaction was studied with a surface-modified redox liposome. A control model, *e.g.* a bare liposome, was also studied for means of comparison. Therefore, the first objective was to synthesize and characterise redox phospholipids that were used to design surface-modified redox liposomes. This was realised through the PLD-catalyzed transphosphatidylation reaction between 1,2-distearoyl-*sn*-glycero-3-phosphocholine and a primary alcohol. The choice of the primary alcohol is what makes this phospholipid headgroup modification original. Here, the chosen electroactive tether is a ferrocene-derivative. Until now, no phospholipid headgroup has been modified with an organometallic unit. This leads to the second objective of this research project, which was the SECM study of the resulting organometallic redox liposome. By approaching an ultramicroelectrode near its surface and by using a sacrificial redox mediator, the redox surface of the liposome was titrated. This was specifically studied by chronoamperometric measurements and the results were compared with the ones obtained for a bare liposome (control biomimetic model). Finally, the third objective was to design and fabricate a novel ring microelectrode. Here, a platinum ring microelectrode was fabricated using novel materials to isolate the electrode. This electrode was first designed to study the biomimetic models previously presented. However, the challenges involved in the fabrication procedure did not allow us to use the ring microelectrode (or micropipet) with the liposomes. The studies were mainly focused on how well, and to what extent the new insulator material worked. This

study was done by experimental and numerical simulations of cyclic voltammetry measurements.

The following thesis is presented in the form of three manuscripts, each representing one of the objectives outlined. Chapter 2 presents the first manuscript, which focuses on the modification of the phospholipid headgroup with an organometallic redox active tether. It also presents the influence of the synthetic conditions over the enzyme (PLD) activity. The second manuscript is presented in Chapter 3. It consists of the synthesis of a more stable organometallic redox phospholipid than the one presented in the previous manuscript and in the electrochemical study of the resulting redox liposome. Chapter 4 details the fabrication of a novel platinum ring microelectrode insulated with silicon oxide. In the context of this research project, disk-UMEs and platinum ring microelectrodes were developed. The disk-UME was first used because numerical simulation data already existed and it was easy to fabricate. As for the ring microelectrode, it was chosen because it is ideal for controlled kinetic studies (microinjection experiments) and thus, was suitable to study biomimetic models, such as liposomes. This manuscript is based on the presentation of the steps involved in the microring design and on the study of the effect of focused ion beam on the insulating layer during the ring exposure step. To do so, numerical simulations were used. Finally, at the beginning of each chapter, the content is described and put into context with that of the other chapters and related to the main objectives of the thesis.

Chapter 2. Synthesis of metal complex modified phospholipids by phospholipase D-catalyzed transphosphatidylation

2.1. Contribution of authors and context

This first manuscript was published in the *ECS Transactions* (v. 19, issue 33, p. 1-10) and is related to a conference presentation given at the 215th ECS Meeting in San Francisco held from May 24-29, 2009. All experiments and the manuscript draft were produced by Debby Correia Ledo under the supervision of Dr. Janine Mauzeroll, Université du Québec à Montréal.

In the literature, various types of redox liposomes are presented. In these models, the electroactive organometallic units are usually encapsulated within the liposome. As for the surface-modified liposomes, only quinone derivatives have been, up until now, reported. These redox liposomes are not appropriated for our ongoing electrochemical studies. Thus, we developed a redox liposome whose surface was modified with a redox active organometallic type tether, namely ferrocene derivatives. The advantage of using ferrocene derivatives is that they have been widely studied and therefore their electrochemical behaviour is well known. Moreover, it is easier to activate the ferrocene tether using a sacrificial analyte compared to other non-organometallic redox liposomes. This manuscript describes the modification of a phospholipid headgroup with

ferrocenemethanol. Since an enzymatic synthesis was chosen for such modification, a study of the enzyme activity is also presented.

2.2. Abstract

The synthesis of ferrocenyl-functionalized phospholipid was achieved through a biphasic transphosphatidylation reaction catalyzed by phospholipase D. Thus, the 1,2-distearoyl-*sn*-glycero-3-phosphocholine headgroup was modified with hydroxymethylferrocene. 1,2-distearoyl-*sn*-glycero-3-phosphocholine was chosen because it bears a choline group required for successful phospholipase D-catalysis. The use of hydroxymethylferrocene, as an electroactive tether, was appropriate since the present transphosphatidylation reaction is specific to primary alcohols. Mass spectrometry and phosphorus nuclear magnetic resonance analysis confirmed the formation of the redox active phospholipid and also revealed downstream instabilities that will need to be resolved prior to use in liposome assemblies.

2.3. Introduction

Liposomes are tuneable biomimetic models whose content and surface properties can be altered readily. Their versatile nature enables them to be used in drug encapsulation and their surface modification serves different purposes such as target delivery, long-circulating vehicles and transfection vectors. They are also used in more fundamental membrane transport studies. We are interested in synthesizing redox active

liposomes in order to study long term liquid-membrane interfacial reactions. The redox active units can be encapsulated within the internal void, be imbedded in the membrane or be bound to either the phospholipid headgroup or tail of the liposome. Liposomes bearing encapsulated and imbedded redox units have been the focus of other work.[57-59] The nature of the redox units used varies and includes among others ruthenium tris-bipyridyl complexes, *N*-(10,12-pentacosadiynoic)-acetylferrocene molecules, ferredoxin analogues, nitro-2,1,3-benzoxadiazol-4-yl units and bis(11-ferrocenylundecyl)-dimethylammonium bromide.[57-61] Liposomes bearing surface bound units are also well-known and include fluorescent tags (quantum dots, 6-carboxyfluorescein, rhodamine 101, perylene tethers[18, 62-64] and carbohydrates units[65]. However, few reports are related to the study of liposomes bearing surface bound redox active units. Up to now, the studies have been restricted to the surface functionalisation of liposomes with quinones.[66-68] Quinone-functionalized liposomes would be good candidates to study surface reactions if not for the fact that quinones auto-oxidize with time, leading to liposome degradation. This characteristic is desirable when studying the release of electroactive, medical or biological material. For our purposes, long-term stability of the liposomes is required. As such, we have elected to modify a phospholipid headgroup with a different electroactive tether (hydromethylferrocene) using a phospholipase D-catalyzed transphosphatidylation reaction.

Phospholipase D (PLD, EC 3.1.4.4) has been used as a synthesis catalyst as a result of a growing interest for natural phospholipids in the industrial and biomedical fields.[31] For example, Wang *et al.* have conducted a comprehensive study on the modification of an L-α-phosphatidylcholine with different organic primary alcohols and

were able to study the chemoselectivity, regioselectivity and stereoselectivity of PLD.[65] To capitalize on the highly selective nature of PLD towards primary alcohols, hydroxymethylferrocene, also known as ferrocenemethanol (FcMeOH), was first used as a potential electroactive tether. FcMeOH is a redox-active organometallic molecule whose electrochemical properties are well known and that had been previously used to produce redox-active dendrimers, *e.g.* ferrocenyl-functionalized poly(propylenimine) (PPI) dendrimers.[69] Herein, we describe, for the first time, a method to synthesize a ferrocenyl-functionalized phospholipid, DSP-OMeFc, by the PLD-catalyzed transphosphatidylation reaction.

2.4. Experimental section

2.4.1. Materials

Tris-acetate salt (reagent grade), sodium dodecyl sulfate (SDS, 99+ % ACS reagent), 2-(*N*-morpholino)ethanesulfonic acid (MES, low moisture content, ≥ 99 %), *o*-phenylenediamine (OPD, 99.5 %), hydroxymethylferrocene (FcMeOH, 97 %), L-α-phosphatidylcholine (PC, from egg yolk, type XI-E, minimum 60 % TLC), phospholipase D (PLD, type II, ≥ 60 U/mg protein, E.C. 3.1.4.4) from *Arachis hypogaea* (peanut), choline oxidase (E.C. 1.1.3.17) from *Alcaligenes* sp. and peroxidase (type I, E.C. 1.11.1.7) from horseradish were purchased and used as received from Sigma-Aldrich. Triton X-100 was purchased from EMD. Tris-HCl (BioUltraPure reagent, > 99.0 %) was purchased from BioShop while calcium chloride ($CaCl_2$, ACS reagent), sodium acetate

(NaOAc, ACS reagent) and ethylenediaminetetraacetic acid (EDTA, ACS reagent) were purchase from Anachemia. 1,2-distearoyl-*sn*-glycero-3-phosphocholine (DSPC, 20 mg/mL in chloroform solution) was purchased from Avanti Polar Lipid Inc. Finally, all reaction solvents were of ACS grade or better.

2.4.2. Methods

2.4.2.1. Phospholipase D activation

Lyophilized PLD powder was activated in two ways. The first procedure consisted in dissolving 2526 units of PLD in 2526 µL of 100 mM NaOAc solution (1 U/µL). DMSO was added to a final concentration of 10 % v/v and served the purpose of cryogenic agent. From this stock solution, aliquots containing 100 units of active PLD in a final 100 µL volume were prepared. The aliquots were frozen in liquid nitrogen and stored at -80 °C. In the second PLD activation procedure, 1000 units of PLD were dissolved in 1 mL of 0.4 M Tris-acetate buffer pH 6.0. This solution was freshly prepared before each synthesis. Finally, PLD aliquots used in the enzymatic activity assays were prepared from a stock solution of 1 U/mL dissolved in nanopure water (Milli-Q Biocel, Milipore).

2.4.2.2. Phospholipase D enzymatic activity assay

Experimental conditions greatly affect PLD enzymatic activity and several techniques have been developed to monitor its activity. These methods include titration

techniques based on pH changes related to the formation of phosphatidic acid, nuclear magnetic resonance measurements that monitor phospholipids structure variations and chromatography coupled with radioactivity assays.[70] An important limitation of these methods, which impairs their widespread use, is their lack of adaptability for high throughput analyses.[70-71] Spectroscopic methods are readily adaptable for high throughput applications and have several advantages that include sampling a wide linear domain of PLD concentrations. In the present microtitration method, PLD concentrations ranging from 0 to 0.3 U/mL are accessible.[71]

Briefly, Figure 2.1 presents the reaction scheme of the PLD enzymatic assay that is based on the colorimetric determination of choline, **3**, using a choline oxidase/horseradish peroxidase reaction. Oxidation of compound **3** by choline oxidase produces stoichiometric amounts of betain (a quaternary ammonium compound, **4**) and hydrogen peroxide (Figure 2.1b). The latter, in presence of peroxidase, catalyzes the oxidation of OPD, **5**, which becomes colored (Figure 2.1c). This reaction product, **6**, is detected by UV-vis analysis at 490 nm using a microplate reader Tecan Infinite M200 (ESBS Scientific, Canada) and its concentration is directly related to the enzyme activity and thus to the PLD active concentration (Figure 2.1a). For a given PLD concentration, only a fraction of it is considered active and this is what is meant by the term «active concentration». The determination of PLD enzymatic activity followed a reported protocol [71] that was modified to account for aliquot preparation from a commercially available PLD strain instead of PLD obtained from natural extracts.

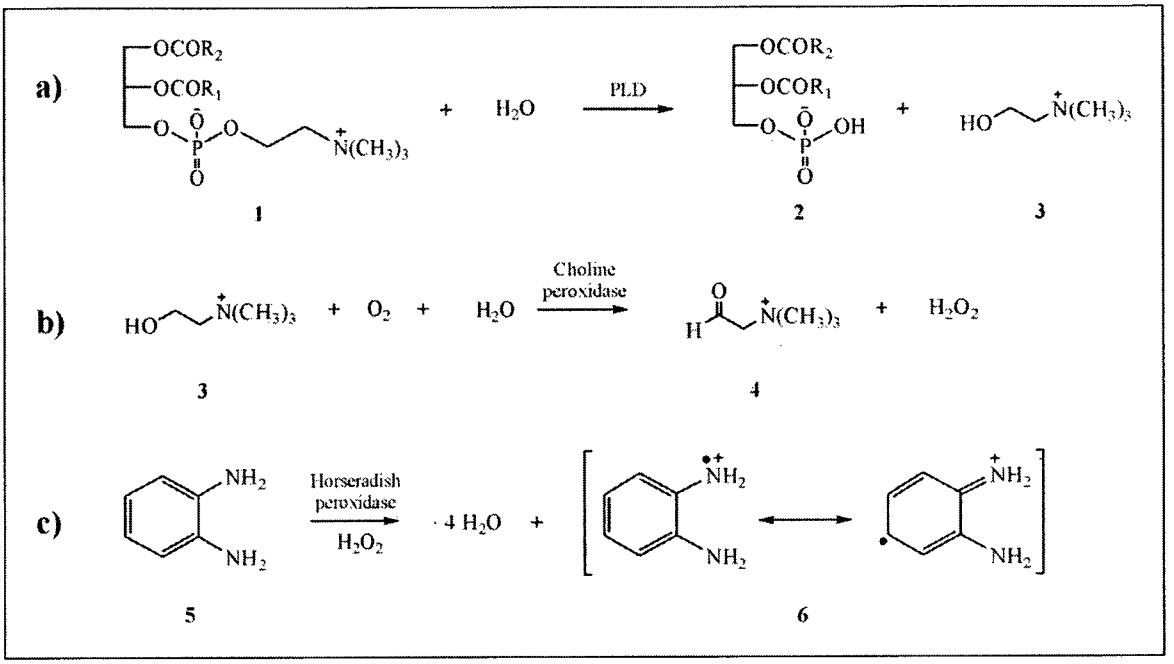

Figure 2.1. Schematic representation of the three reactions involved in the phospholipase D enzymatic activity assay.

2.4.2.3. Redox phospholipid syntheses

The redox phospholipid syntheses were developed based on the work of Wang *et al.*[65] and Dong and Su-jia[25]. Monophasic transphosphatidylation reactions, syntheses A and B, were performed in a non-aqueous environment where 7.9 µmole of DSPC and 47.5 µmole of FcMeOH are dissolved in 5 mL of anhydrous chloroform. Consistent with literature,[65] a 1:6 lipid to alcohol ratio was maintained. Reaction conditions differ for synthesis A and B. In synthesis A, 50 units of PLD (activated using the first procedure and then lyophilized[72]) were added to the reaction mixture that was kept under agitation at 38 °C for 48 hours. In synthesis B, 100 units of PLD were used while reducing the reaction time to 4 hours.

Biphasic transphosphatidylation syntheses A' and B' were carried out in a biphasic media where a 1:8 aqueous to organic phase ratio was maintained. In the case of syntheses A' and B', the reaction conditions are similar to those of syntheses A and B respectively with the exception that the PLD dissolution was carried out in the aqueous phase.

Finally, the optimized biphasic synthesis C' was prepared by mixing 20 mM of DSPC and 6.67 mM of FcMeOH (3:1 lipid to alcohol ratio) in 3 mL of ethyl ether. Since DSPC was already dissolved in chloroform, the latter was evaporated under argon before adding it to ethyl ether. 1000 units of PLD (activated using the second procedure) were added to the ether phase. Here, the PLD solution acts as the aqueous phase with an aqueous organic phase ratio of 1:3. All were kept under agitation for more than 5 days at 38 °C.

2.4.2.4. Product characterisation

Prior to purification, the crude sample was characterized by mass spectrometry (MS) and 31-phosphorus nuclear magnetic resonance (^{31}P NMR). For the MS analyses, the sample was dissolved in methanol and directly injected into the ionizer (Waters Micromass ZQ, positive electrospray ionization (ESI)). NMR experiments were carried out at 298 K on a Varian Inova 600 MHz spectrometer equipped with a double resonance probe operating at 242.86 MHz for ^{31}P. The spectra were recorded using single 90 degree pulses and ^{1}H continuous wave decoupling during the acquisition. A total of 32 scans

with a recycle delay of 3 seconds were accumulated. All samples were dissolved in a $CDCl_3$:CD_2OD 2:1 (v/v) mixture.[73]

2.5. Results and discussion

Herein, we describe a means by which lipid functionalisation can be achieved using a PLD-catalyzed transesterification reaction. Figure 2.2 presents the headgroup modification of DSPC, **7**, with the primary alcohol FcMeOH, **8**, through a PLD-catalyzed transphosphatidylation reaction that yields the desired redox active phospholipid, **9**, phosphatidic acid, a byproduct, **10**, and choline, **3**.

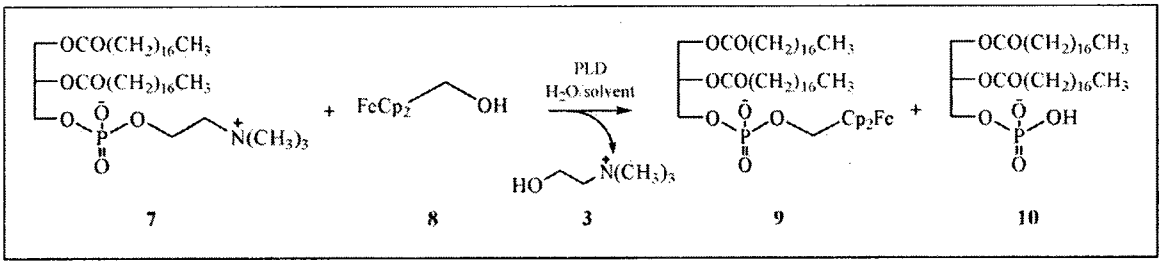

Figure 2.2. Schematic representation of DPSC, **7**, headgroup modification by FcMeOH, **8**, through a PLD-assisted transphosphatidylation.

Phospholipase D is an enzyme that catalyzes the hydrolysis of the phosphodiester bonds of glycerophospholipids. In presence of a primary alcohol, PLD catalyzes the transesterification reaction, also known as transphosphatidylation. This reaction, which is specific to choline bearing molecules, consists in substituting the phosphatidyl group of a phosphatidylcholine by a primary alcohol.[25, 27, 31, 37, 65] Here, DSPC, **7**, was chosen as the modifiable lipid because its behavior in model membranes has been extensively studied

as it can readily be applied to classical liposome assembly protocols, such as the double emulsion method, and it is a cell membrane constituent. The choice of primary alcohol, FcMeOH, **8**, as the electroactive tether, was motivated by the fact that it is commercially available and is a well behaved reversible redox mediator. A cyclic voltammogram (Figure 2.3) recorded at a 25 μm diameter Pt microelectrode presents the classical sigmoidal shape characteristic of microelectrodes where the steady state current, i_{ss}, is directly related to the bulk concentration of FcMeOH in solution. Finally, the use of FcMeOH in the fabrication of ferrocenyl-functionalized poly(propylenimine) (PPI) dendrimers was also an encouraging parallel study that suggested that FcMeOH might be amenable to surface functionalisation of liposomes.[69]

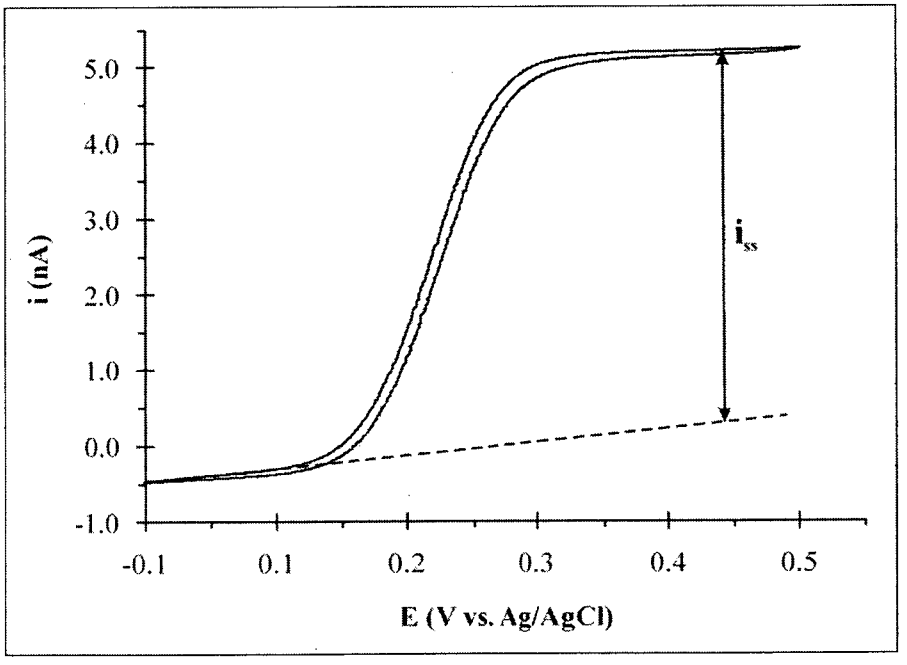

Figure 2.3. Cyclic voltammogram (CV) of a 1 mM ferrocenemethanol solution in 0.1 M KCl recorded at a 25 μm diameter Pt microelectrode at a scan rate of 10 mV/s.

In enzyme-assisted synthesis, it is important to control the parameters related to the enzyme activity, such as the enzyme strain, environment and reaction temperature. There are several PLD strains, but PLD from *Streptomyces sp.*, *Arachis hypogaea* (peanut) or cabbage are the most commonly used for transphosphatidylation reaction. Here, PLD from *Arachis hypogaea* (peanut) was chosen because it is accessible commercially and its properties are well known.[29-30, 35-36]

2.5.1. Phospholipase D enzymatic activity determination

Phospholipase DPLD activity is strongly dependent on storage conditions and preparation practices (Figure 2.4). Under optimal conditions (pH 6, freshly activated PLD), the measured absorbances (λ = 490 nm) of 0.3, 0.2 and 0.1 U/mL aliquots were 0.94, 0.61 and 0.46 respectively. These values are higher than those presented in the literature for the same concentrations of PLD.[71] Phospholipase D strain and its source (commercial vs. natural extracts) may explain the fact that the absorbance values presented here exhibit a six fold increase.

Phospholipase D aliquot storage is an important experimental parameter that should be controlled during enzyme-assisted synthesis to ensure enzyme stability and retain activity. Enzyme storage of PLD aliquots at -80 °C for a week results in a general loss of activity. As presented in Figure 2.4, for identical PLD concentrations, the absorbance values of stored PLD aliquots were 0.49, 0.30 and 0.21 respectively. This two fold decrease in enzyme activity as compared to that obtained with fresh aliquots can be

explained by partial enzyme denaturation due to exposure to a storage cold temperature that potentially exceeds the cold denaturing temperature of PLD.[74]

Enzyme preparation is also critical in terms of pH to retain activity. Phospholipase D activity is optimal in a slightly acidic environment, *e.g.* at pH 5-6.[75] In a more basic environment, pH 8, the corresponding PLD activity absorbance values present a two-fold decrease in intensity similar to that observed when studying the effect of storage. Successful optimization of the transphosphatidylation reaction therefore requires the use of fresh PLD aliquots that have been activated using the second activation procedure described above.

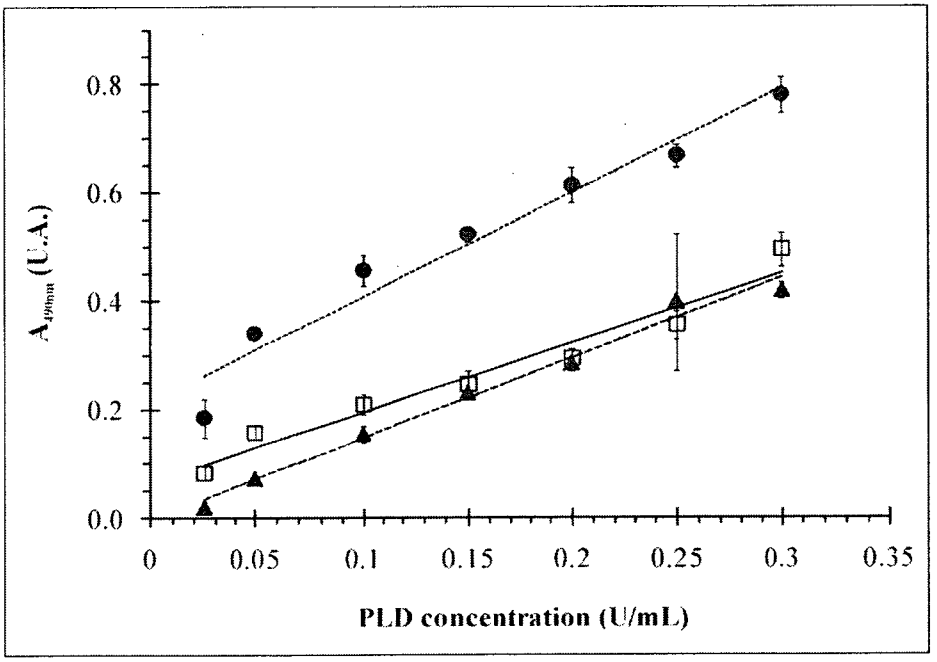

Figure 2.4. Calibration curves of the phospholipase D enzymatic activity assay at pH 6 using aliquots of freshly activated PLD (•), following storage at -80 °C (□) and at pH 8 (▲). The error bars represent 95% confidence intervals (N=5) and may be within the data marker.

2.5.2. Synthetic approaches to redox phospholipids

To proceed with the synthesis of **9**, the reaction conditions described in Table 2.1 were used. Transphosphatidylation reactions can be performed in either a monophasic or biphasic system.[25, 37, 65] Monophasic transphosphatidylation reactions involve the use of a single organic phase that prevents the formation the phosphatidic acid byproduct, **10**, and therefore should provide higher yields of **9**. Unfortunately, monophasic reactions subject the enzyme to an uncontrolled pH environment that significantly reduces its activity. In the characterization of both developed monophasic syntheses (A and B), only the starting reagents, **7** and **8**, were observed. Further attempts to activate PLD using a 100 mM NaOAc solution and subsequent lyophilisation did not improve the outcome of the monophasic syntheses.[65, 72]

Table 2.1. Biphasic and monophasic syntheses parameters.

	Monophasique syntheses		**Biphasique syntheses**		
	A	**B**	**A'**	**B'**	**C'**
Solvent	$CHCl_3$	$CHCl_3$	$CHCl_3$	$CHCl_3$	$(CH_3CH_2)O$
Aqueous/organic phase ratio	—	—	1 : 8	1 : 8	1 : 3
Lipid/alcohol ratio	1 : 6	1 : 6	1 : 6	1 : 6	3 : 1
PLD (units)	50	100	50	100	1000
Reaction time (hours)	48	4	48	4	> 48

In the biphasic system, the transphosphatidylation reaction occurs at the interface of the aqueous and organic phase (Figure 2.5a). As a consequence, in the biphasic reaction, the enzyme does not significantly interact with the organic phase. Three syntheses were developed (A', B' and C'). Given the hydrophilic nature of the

phospholipid headgroup, it is expected that its modification would mainly occur in the aqueous phase. Hence, the enzyme and primary alcohol must have an appreciable solubility in the aqueous phase to ensure efficient synthesis of product **9**. Synthesis A' and B' were developed on the basis of successful reports that used carbohydrates containing primary alcohols.[25, 65] In these syntheses, a lipid to alcohol ratio of 1:6 was used in a total reaction volume that did not exceed 5.6 mL but did not produce appreciable yields of **9**. Only the reagents **7** and **8** were observe by the MS analyses.

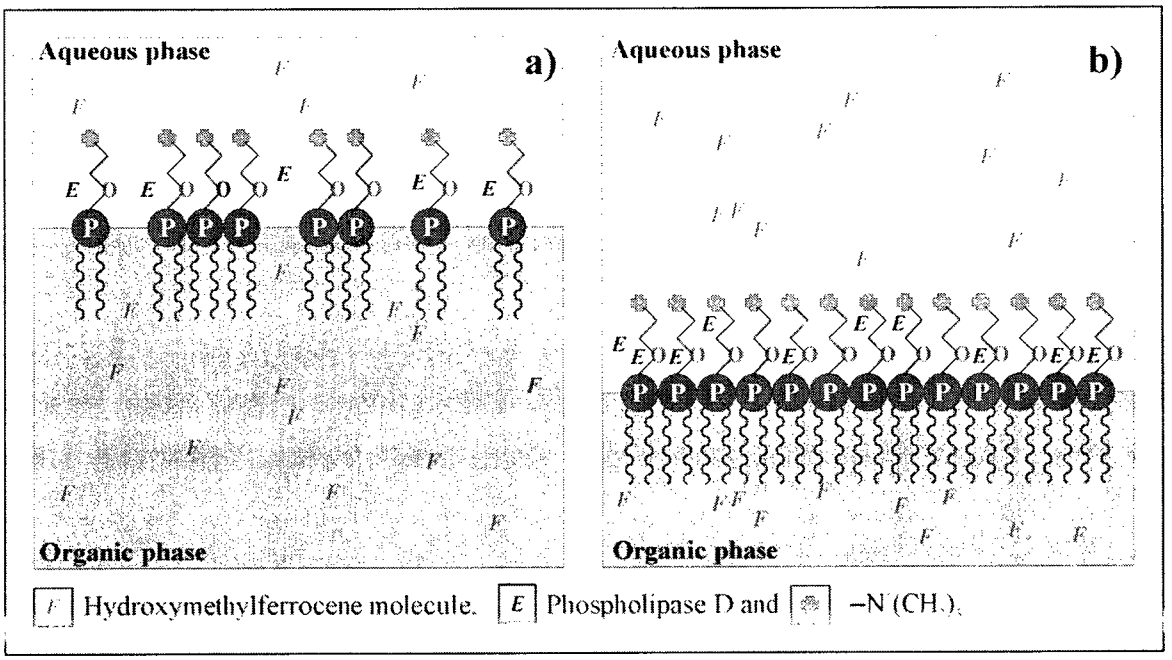

Figure 2. 5. Schematic representation of the biphasic synthesis a) A' and B' and b) C'.

Synthesis C' was however successful in forming redox phospholipids. In the present reaction system, FcMeOH, **8**, is an organometallic primary alcohol that has a maximum solubility in aqueous solutions on the order of 1mM. In the biphasic system, a considerable fraction of the primary alcohol is extracted in the organic phase. As such, optimization of the resulting transphosphatidylation reaction implied (i) increasing the

relative distribution of FcMeOH in the aqueous phase and (ii) increasing the number of available reaction sites. This was accomplished in reaction C' by changing the solvent environment from chloroform to ethyl ether, reducing the aqueous to organic phase ratio from 1:8 to 1:3, increasing the lipid to alcohol ratio from 1:6 to 3:1 and increasing PLD concentration (Figure 2.5b). Changing the solvent environment was advantageous because both DSPC and FcMeOH have reduced solubility in $(CH_3CH_2)_2O$. This change is consistent with previous reports that demonstrated a two fold increase in reaction yields upon a similar solvent substitution.[25] Reduction of the aqueous to organic phase ratio increased the extraction power of the aqueous phase towards **8.** Increasing the lipid to alcohol ratio increased the number of interfacial phospholipid headgroups available for transphosphatidylation while increasing PLD concentrations ensures a fast turn-over rate of the interfacial reaction even though PLD is never in direct contact with the organic solvent. The formation of the redox phospholipid, **9**, was observed by MS and ^{31}P NMR.

2.5.3. Product characterisation

The crude sample was analysed by MS and revealed $[M+H]^+$ peaks of DSPC, FcMeOH and redox phospholipid at *m/z* 791 (100 %), *m/z* 217 (relative intensity not determined) and *m/z* 903 (10.2 %) respectively. $[M+Na]^+$ peaks were also observed at *m/z* 813 (90.8 %), *m/z* 239 (relative intensity not determined) and *m/z* 925 (34.7 %) respectively. The presence of peaks at *m/z* 903 and *m/z* 925 confirms that the enzyme-assisted synthesis C' was successful.

^{31}P NMR analyses also confirmed successful synthesis of **9**. In Figure 2.6a, the DSPC signal is observed at chemical shift of 22.1 ppm. Following enzyme-assisted synthesis, a slight downfield shift of the DSPC chemical shift to 23.8 ppm is observed (Figures 2.6b and c). In Figure 2.6b the upfield signal observed at chemical shift 0.25 ppm is assigned to the redox phospholipid. This peak cannot be assigned to the phosphatidic acid byproduct since, according to literature, its chemical shift is 2.39 ppm.[73]

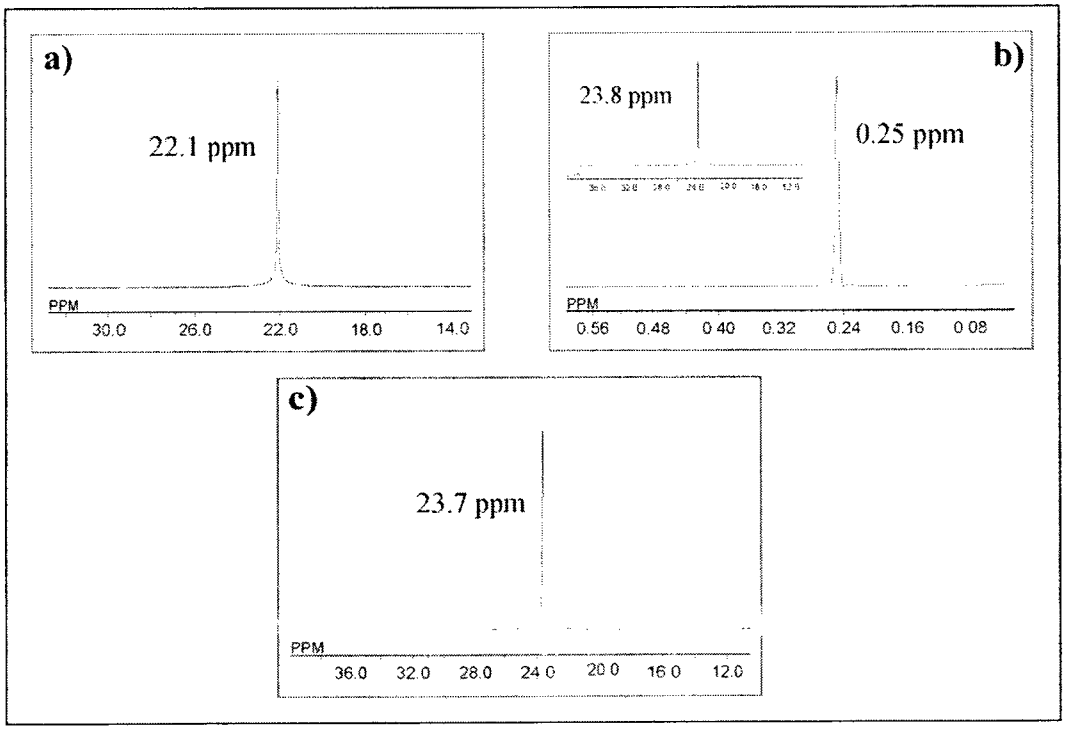

Figure 2.6. ^{31}P NMR of a) DSPC, **7**, b) redox phospholipid (**9**, DSP-OMeFc) synthesized by a PLD-assisted transphosphatidylation between **7** and **8** and c) a PLD-assisted transphosphatidylation following decomposition of compound 9 within a few hours. The spectra were referenced to H_3PO_4.

Finally, it is important to note that product **9** displays an instability that results in a loss of ^{31}P NMR signal with time (Figure 2.6c). This instability could be related to the

benzylic nature of compound **9** that increases the leaving group capabilities of the redox phospholipid headgroup. The consistent presence of water and choline in the reaction mixture can lead to a cleavage of the P-O and/or O-CH_2 bonds through a hydrolysis or S_N2 reaction. Efforts are presently underway to improve the overall stability of the redox lipids by using aliphatic primary alcohols.

2.6. Conclusion

In this work, the biphasic transphosphatidylation reaction was successfully used to modify the headgroup of a phospholipid with an organometallic electroactive tether. The transphosphatidylation reaction catalyzed by PLD is specific to lipid bearing a choline function and primary alcohols. Thus, the phosphorus headgroup of DSPC was modified with the redox agent and primary alcohol, FcMeOH. The resulting redox DSPC, DSP-OMeFc, was obtained and characterized by MS and ^{31}P NMR. The product instabilities observed are thought to be related to the benzylic character of the product. It is suggested that the presence of choline and water in the reaction mixture favours undesired hydrolysis or S_N2 thus cleaving the P-O and O-CH_2 bonds. By changing the nature of the primary alcohol and the experimental conditions, it should be possible to obtain a stable aliphatic redox modified DSPC that would be applicable to the formation of redox liposomes. These can in turn serve as biomimetic models to study surface reaction at membranes.

Chapter 3. Synthesis of a redox active ethyl-ferrocene phospholipid by transphosphatidylation reaction and chronoamperometry study of the corresponding redox liposome

3.1. Contribution of authors and context

This manuscript will soon be submitted to the *Journal of Lipid Research*. The experimental results presented here were part of a conference presentation that will be given at the 93rd Canadian Chemistry Conference and Exhibition held in Toronto from May 29-June 2, 2010. Once again, all experiments were performed and the manuscript drafted by Debby Correia Ledo under the supervision of Dr. Janine Mauzeroll, Université du Québec à Montréal. The ^{31}P NMR measurements were performed with Dr. Alexandre Arnold, Université du Québec à Montréal, who is also a contributing author to the manuscript.

This second manuscript is in the same vein as the first one. However, the study of the proposed redox liposome is actually assessed here and the premises of the study of surface bound reactions are presented. The modification of the phospholipid headgroup with ferrocenemethanol led to the synthesis of an unstable product in presence of water in the reaction medium. By following a similar synthetic route as that previously described, the phospholipid headgroup was modified once again but using ferrocene-ethanol as the electroactive tether. The result was a stable organometallic redox active phospholipid. In

this manuscript, not only the synthesis of a ferrocenyl phospholipid is presented, but proof that the tether was covalently bound to the phosphorus atom is also given. In addition, preliminary electrochemical measurements of the resulting redox liposome demonstrate that its surface was indeed electroactive and that it is possible to modulate its electrochemical response.

3.2. Abstract

Liposome surface functionalisation remains a key issue in the ever expanding field of drug targeting and delivery. Our interest lies in the development of long-lived redox active liposomes. Herein, the design and characterisation of a stable organometallic redox liposome are presented for the first time. Synthesis of the organometallic redox active phospholipid was successfully achieved through PLD-catalyzed transphosphatidylation reaction between a choline bearing phospholipid and an organometallic redox active primary alcohol. Solid state ^{31}P NMR, IR and MS analyses confirmed the successful attachment of the ferrocene derivative to the phosphorus atom of the phospholipid headgroup. Once assembled into stable and large diameter redox liposomes, the electrochemical activity of individual liposomes over time was studied. The resulting liposomes are ideal biomimetic models that will be used to eventually study surface bound electroactive reactions at membranes.

3.3. Introduction

Liposomes are coveted biomimetic models that are commonly used in drug target and delivery studies. Tuneable models, their internal void and surfaces can readily be modified totally or partially. Although surface functionalisation strategies are diverse and well established, liposome surface functionalisation with electroactive units has been limited to organic or quinone[66-67, 76-77] based electroactive pendents. The latter were also found to be unstable over time.

The use of organometallic pendents to functionalize liposome surfaces remains unexplored and the only available reported study suffered from severe redox phospholipid instability[78] that prevented the formation of organometallic redox active liposomes. Ferrocene-modified liposomes should be ideal biomimetic membrane models that present straightforward electrochemical behaviour combined with stability, as largely documented in two dimensional self-assembled systems.[11, 79]

Herein, phospholipid headgroups are modified with a ferrocene derivative prior to their assembly into liposomes. To do so, an enzymatic synthesis based on a transphosphatidylation reaction was chosen to covalently bind a ferrocene derivative having a primary alcohol function to the phosphorus of a phosphatidylcholine. Transphosphatidylation reactions have been successful in modifying the phosphatidylcholine headgroup through the catalytic activity of phospholipase D,[25, 33, 37, 65] which is dependent on the presence of a choline bearing phospholipid and a primary alcohol, which in the present case is ferrocene-ethanol.

Modification of the phosphatidylcholine headgroup and attachment of the organometallic pendent was confirmed by solid state 31-phosphorus nuclear magnetic resonance, infrared and mass spectrometry analyses. Cyclic voltammetry analyses revealed the electrochemical activity of the organometallic redox phospholipid.

Finally, chronoamperometric measurements performed on sedimented liposomes confirmed that redox liposomes produced using the double emulsion technique[13, 17, 22, 80-81] from the redox active phospholipids were electroactive and could be titrated by potassium hexachloroiridate (III). On the basis of these results, it is expected that redox active liposomes produced using these methods, should provide a much needed model system that will enable detail studies of membrane bound electrochemical reactions.

3.4. Experimental section

3.4.1. Chemicals

1,2-distearoyl-*sn*-glycero-3-phosphocholine (DSPC, 20 mg/mL in chloroform and powder form), 1,2-dioctadecanoyl-*sn*-glycero-3-phospho-(1'-*rac*-glycerol) (sodium salt) (DSPG, 25 mg/mL in chloroform) and 1,2-dibutyryl-*sn*-glycero-3-phosphocholine (04:0 PC) were purchased from Avanti Polar Lipids Inc. Ferroceneacetic acid (98 %), ferrocenemethanol (FcMeOH, 97 %), Trizma® acetate (reagent grade), borane dimethyl sulphide complex solution (BH_3, 2.0 M in toluene), potassium hexachloroiridate (III) (K_3IrCl_6) and phospholipase D (PLD, type II, $\geq$ 60 U/mg protein, E.C. 3.1.4.4 from

Arachis hypogaea (peanut)) were purchased from Sigma Aldrich. Ammonium chloride (NH_4Cl, ACS 99 %), potassium chloride (KCl, ACS 99 %), magnesium sulphate ($MgSO_4$ anhydrous, ACS 99 %) and sucrose crystal (ACS) were all purchased from Anachemia. D(+)-glucose (anhydrous, biological grade) was purchased from Fisher Scientific and tetraethylammonium tetrafluoroborate (TEA-BF_4, 99 %) was purchased from Alfa Aesar. Finally, all commercially available solvents were reagent grade and used without further purification or dried according to standard procedures.

3.4.2. Synthesis of the ferrocene-ethanol

To a solution of ferroceneacetic acid (500 mg, 2.09 mmoles) in anhydrous THF (6 mL), stirred in an ice bath, BH_3 (2.0 M toluene, 2.10 mL) was added drop by drop over 15 minutes. The reaction mixture was left under reflux overnight. The excess BH_3 was neutralized using a 1 M NH_4Cl aqueous solution. The organic phase was washed with water and NaCl brine, dried over $MgSO_4$ and evaporated in vacuo. The residue was purified by recrystallisation in hexane to give **2** (97 %) as an orange solid.

3.4.3. Synthesis of the redox phospholipids

The synthesis of the redox phospholipids is a modification of our previous protocol[78] and was inspired by the work of Wang *et. al.*[65] and Dong and Su-jia[25]. To a solution of 1,2-distearoyl-*sn*-glycero-3-phosphocholine (**3**, 47.41 mg, 20mM) in ethyl ether (3 mL), ferrocene-ethanol (**2**, 4.60 mg, 6.67 mM) was added. To this mixture,

1000 units of PLD freshly activated in 1 mL buffer solution 0.4 M Trizma acetate at pH 6.0 was added. The mixture was heated at 37 °C for at least 96 hours under constant and vigorous stiring. The excess ferrocene-ethanol (FcEtOH) was extracted with iced ethyl ether and the aqueous phase was separated and extracted with chloroform. The organic phase was evaporated in vacuo to give a mixture of phospholipid/redox phospholipid (**3/5**). The same protocol was repeated using 1,2-dibutyryl-*sn*-glycero-3-phosphocholine (**4**, 23.84 mg, 20mM) in ethyl ether (3 mL) in order to obtained the mixture **4/6**.

3.4.4. Product characterisation

Samples were characterised by solid state 31-phosphorus nuclear magnetic resonance (^{31}P NMR), infrared (IR) and mass spectrometry (MS). Solid state ^{31}P NMR experiments were carried out at 298 K on a Varian Inova 600 MHz spectrometer equipped with a double resonance probe operating at 242.86 MHz for ^{31}P. The spectra were recorded at the magic angle (54.7°) without and with sample rotation at 5 kHz. A recycle delay of 3 s longer than T1 was imposed to insure that the peak integrations were quantitative.[82-83] The IR analyses were carried out on a Nicolet 6700 FT-IR (Thermo Scientific). The acquisition was done using OMNIC 8.0 software with 64 scans, a resolution of 8 and a baseline correction for CO_2. Finally, the MS analyses were realised by dissolving the samples in methanol and directly injecting them into the ioniser (Waters Micromass ZQ, positive electrospray ionization (ESI)).

3.4.5. Liposome formation protocols

3.4.5.1. Control liposomes

First, an emulsion was prepared by combining 1,2-distearoyl-*sn*-glycero-3-phosphocholine dissolved in chloroform (**3**, 3 μmoles), 1,2-dioctadecanoyl-*sn*-glycero-3-phospho-(1'-*rac*-glycerol) dissolved in chloroform (1 μmole), 1 mL of 215 mM sucrose solution and 1 mL of chloroform. The mixture was vortexed for 45 seconds. A second emulsion was prepared by combining once more 1,2-distearoyl-*sn*-glycero-3-phosphocholine dissolved in chloroform (**3**, 3 μmoles), 1,2-dioctadecanoyl-*sn*-glycero-3-phospho-(1'-*rac*-glycerol) dissolved in chloroform (1 μmole), 2.5 mL of a 215 mM sucrose solution and 0.5 mL of diethyl ether. Sucrose must be present in the internal void of the liposome to promote liposome sedimentation, which is required in later electrochemical measurements. The mixture was vortexed for 15 seconds. The two emulsions were then combined and vortexed for 10 seconds. The mixture was transferred into a round flask and heated at 65-67 °C for one hour and half under argon flux. Subsequently, the entire mixture was transferred and centrifuged for 30 minutes at 1500 rpm. Control liposomes were recuperated and stored in 215 mM sucrose solution.

3.4.5.2. Redox liposomes

A protocol similar to that presented for the control liposomes was used to produce redox liposomes. Specifically, the pure DSPC fraction was replaced by a mixture of DSPC/redox DSPC.

3.4.6. Electrochemical measurements

A scanning electrochemical microscope (HEKA Elektronik) mounted on an inverted microscope (Nikon Eclipse TE2000-U) was used to perform the different electrochemical measurements as well as to monitor the tip to substrate and tip to liposome distance. The complete setup was detailed previously.[84]

The measurements were performed in a Teflon electrochemical cell with a conventional three-electrode configuration. All electrochemical measurements were performed using a 25 μm diameter platinum microelectrode with an RG = 4. The RG value is the ratio of the radii of the outer glass insulator and metal wire of the microelectrode.[47] A platinum wire served as the counter electrode while a silver wire pre-coated with silver chloride was used as the reference electrode. The bottom of the cell was a microscope glass slide.

3.4.6.1. Cyclic voltammetry measurements

Ferrocene-ethanol, redox DSPC and potassium hexachloroiridate (III) were studied by cyclic voltammetry. The following four electrolytic solutions were freshly prepared and studied: (i) 1 mM ferrocene-ethanol in an aqueous solution 0.1 M KCl, (ii) 1 mM ferrocene-ethanol in acetonitrile 0.1 M TEA-BF_4, (iii) 1 mM redox DSPC (DSP-OCH_2CH_2Fc) in acetonitrile 0.1 M TEA-BF_4 and (iv) 1 mM potassium hexachloroiridate (III) in an aqueous solution 50 mM glucose/0.1 M KCl. The scan rate was varied between 100 mV/s and 10 mV/s and all electrolytic solutions were degassed with argon for

15 minutes before being studied. All aqueous solutions were prepared using Milli-Q water (Millipore, Biocel, 18.2 MΩ). Finally, the cyclic voltammograms obtained in organic solution were all referenced to Ag/AgCl and normalized versus ferrocene-ethanol potential in aqueous solution.

3.4.6.2. Tip positioning and scanning electrochemical microscopy measurements

The microelectrode was prepositioned in air in the center of the optical axis of the underlying objectives of the inverted microscope. Once submerged in 1 mM potassium hexachloroiridate (III) in an aqueous solution 0.1 M KCl, a negative approach curve was recorded over the glass substrate to evaluate the effective zero tip to substrate distance. The microelectrode was biased at 850 mV and moved towards the surface with a scan rate of 1 μm/s. The measured approach curve was consistent with pure negative feedback behaviour and was fitted with the analytical approximations.[47] The tip was then positioned 250 μm above its zero distance, prior to the injection of a liposome aliquot, which sedimented at the bottom of the cell. Using the x-y motorized microscope stage, the electrochemical cell was positioned until a suitable liposome was found and positioned at the center of the optical axis of the objective of the microscope. Using the microscope optics it was possible to continuously monitor the studied liposomes and observe bursting. After targeting an individual immobilized liposome, the liposome size was measured and the tip was manually brought down to a tip to liposome distance of 20 μm (exactly). The microelectrode was once again biased for a few seconds to monitor

the current and returned to standby mode before starting the chronoamperometry measurement.

An oxidative potential between 850 mV and 875 mV was applied at the tip for one hour and the current versus time signal was monitored throughout the measurement. The measured currents were normalized by the background response of the control liposome recorded at an identical tip to liposome distance.

3.5 Results and discussion

3.5.1. Redox phospholipid synthesis

Herein, we report the design of stable redox active liposomes that covalently bound an organometallic electroactive pendent. The redox active molecules were covalently bound to the phospholipid headgroup through a PLD-catalyzed transphosphatidylation reaction between a choline bearing phospholipid and a primary alcohol containing a ferrocene derivative. Previously, the synthesis of a redox DSPC bearing a ferrocenemethanol function (DSP-OCH_2Fc) presented stability issues that prevented the successful formation of redox liposomes.[78] The DSP-OCH_2Fc was unstable because the redox headgroup (-OCH_2Fc) underwent hydrolysis and/or S_N2 reactions, which favoured the formation of phosphatidic acid instead of the DSP-OCH_2Fc. To overcome this limitation, it was hypothesized that increasing the alkyl chain length between the phosphorus and the ferrocene group should further stabilise the redox active phospholipid reaction product.

To this end, ferrocene-ethanol, **2**, was synthesised through the reduction of the parent carboxylic acid compound, **1** using BH_3 or $LiAlH_4$ as the reducing agent (Figure 3.1). A yield of 97 % was obtained after purification and product **2** was characterised by mass spectrometry (ESI-MS) and ^1H NMR. The *m/z* 230 (100%) and 214 (65%) indicate that ferrocene-ethanol has been synthesised and the iron isotopic ratio was identify as *m/z* 910 ($\leq$ 5%). The ^1H NMR analysis indicated no other peaks than those assigned to **2**. ^1H NMR (600 MHz, $(CD_3)_2SO$) δ: 2.43 (t, J = 7.14 Hz and J = 7.31 Hz, 2H, $C\underline{H_2}CH_2O$), 3.51 (q, J = 7.06 Hz, 2H, $CH_2C\underline{H_2}O$), 4.02 (m, 2H, H_{Fc}), 4.09 (s, 7H, H_{Fc}), 4.50 (t, J = 5.25 Hz and J = 5.25 Hz, 1H, OH).

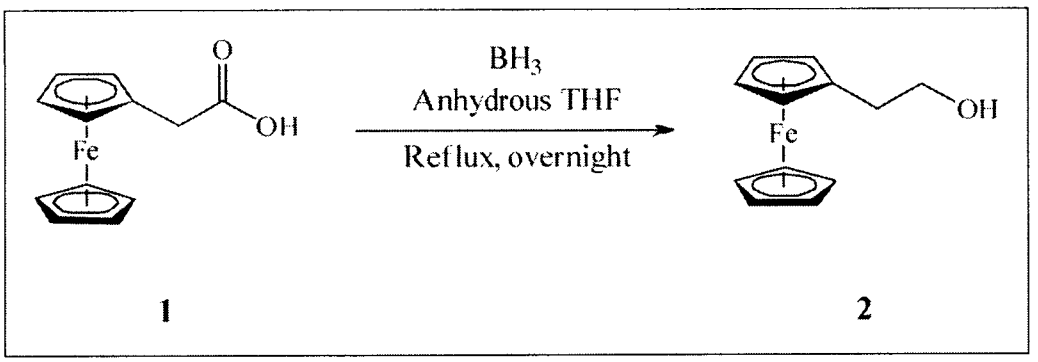

Figure 3.1. Schematic representation of the synthesis of ferrocene-ethanol, **2**, from a reduction of ferroceneacetic acid, **1**, by BH_3.

The PLD-catalyzed transphosphatidylation reaction between DSPC, **3**, and ferrocene-ethanol, **2**, was then performed (Figure 3.2) using a modified protocol from previous work.[78] These modifications included PLD activation by dissolving 1000 units in 1 mL buffer solution Trizma acetate 0.4 M at pH 6.0. Moreover, DSPC was used directly in powder and a purification step was introduced to separate the phospholipids (non-modified and redox modified).

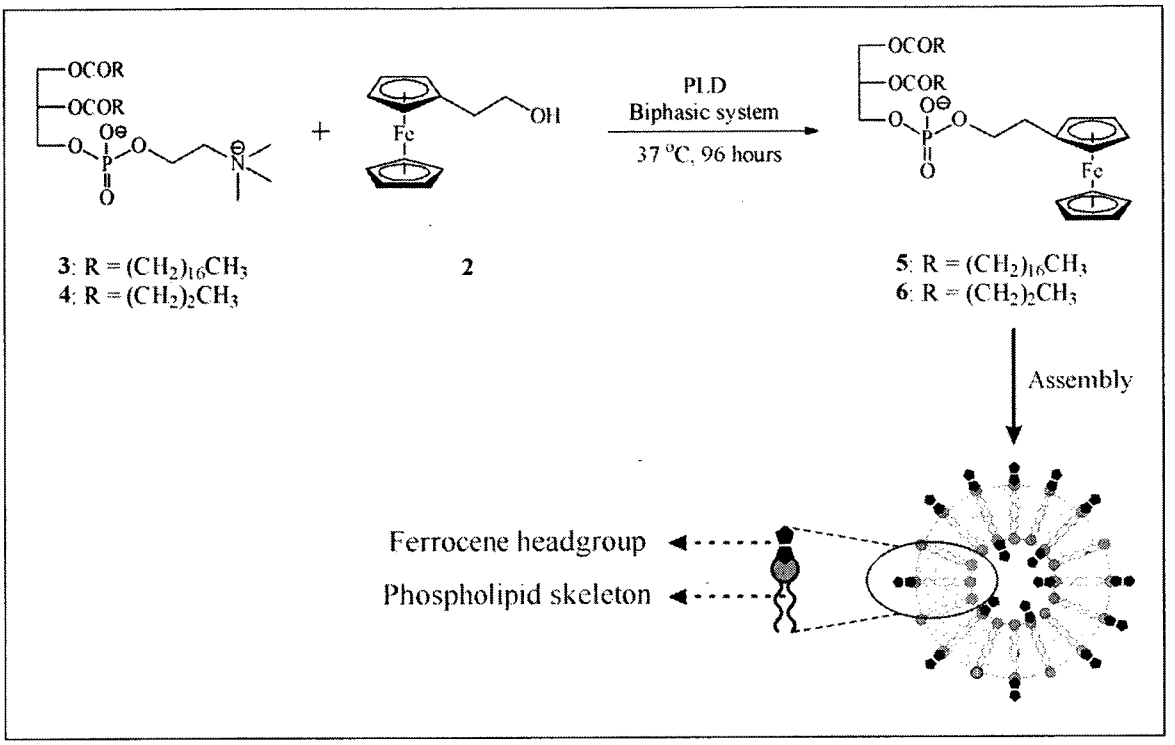

Figure 3.2. Schematic representation of the synthesis of a redox phospholipids, **5** and **6**, through a PLD-catalyzed transphosphatidylation reaction between ferrocene-ethanol, **2**, and a choline bearing phospholipid such as 1,2-distearoyl-*sn*-glycero-3-phosphocholine, **3**, and 1,2-dibutyryl-*sn*-glycero-3-phosphocholine, **4**.

3.5.2. Redox phospholipid characterisation

Purification of the reaction mixture was limited to the separation of phospholipids, **3** and **5**, from the PLD enzyme and the excess of alcohol. Since DSPC is needed again during the liposome formation through the double emulsion technique, it was not separated from the redox phospholipid. Redox DSPC characterisation and DSPC/DSP-OCH_2CH_2Fc ratio quantification was achieved through solid state phosphorus NMR (Figure 3.3). The study of phospholipids by solid-state ^{31}P NMR is a well established technique.[41-42, 85] Spectral analysis is greatly simplified with respect to

^{1}H NMR since each phospholipid contains a single phosphorus atom per headgroup. In addition, speciation should be possible because the headgroup modification with ferrocene-ethanol, a well known electron donor, is likely to alter the shielding of the ^{31}P nucleus and thus its chemical shift.

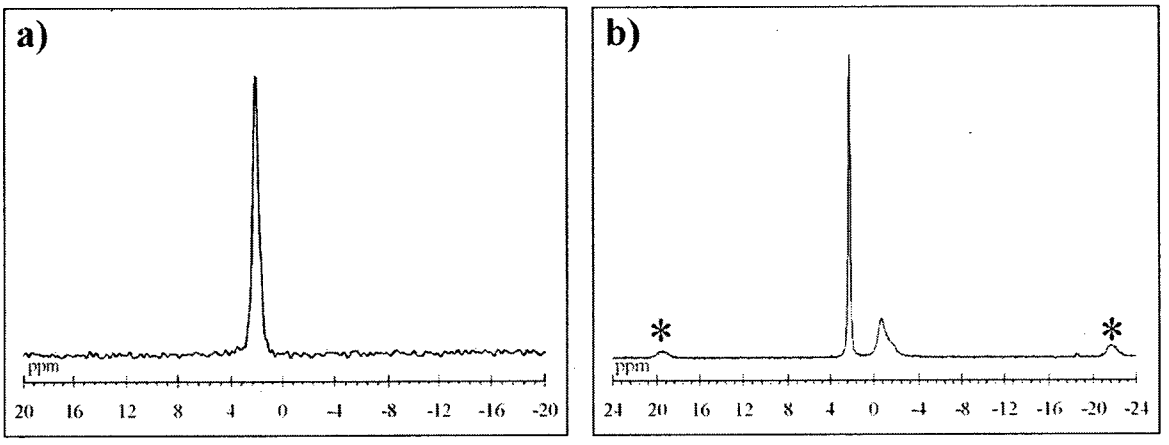

Figure 3.3. ^{31}P NMR solid state spectra of a DSPC/DSP-OCH_2CH_2Fc 1:0.6 mixture. a) Static spectra and b) high resolution spectra with a magic angle spinning at 5 kHz. Rotating sidebands are identified by *.

It is important to mention that the samples studied by solid state phosphorus NMR were hydrated, which implies that the phospholipids can adopt different morphologies such as multilamellar vesicles (MLVs), small unilamellar vesicles (SUVs) or micelles. In static spectra, objects which slowly reorient themselves in the magnetic field, such as MLVs, will display broad ^{31}P spectra that reflect the chemical shift anisotropy interaction.[41-42, 85] In contrast, small objects that reorient rapidly, such as SUVs or micelles, will display a spectra composed of sharp peaks akin to those obtained in liquid state NMR. The effect of the ^{31}P chemical shift anisotropy can however be averaged out by fast spinning of the sample at angle of 54.7° with respect to the magnetic field (Magic-Angle Spinning or MAS). The resulting spectra were composed of a set of spinning

sidebands with relative intensities that reflect the chemical shift interaction tensor.[86] If the spinning speed is fast enough, the spinning sidebands will disappear and only the center sideband will remain.

Figure 3.3a displays the static and the 5 kHz MAS spectra. Only one narrow peak at 2.18 ppm is observed on the static spectrum (Figure 3a). Its unusual chemical shift for phospholipids[41] and shape (narrow) indicates that it is likely to be the redox DSCP, DSP-OCH_2CH_2Fc.

The MAS spectrum (Figure 3.3b) is composed of the same sharp peak at 2.18 ppm and a spinning sideband manifold centered at -0.77 ppm. The spinning sideband spectrum and chemical shift are typical of MLVs of phospholipids, it is thus reasonable to assign it to unmodified DSPC. We believe that the broad DSPC spectrum is within the noise in the static spectrum but would be detected with a longer acquisition time. It thus appears that DSP-OCH_2CH_2Fc forms small isotropic objects such as micelles or SUVs which reorient fast in the magnetic field whereas unmodified DSPC forms MLVs.

31-Phosphorus nuclear magnetic resonance analysis demonstrated that two different phospholipids, DSPC and DSP-OCH_2CH_2Fc, are present in the purified mixture. The covalent nature of the ferrocene unit attachment to the phospholipid headgroup is supported by infrared analyses. In the 3000 cm^{-1} region, DSPC has a ν(C–H) band at 3376 cm^{-1}, which is consistent with the literature.[87] In the same region, DSP-OCH_2CH_2Fc has an additional contribution assigned to the ν(C–H) at 3231 cm^{-1} band of the ferrocene unit. Also, the two low intensity ferrocene ring modes,[87] not present in the DSPC spectra, are observed in the DSP-OCH_2CH_2Fc spectra at 605 cm^{-1} and 1400 cm^{-1}. Finally and

most importantly, the redox DSPC spectra of ν(P=O) at 1236 cm^{-1} is 20 cm^{-1} downshifted as compared to the DSPC phosphorus band, which is at 1254 cm^{-1}. This shift is significant and indicative of a phospholipid headgroup modification. It is expected that the zwitterionic character of the choline function present in the DSPC allows for a six member like reorganisation that will not occur once the choline has been replaced by the ferrocene unit and this results in a shift of the expected P=O mode.

The DSPC/DSP-OCH_2CH_2Fc mixture was also characterised by mass spectrometry analyses. On the MS spectrum of redox DSPC **5** ions at *m/z* $[M+H^+]$ 912 and at *m/z* $[M+Na^+]$ 934 was observed. A comparison with the expected *m/z* exhibits a four unit difference which has been attributed to the loss of 4 protons. This difference cannot fully be explained at present, but it is thought to be related to the post transphosphatidylation activity of the PLD or it can be a result of a gas phase reaction during the ionisation process of the MS. In order to investigate the possible location and nature of the modifications responsible for this change in the expected mass, several control synthesis were performed and characterised by MS (Table 3.1)

Table 3.1. Summary of the protocol conditions, analyses and mass spectrometry results for PLD-catalyzed transphosphatidylation control reactions.

	Starting reagents			Expected product	Analyses	MS results (*m/z*)	
	Lipid	Primary alcohol	Enzyme			$[M+H^+]$	$[M+Na^+]$
a	DSPC	FcEtOH	Yes	5	^{31}PNMR/ MS/IR	912	934
b	4	FcEtOH	Yes	6	MS	520	542
c	4	(S)-prolinol	Yes	9	MS	395	nd
d	DSPC	None	None	DSPC	MS/IR	791	813
e	None	FcEtOH	None	FcEtOH	MS/IR	230	253

Modification to the alkyl chain of the redox phospholipid were first suspected based on the observed MS fragmentation pattern *m/z* [M+H$^+$] 524 and *m/z* [M+Na$^+$] 546 of redox phospholipid **5** (Trial a). The fragments respectively correspond to the ionisation of the lipid between carbon 3 and 4 of the phospholipid alkyl tails which is also the mass of redox phospholipid **6**. Following the synthesis of redox phospholipid **6** through the PLD-catalyzed transphosphatidylation reaction between phospholipid **4** and ferrocene-ethanol, the observed MS spectrum presented ions at *m/z* [M+H$^+$] 520 and at *m/z* [M+Na$^+$] 542 (Trial b). The discrepancy in expected *m/z* is still observed and is not induced by the reaction environment because the expected mass of phospholipid **3** is obtained when subjected to reaction conditions in absence of alcohol or enzyme (Trial d). These results therefore suggest that the modification to product **4** occurs possibly between the phosphorus and the ferrocene group. Of course, if this discrepancy occurs during a gas phase reaction during ionisation, the modification might as well be on the terminal carbons of redox phospholipid **4**. Modification to the pendent unit between the phospholipid headgroup and ferrocene was investigated next (Trial c). When the PLD-catalyzed transphosphatidylation reaction was repeated by replacing the FcEtOH by the (S)-prolinol (Figure 3.4), the expected and observed *m/z* fragments were the same (*m/z* [M+H$^+$] 395). This agrees with the literature[65] and also suggests that the discrepancy in observed mass is dependent on the presence of the ferrocene unit. It was also conclude that the modification occurs either following the transphosphatidylation reaction since in presence of all reagents, except DSPC, no mass discrepancy in the observed *m/z* of ferrocene-ethanol is observed. Again, another possibility is an uncontrollable gas phase reaction in the MS.

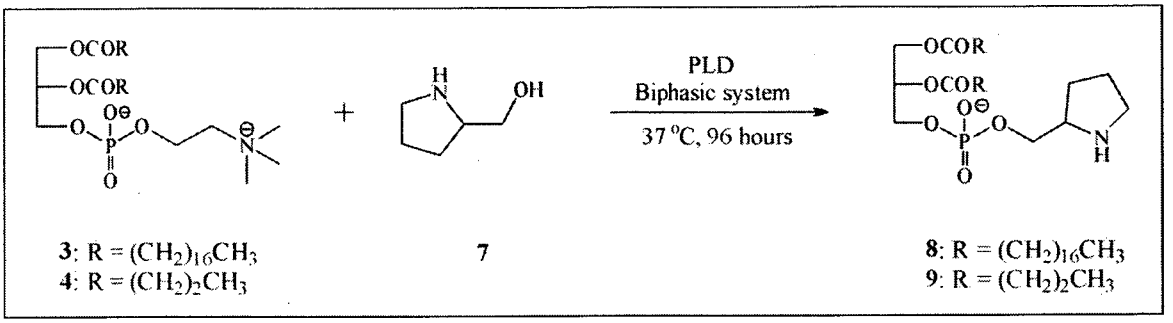

Figure 3.4. Schematic representation of the synthesis of modified headgroup phospholipid, **8** and **9**, through a PLD-catalyzed transphosphatidylation reaction between (S)-(+)-2-pyrrolidinemethanol ((S)-prolinol, **7**) and a choline bearing phospholipid such as 1,2-distearoyl-*sn*-glycero-3-phosphocholine, **3**, and 1,2-dibutyryl-*sn*-glycero-3-phosphocholine, **4**.

Regardless of the discrepancy in expected *m/z*, DSP-OCH_2CH_2Fc provides a stable electroactive behavior as presented on the cyclic voltammogram in Figure 3.5. As expected, pendent substitutions of organometallic complexes lead to shifts in the measured standard potential.[88] Attachment of the ferrocene-ethanol to DSPC results in a modest anodic shift of standard potential from 205 mV for ferrocene-ethanol to 274 mV for DSP-OCH_2CH_2Fc in acetonitrile. Also, the increased molecular weight of the DSP-OCH_2CH_2Fc, as compared to ferrocene-ethanol, reduces the observed anodic steady state current measured at microelectrodes during cyclic voltammetry for a given concentration. As a result, a diffusion coefficient of 3.2×10^{-5} cm^2/s has been determined for ferrocene-ethanol in acetonitrile and a value of 1.9×10^{-6} cm^2/s for DSP-OCH_2CH_2Fc under the same conditions.

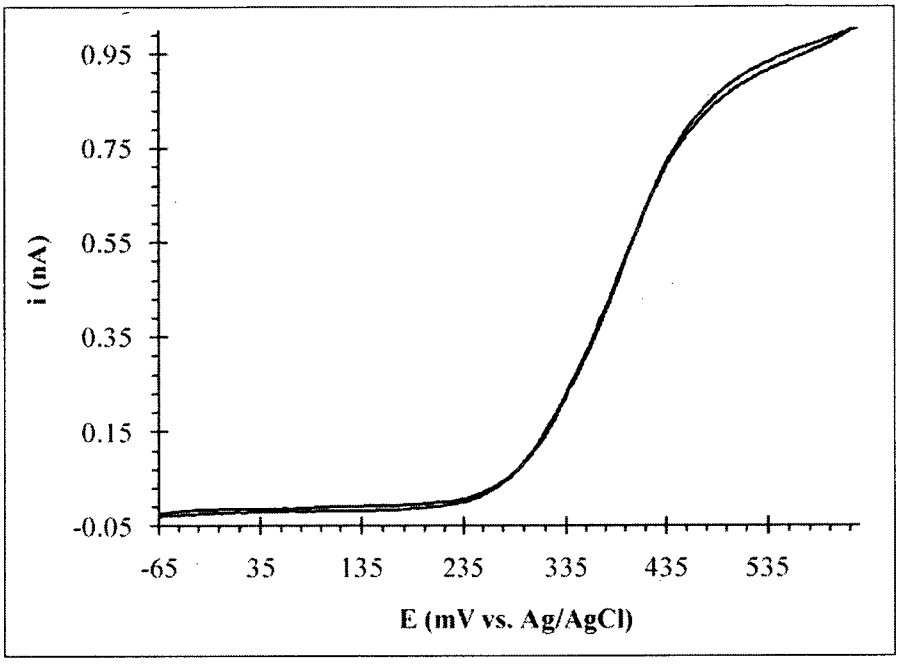

Figure 3.5. Cyclic voltammogram (CV) of 1 mM redox phospholipid (DSP-OCH_2CH_2Fc, **4**) solution in 0.1 M tetrabutylammonium tetrafluoroborate solution in acetonitrile. CVs were recorded at a 25 μm diameter microelectrode at a 10 mV/s scan rate.

3.5.3. Electrochemical study of the redox liposomes

Having synthesized and characterized a stable electroactive phospholipid, the formation of a redox active liposome was achieved using a double emulsion technique from a 1,2-dioctadecanoyl-*sn*-glycero-3-phospho-(1'-*rac*-glycerol) (DSPG), 1,2-distearoyl-*sn*-glycero-3-phosphocholine (DSPC) and 1,2-distearoyl-*sn*-glycero-3-phospho-1-ethylferrocene (DSP-OCH_2CH_2Fc) mixture. Given that the ^{31}P NMR established 1:0.6 DSPC/ DSP-OCH_2CH_2Fc ratio, it is estimated that the surface concentration of reduced ferrocene units exposed to the external solution on a single redox liposome is at most 15%. Given their probable partition in both leaflets of the

membranes, the redox units are considered quite dilute, which suggests that neighbouring effects following oxidation are negligible.

To promote immobilisation of the liposomes to the bottom of the electrochemical cell during chronoamperometry, the double emulsion liposome protocol was modified to include sucrose (ρ=1.59 g/cm^3) in the internal void of the liposomes. During chronoamperometric measurements glucose (ρ=1.54 g/cm^3) would be added to the external electrolyte, which would lead to liposome sedimentation based on the differential density of the respective sugars. Also, the double emulsion protocol was adjusted to prevent bursting of the liposomes through careful osmolality control of the internal and external solution. A measured osmolality of 245 mOsm was used throughout and provided stable liposomes that could be electrochemically studied for several hours. Figure 3.6a presents the optical micrographs of the large stable liposome (100-250 μm diameter) routinely produced by the modified double emulsion method. Such large dimension liposomes enabled single liposome monitoring when using conventional microelectrode tip (25 μm diameter Pt) (Figure 3.6a).

To establish the redox activity of the resulting liposomes, the reduced ferrocene headgroups were oxidized using a sacrificial redox couple, $[IrCl_6]^{3-/2-}$ [69, 89] Thermodynamically, the electron transfer between ferrocene moieties of the liposome and K_3IrCl_6 is favourable.[69] In the context of a SECM experiment, $[IrCl_6]^{3-}$ is oxidized at the microelectrode positioned directly above the liposome (Figure 3.6b). $[IrCl_6]^{2-}$ diffuses to the surface of the liposome where it is spontaneously reduced to $[IrCl_6]^{3-}$ by the ferrocene units on the liposome. $[IrCl_6]^{3-}$ diffuses back to the tip to produce an enhancement in oxidized current measured at the microelectrode (Figure 3.6b). This

enhanced material flux only occurs for short microelectrode to liposome distances characteristic of the feedback mode of SECM.

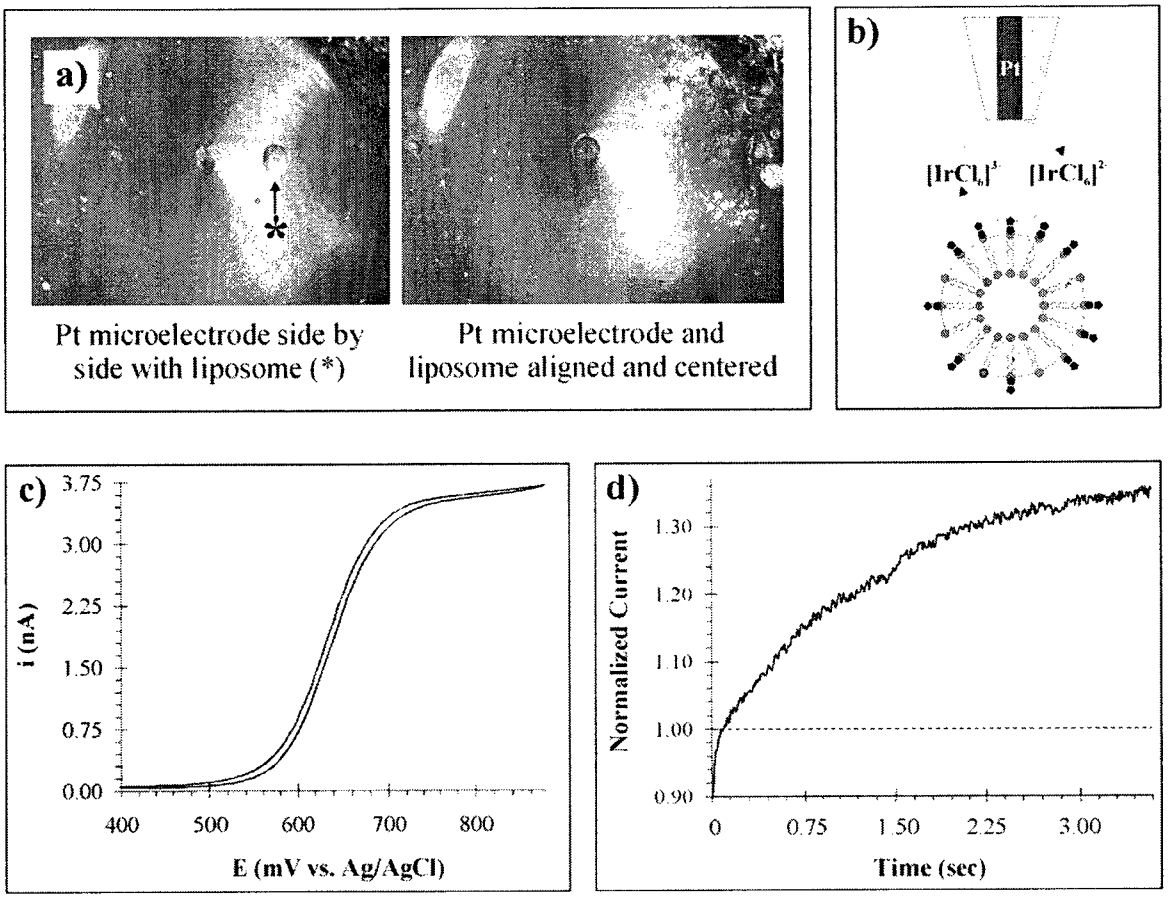

Figure 3.6. a) Optical images presenting the microelectrode tip side by side with the liposome to be studied (left) and aligned and centered with one another (right). b) Schematic representation of the oxidation of $[IrCl_6]^{3-}$ at the tip of a 25 µm microelectrode which will diffuse to the redox phospholipid surface where it oxidizes the ferrocene headgroups. c) Cyclic voltammogram of a 1 mM potassium hexacholoroiridate (III) (K_3IrCl_6) solution in a 50 mM glucose and 0.1 M KCl aqueous solution. CV was recorded at a 25 µm diameter microelectrode at a 10 mV/s scan rate. d) Chronoamperometry measurements over a bare liposome (---) and a redox liposome (—). The current vs. time curves were recorded at a 25 µm diameter microelectrode in a 1 mM potassium hexachloroiridate (III) (K_3IrCl_6) solution in a 50 mM glucose and 0.1 M KCl aqueous solution and the tip to distance was 20 µm.

The chronoamperometric measurements described above were carried out on control liposomes, devoid of DSP-OCH_2CH_2Fc, and redox liposomes. Based on the $[IrCl_6]^{3-}$ cyclic voltammetry (Figure 3.6c), an applied mass transport limited bias ranging from 850 mV and 875 mV was consistently used during the electrochemical study of both control and redox liposome experiments. The microelectrode to liposome distance at which the current time profile was measured was also always the same. The response of the control liposome provided a background response that was used to normalise the response observed at the redox liposomes. Figure 3.6d presents the normalised current response of the control and redox liposomes. The response measured at the control liposome is unaffected by the presence of the oxidized species, $[IrCl_6]^{2-}$, generated at the nearby microelectrode. In contrast, the surface of the redox liposome is electroactive and reacts with the $[IrCl_6]^{2-}$ species that diffuses in the cleft to the microelectrode surface, which regenerates $[IrCl_6]^{3-}$species. This regeneration reaction occurs and produces an additional flux of $[IrCl_6]^{3-}$ species, within a few microseconds, that leads to an increase of the current measured at the microelectrode. It is noteworthy that the chronoamperometric curve seems to stabilise over time and reach a stable turnover rate. At very long times, the current stabilisation cannot be maintained with the depletion of the surface available ferrocene units and a decrease in current returning to baseline is expected. This is however rarely observed, because the liposomes tend to burst before being completely depleted. During the measurements, a lamp was used for optical microscopy imaging. This caused evaporation of the electrolyte solution and thus, the osmolality of the latter solution was modified. It no longer equalled the osmolality of the sucrose solution encapsulated within the liposome internal void, which lead to the liposome degradation.

Finally, it was possible to determine the number of molecules of ferrocene that were most likely probed during the chronoamperometry measurement. Approximately, $3.9x10^{-18}$ moles of ferrocene units was calculated using the measured current, which is consistent with the number of ferrocene units estimated during the liposome assembly, if one consider that not all of the ferrocene units were probe and that at the best only 50 % of what was added is exposed to the electrolyte solution.

3.6. Conclusion

In this study, a stable organometallic modified phospholipid through the covalent attachment of ferrocene-ethanol to DSPC using an enzymatic transphosphatidylation reaction was synthesized and characterised for the first time. It was also demonstrated that it is possible to functionalise the surface of a liposome with this organometallic phospholipid and that the electrochemical activity of the liposome with time can be probed using potassium hexachloroiridate (III) as a sacrificial redox mediator. The ability to use phospholipase D to attach different organometallic pendents to phospholipid headgroups and success in forming stable redox liposomes is important in the development of simple biomimetic models that will enable to study membrane bound electrochemical reaction. Also, from a drug target design, it could also be interesting to vary the nature and standard potential of the pendent units to monitor the effect of the apparent electrochemical activity of the liposome on target or delivery strategy outcome.

Chapter 4. The detrimental effects of focused ion beam machining on the electrochemical response of silicon oxide insulated platinum microring sensors

4.1. Contribution of authors and context

This third manuscript will soon be submitted to the *Chemical Science*, a new journal of the Royal Society of Chemistry (RSC publications). All experiments, and the manuscript draft, was performed and prepared by Debby Correia Ledo under the supervision of Dr. Janine Mauzeroll, Université du Québec à Montréal. The numerical simulations were performed, by or with the help, of Dr. Renaud Cornut, Université du Québec à Montréal, who specialises into theoretical chemistry. Dr. Cornut is also a contributing author to the manuscript.

The third manuscript presents the results obtained for the final work of this thesis. The long term objective of this work is to include transmembrane proteins in the liposome bilayer. Therefore, transport studies through these proteins (assisted-diffusion) require controlled injection microelectrode sensors. As such, the design of a similar sensor was undertaken in this thesis in order to pave the way for future studies on our group. This manuscript presents the fabrication steps and characterisation of a platinum ring microelectrode. The design of the probe is novel itself. Compared to what is already demonstrated in the literature, our probe is not made from an alloy but rather from pure

platinum. Also, silicon oxide, an unusual material for insulator, was used instead of the typical electrophoretic paints and non-conductive polymers. Numerical simulations were used to analyze the effect of the ring exposure procedure on the insulator layer. By modifying our existing protocol to reduce silicon oxide porosity following focused ion beam treatment, it should be possible to obtain pure platinum ring micropipette SECM probes that could be used in injection experiments on liposomes.

4.2. Abstract

The fabrication and electrochemical characterisation of a platinum ring microelectrode is described. To study transport and injection dynamics by scanning electrochemical microscopy, a simplified five step protocol, consisting of capillary pulling, metal coating, electrical connection, insulator coating and ring milling, is put forth. Briefly, the microring electrodes were prepared by insulating pure platinum-coated quartz micropipets with silicon oxide and exposing the ring portion by focused ion beam milling. The microelectrodes were characterised by scanning electron microscopy and cyclic voltammetry. Scanning electron microscopy images shows that the proposed protocol leads to the fabrication of reproducible 10 μm diameter average ring microelectrodes. However, cyclic voltammetry results shows that the focused ion beam milling of the microelectrode tip weakened the insulating properties of the silicon oxide. As discussed on the basis of numerical results, increased porosity of the silicon oxide layer lead to an enhanced contribution from lateral diffusion of the electroactive species to the measured current, which limits the use of the microring probe as a local sensor.

4.3. Introduction

Innovation in probe design has been at the heart of scanning electrochemical microscopy (SECM) development. The most commonly used SECM probe is the solid disk-shape ultramicroelectrode (UME).[47, 52] Besides microdisks, ring, hemispherical, spherical and finite conical (or etched) microelectrodes are also regularly used.[50, 52] Their dimensions are small on at least one dimension and they quickly achieve mass transfer limited currents. Thus, UMEs are versatile electrodes that have unique electrochemical behavior.[52]

The ring geometry is of interest to our ongoing SECM studies that relate transmembrane transport mechanism studies and electrochemical response monitoring during solution dispensing experiments on different substrates, such as living cells. Recently, a biomimetic model, an organometallic redox liposome, has been designed to study surface bound electroactive reactions at membranes.[78, 90] The study of such liposomes with a ring microelectrode would allow extraction of electrochemical and kinetic information on surface bound reactions. The micropipet sensor would be able to accurately titrate surface bound units based on the controlled injection of a diffusing electroactive solution.[91-92] Therefore, microring electrodes are ideal SECM probes for biological molecular transport studies and they also allow the SECM technique to be combined with other techniques, such as near field scanning optical microscopy (NSOM) or atomic force microscopy (AFM).[52] Finally, the signal-to-background and signal-to-noise ratios are also improved for different transient voltammetry forms.[91-95]

Various studies have reported the fabrication and electrochemical characterisation of gold ring microelectrodes as suitable SECM probes.[96-98] Gold metal is often used for designing microrings because it is mechanically stable and has a reasonable adhesion to curved glass surfaces that do not require chromium or aluminum adhesion underlayers.[96] In addition, some studies reported the fabrication and the use of platinum microring electrodes. These microelectrodes are often prepared from a platinum/titanum (Pt/Ti) alloy,[99] that promotes adhesion to both glass and insulating layers. Here, we report the fabrication of a ring microelectrode made of pure platinum. The use of Pt/Ti alloy was avoided because it may influence the electrochemical response and reactivity of the electrode surface.

As for the microelectrode insulating sheath, electrophoretic paints[96, 100-105] or non-conductive polymers[99, 106-109] were mostly used. Herein, the insulation of the pure platinum ring microelectrode with a novel insulating material, silicon oxide, is reported. To improve on the recurring disadvantages of polymer based insulators, such as aging, controlled composition, mechanical stability and chemical stability, the use of a silicon oxide layer was investigated.

Although the optical microscopy studies suggested ideal microring geometry, in depth, electrochemical experiments and numerical simulations lead us to conclude that focused ion beam milling of the ring microelectrode increases the silicon oxide film porosity and limits the use of the resulting probe as a local electrochemical sensor.

4.4 Theory

4.4.1 Model presentation[110-111]

The SECM diffusion problem at a ring microelectrode is simulated using cylindrical coordinates (Figure 4.1). The coordinate axes, R and Z, are respectively parallel and normal to the surface of the ring microelectrode and the origin is set at the center of the internal void. Characteristic dimensions of the probe, $r_{g,int}$, a, b and r_g, are definied as the radius of the internal void, the inner radius, the outer radius and the total radius of the microelectrode respectively. Numerical simulations of the current and concentration profiles of a ring microelectrode have been presented previously.[92] Here, the previously used model is modified in order to simulate the current versus potential profile for a ring micropipet where the insulating sheath have been modified so it no longer isolates well the micropipet. The affect of a non-perfectly insulating layer on the observed current is specifically studied by numerical simulation.

During SECM measurements, the microelectrode is immersed in an electrolyte solution containing only one redox active mediator. Assuming that the only redox mediator is the oxidized chemical species, O, the reduced species, R, would be generated at the microelectrode tip during the mass transfer limited reduction reaction when the probe is biased.

$$O + ne^- \longrightarrow R \qquad \text{(Rx. 4.1)}$$

where n is the number of electrons exchanged during the reaction at the microelectrode tip.

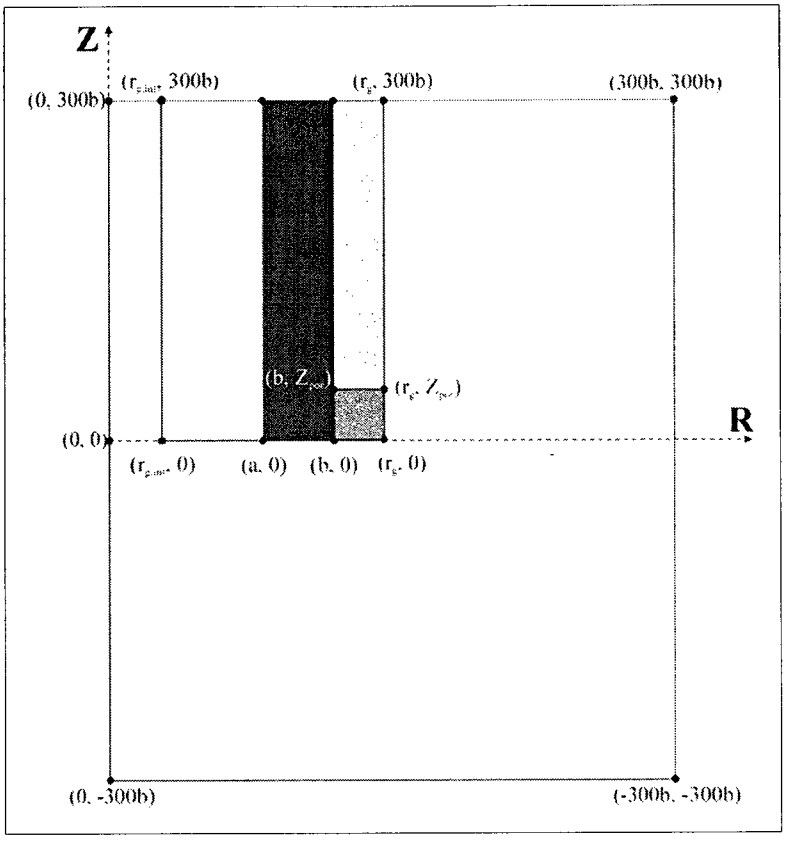

Figure 4.1. Geometry of a SECM ring microelectrode in cylindrical coordinates.

Generally, for such type of measurement, convection and migration processes are neglected. Thus, only the diffusive flux at the microelectrode tip is simulated. The diffusion or flux of oxidized species at the tip surface is known as the steady-state diffusion and is described by Fick's law:

$$0 = D_O\left[\frac{\partial^2 C_O}{\partial R^2} + \left(\frac{1}{R}\right)\left(\frac{\partial C_O}{\partial R}\right) + \frac{\partial^2 C_O}{\partial Z^2}\right] \qquad \text{(Eq. 4.1)}$$

where C_O is the local concentration of the redox active mediator and D_O is the diffusion coefficient of that same mediator and R and Z are respectively the radial and axial coordinates of the cylindrical geometry. Integration of this flux density across the conductive surface of the ring-UME leads to the steady-state limiting current, i_T:

$$i_T = nFD_O \iint_{\substack{active \\ surface}} \vec{\nabla} C_O . \vec{n} ds \qquad \text{(Eq. 4.2)}$$

where n is the number of electrons exchanged during the reaction, F is Faraday's constant, $\vec{\nabla} C_O$ is the gradient of the reacting species, $\vec{n}$ is the vector normal to surface and ds is the surface element.

Considering that the diffusion coefficient of O species, D_O, is equal to that of R species, D_R, the quasi-reversible boundary condition at the tip conductive surface can be written as following:

$$D_O \vec{\nabla} C_O \vec{n} = -k_f C_O + k_b (C_O^0 - C_O) \qquad \text{(Eq. 4.3)}$$

where k_f and k_b are respectively the forward and backward first-order heterogeneous rate constant, and C_O^0 is the oxidized species initial bulk concentration in solution.

The first-order heterogeneous rate constant, k_f and k_b, are depend on the applied potential. Butler-Volmer's expression is generally used to express that dependency.

$$k_f = k^0 exp\left[\frac{-\alpha(E - E^0)}{RT}\right] \qquad \text{(Eq. 4.4a)}$$

$$k_b = k^0 exp\left[\frac{(1-\alpha)(E - E^0)}{RT}\right] \qquad \text{(Eq. 4.4b)}$$

where E and E^0 are respectively the open circuit potential and the formal potential of the microring, k^0 is the standard rate constant, and α is the transfer coefficient.

The boundary conditions representing the internal part of microelectrode are given by :

$$\frac{\partial C_O}{\partial Z} = 0 \qquad \text{for } Z = 300b \text{ and } 0 < R < r_{g,int} \qquad \text{(Eq. 4.5a)}$$

$$\frac{\partial C_O}{\partial Z} = 0 \qquad \text{for } Z = 0 \text{ and } r_{g,int} < R < a \qquad \text{(Eq. 4.5b)}$$

$$\frac{\partial C_O}{\partial R} = 0 \qquad \text{for } 0 < Z < 300b \text{ and } R = r_{g,int} \qquad \text{(Eq. 4.5c)}$$

The boundary conditions representing the external part of the microelectrode represent two different simulating situations: (i) a porous silicon oxide insulating layer or (ii) a totally stripped insulating silicon oxide layer. For a porous silicon oxide layer, the boundary conditions are given by:

$$\frac{\partial C_O}{\partial R} = 0 \qquad \text{for } Z_{por} < Z < 300b \text{ and } R = r_g \qquad \text{(Eq. 4.6a)}$$

$$\frac{\partial C_O}{\partial R} = 0 \qquad \text{for } Z = Z_{por} \text{ and } b < R < r_g \qquad \text{(Eq. 4.6b)}$$

where Z_{por} represents the height over which silicon oxide cannot be considered as a perfect insulator. In this region, complex transport process involving the motion of species through pores variously connected could be represented by a diffusion process with apparent diffusion coefficient, $D_{O,por.}$ This leads to the following conservation of flux at solution-porous silicon oxide interface:

$$D_{O,por}\left(\frac{\partial C_O}{\partial R}\right)_{R=r_{g,-}} = D_O\left(\frac{\partial C_O}{\partial R}\right)_{R=r_{g,+}} \qquad \text{for } 0 < Z < Z_{por} \qquad \text{(Eq. 4.7a)}$$

$$D_{O,por}\left(\frac{\partial C_O}{\partial Z}\right)_{Z=0} = D_O\left(\frac{\partial C_O}{\partial Z}\right)_{Z=0} \qquad \text{for } 0 < R < r_g \qquad \text{(Eq. 4.7b)}$$

In the case where the silicon oxide layer is completely stripped from the platinum underlayer, the above equations still apply and $D_{O,por}=D_O$ must then be considered instead. This situation is first presented in the following theoretical discussion.

Finally, the bulk conditions, or simulation space limits are described as follow:

$$C_O = 1 \qquad \text{for } Z = -300b \text{ and } r_g < R < 300b \qquad \text{(Eq. 4.8a)}$$

$$C_O = 1 \qquad \text{for } -300b < Z < 300b \text{ and } R = 300b \qquad \text{(Eq. 4.8b)}$$

4.4.2 Numerical simulations

The previous equations were solved by numerical simulation using commercially available software COMSOL Multiphysics version 3.5. It solves partial differential equation systems using the finite element method. In order to have accurate evaluation of the current, some verifications were first performed. For example, it has been verified that the current obtained using a simulation domain of 300b was not significantly different than that obtained with larger domains. In addition, the meshing was densified where large current density occurred, e.g. ($R=b$, $Z=0$) and ($R=a$, $Z=0$). This overall verification procedure leads to a simulated current that has a tolerance level below 0.1 %.

4.5 Experimental section

4.5.1 Materials

Quartz glass capillaries (length 75 mm/o.d. 1.0 mm/i.d. 0.70 mm) were from World Precision Instruments. Platinum pellets (Pt 99.99 % pure, 1/8'' diameter x 1/8'' long, #EVMPT40SHOT), silicon oxide beads (SiO_x 99.9 % pure, 3-6 mm size, #EVMSIO303-6D) and fabmate graphite evaporation crucible liner (0.24cc, 0.750 top OD x 0.162 H), were all purchased from Kurt J. Lester Company, Material Group. SiO_x evaporation boat (#ME9-005TA) was purchased from R. D. Mathis. Ferrocenemethanol (FcMeOH, 97%, Sigma-Aldrich) and potassium chloride (KCl, ACS 99%, Anachemia) were used as received. Milli-Q water (Millipore, Biocel, 18.2 MΩ) was used to prepare all solutions and all commercially available solvents were reagent grade and used without further purification and were dried according to standard procedures.

4.5.2 Ring microelectrode preparation

Quartz glass capillaries were pulled with a micropipet laser-puller (model P2000, Sutter Instruments). Prior to pulling, the glass capillaries were cleaned by sonication in isopropanol for 10 minutes and once more in acetone for another 10 minutes. They were washed thoroughly with Milli Q water, and dried under nitrogen flux. The parameters used in the pulling step were chosen to produce short pipet tips. The obtained program was found by trial and error and was modified as needed, since the performance of the laser-puller change slightly over time. The software parameters were as follow:

line 1. heat 700: filament 4: velocity 55: delay 130: pull 45

The micropipets ends were then coated with platinum by E-beam evaporation under vacuum while keeping the micropipets under constant rotation using a power supply (62530 dual PS, Hew) and applying a potential of 3 V (0.5 A). Electrical contact to the platinum coating was made using a copper wire with silver epoxy and heat curing at 120 °C for 15 minutes. Then, a silicon oxide layer was thermally evaporated onto the platinum-coated micropipet to ensure insulation of the pipet. Finally, the platinum ring was exposed by focused ion beam milling of the tip (FIB DB 235 from FEI). The experimental parameters were optimized for each given micropipet, but generally, a rough cut was made at 7-20 nA followed by surface polishing at 1-3 nA current (ionic currents using Ga^{+}). Scanning electron microscopy imaging (SEM) was used to characterise the micropipet prior to and after the coatings.

4.5.3 Electrochemical measurements

Cyclic voltammetry measurements were performed in a Teflon electrochemical cell with a conventional three-electrode configuration. The platinum ring microelectrode was the working electrode while a platinum wire and a silver wire pre-coated with silver chloride served as the counter and reference electrodes respectively. The cyclic voltammetry experiments were carried out in a 1 mM ferrocenemethanol/0.1 M KCl aqueous solution using a scanning electrochemical microscope instrument (HEKA Elektronik).

4.6 Results and discussion

4.6.1 Microring electrode design

The development of a successful micropipet design was dependent on the careful optimisation of the deposition parameters. The platinum layer must be mechanically stable to prevent stripping once it is immersed in the electrolyte solution. As for the silicon oxide, the deposit must provide appropriate insulating properties while also readily adhering to the platinum underlayer. Several combinations of platinum and silicon oxide layer and surface roughening procedures were investigated and are summarised in Table 4.1.

Table 4.1. Summary of the results obtained from the various optimisation trials.

	Pt thickness†	**SiO_x thickness†**	**Analyses**	**Results**
A	Yes	No	Immersion in electrolyte solution for 24h	(i) No stripping of the Pt layer
B	1400-2000 Å	>670 Å	SEM CV	(i) No CV signal. (ii) Stripping of both layers.
C	1400-2000 Å	670 Å	FIB/SEM CV	(i) No CV signal. (ii) Stripping of both layers.
D	1400 Å	1800 Å	FIB/SEM CV	(i) CV observed only for first cycle. (ii) Stripping of both layers with cycling.
E*	3500 Å	12 750 Å	SEM/FIB CV	(i) CV observed. (ii) No stripping upon cycling

† Nominal thickness values.
*The micropipets were treated as follow: chemical etching of the capillary prior to Pt deposition or O_2 plasma treatment of the capillary prior to SiO_x deposition.

After cleaning of the quartz capillary, a layer of platinum was first evaporated. The physical and mechanical stability of the platinum layer was first tested. The deposit was physically rubbed and then immersed in an electrolyte solution for several hours and no stripping of the platinum layer was observed (Trial A). It was supposed that the capillary curvature combined with the deposition technique (evaporation and not sputtering) may be one of the reasons for the physical and mechanical stability of the deposit. The use of quartz instead of a borosilicate glass may also have contributed to the observed stability.

A 1400-2000 Å thick platinum layer followed by a 670 Å silicon oxide layer were evaporated on a laser-pulled quartz capillary. The resulting microelectrode was characterized by cyclic voltammetry (CV), which did not show any electrochemical signal. Moreover, the two layers, the platinum and the silicon oxide, peeled-off (Trial B). We hypothesized that the physical contact between the two deposits was not good enough and thus, the electrolyte solution could seeped between the two layers. This probably caused first the peeling of the silicon oxide layer, which causes than the peeling of the platinum layer. It was also assumed that the platinum surface was not well exposed, e.g. it was partially or totally covered with silicon oxide. Following the exposure of the platinum ring by focused ion beam, similar results as that obtained in Trial B were observed (Trial C).

To overcome the peeling issue and to make sure that the absence of electrochemical signal was not due to insufficient platinum deposition, platinum and silicon oxide thicknesses were increased. Once again, following focused ion beam milling, the microring sensor was tested by cyclic voltammetry. An electrochemical

response was observed only for the first cycle. During subsequent cycling, both layers peeled-off (Trial D).

The stability issues appear to come from poor contact between the platinum and the silicon oxide. To overcome this situation, the micropipets were treated in two different ways, either by surface chemical etching or by oxygen plasma etching. Trial E summarises the most successful result. The idea of treating the quartz capillary prior to the metal deposition, came from the fact that in the literature, Matsue and co-workers[99] modified the surface of microcapillaries with fluorosilane by gas-phase silanization in a nitrogen atmosphere. This surface modification was necessary to prevent cell adhesion on the microelectrode; here it was rather to increase surface roughness by chemical etching in order to improve the adherence of platinum, which can lead to the improvement of the silicon oxide mechanical stability as well. In a similar way, the platinum surface roughness was increased by oxygen plasma treatment in order to improve silicon oxide adherence on the platinum once again. Therefore, the micropipets designed during this trial (i) did not undergo any specific treatment, (ii) were chemically etched before the deposition of the platinum layer and (iii) were treated with oxygen plasma prior to the silicon oxide deposition. For the first two conditions, a cyclic voltammogram was obtained and several cycles have been made. With increasing cycling, the layers tended to peel-off partially. Considering such results, the platinum-coated micropipets were treated with oxygen plasma prior to the silicon oxide evaporation. A cyclic voltammogram was observed for the first cycle and even under intense cycling both layers stayed unchanged (mechanically resistant). The plasma treatment appears to

strengthen and improve the physical contact between the platinum and the silicon oxide minimizing the possibility for the solution to seep between the layers.

4.6.2 Imaging of the ring microelectrode

The focused ion beam (FIB) setup was also equipped with a scanning electron microscope (SEM). Figure 4.2 presents the SEM images taken before and after exposing the platinum ring by FIB. These images were used to characterise the microelectrode tip once completed (Figure 4.2a and 4.2b) and to verify the quality and the thickness of the successive deposits of platinum and silicon oxide (Figure 4.2c). It also allowed for an estimation of the microelectrode diameter.

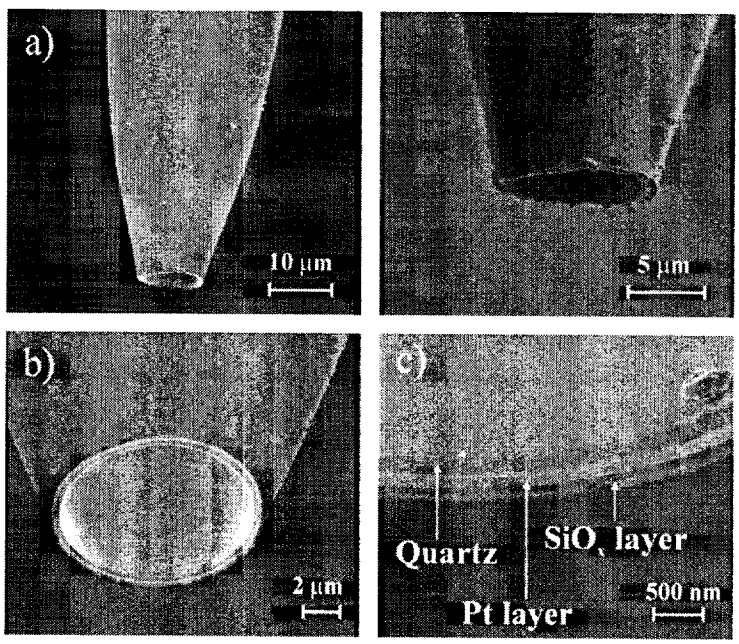

Figure 4.2. SEM images of platinum-coated quartz micropipet insulated with silicon oxide a) prior and b) after exposure of the platinum ring by focused ion beam milling, c) Close up of the micropipet tip showing the platinum ring and the insulating layer.

Despite the successive deposition of the layers, the microelectrode tip was still about 10 μm in diameter. A magnification of the tip shows that the silicon oxide layer covers it entirely, which justifies exposing the tip by focused ion beam milling. The advantage of this technique lies in the fact that it allows a very fine cut of the tip and even a polishing of the microring surface if necessary. This will depend on the beam intensity at which the experiment is realised. A clear and better estimation of the thickness of each layer was possible with the SEM images. The resulting milled Pt microring sensors were electrochemically characterised by cyclic voltammetry. The results were fitted to numerical simulations and this is discussed in the next section.

4.6.3 Theoretical discussion on electrochemical measurements

After imaging the micropipet tips, electrochemical characterisation was necessary to identify to what extent the microring electrode was insulated and to better understand how the surrounding silicon oxide layer influences the observed current. Thus, a ring microelectrode was tested by cyclic voltammetry in a 1 mM ferrocenemethanol/0.1 M KCl aqueous solution (Figure 4.3). The observed current is about 17.5 nA, which represents a 10 fold increase compared to the expected value given by equation 9:[92]

$$i_{T,\infty} = nFD_O c_O^0 \left(\frac{\pi^2 (a+b)}{\ln\left[16 \frac{b+a}{b-a}\right]} \right) \qquad \text{(Eq. 4.9)}$$

where a and b, the inner and outer radii, are both 11.4 μm, as extracted from SEM images. This suggests that 10 % of the current comes from the actual platinum ring and

90 % is due to another conductive source. Therefore, it was hypothesized that an edge was exposed at the beginning of the tip during the focused ion beam procedure. When exposing the ring platinum by focused ion beam milling, Ga^+ ions are not necessarily confined to the beam. It is likely that these ions etched part of the insulating layer that is near the cut line. This may create a conductive edge at the tip, which can contribute to a current increase. This etching effect limits the use of several polymer based insulator layers as there was a different etching rate between glass, metal or insulator layers. Using numerical simulations, this hypothesis was first assessed.

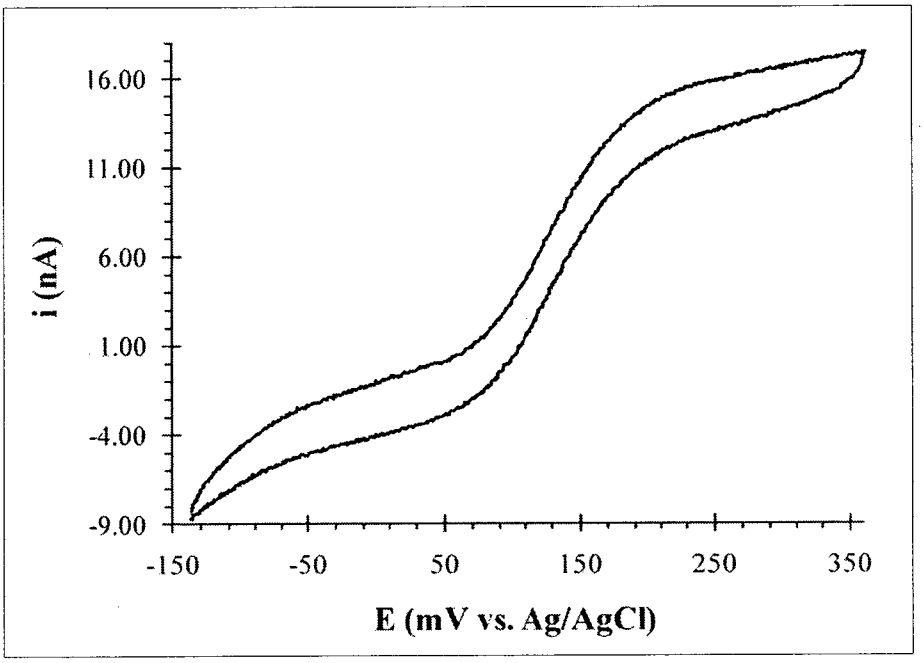

Figure 4.3. Cyclic voltammogram (CV) of 1 mM ferrocene-methanol/0.1 M KCl aqueous solution recorded at a platinum ring microelectrode as the working electrode at a 10 mV/s scan rate.

Here, the numerical simulations describing the cyclic voltammetry curves for a ring microelectrode having a conductive edge are presented. It requires the calculation of the steady-state currents over a potential range for an edge limited to $0<Z_{por}<10b$ (Figure

4.4a). The experimental cyclic voltammogram was then fitted to these theoretical curves (Figure 4.4b). An edge of 6.25*b* height was determined. This result does not agree with the SEM images. A small edge height was expected since it was not directly identified on the images and when it is, the height is around 1.95 µm. Therefore, the Ga^+ ions probably do not etch the entire insulating layer from the microelectrode tip as first proposed.

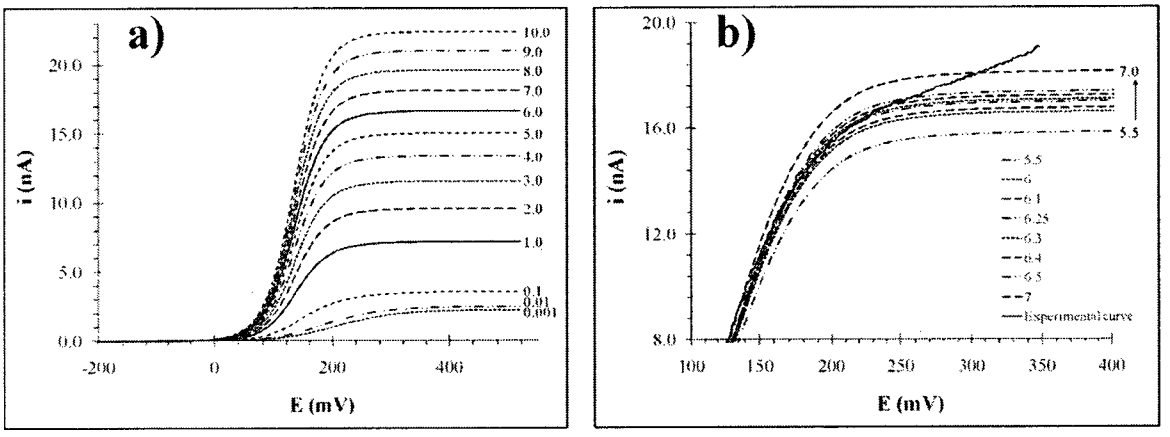

Figure 4.4. a) Dimensionless currents as a function of the potential range simulated for edge heights limited to $0<Z_{por}<10b$. b) Fitting of the experimental cyclic voltammogram to the theoretical data where an edge of 6.25*b* height was determined.

Following these results, it was hypothesis instead that the insulating properties of the silicon oxide are diminished or weakened during the focused ion beam procedure. During the tip milling, the silicon oxide layer becomes sufficient porous to allow diffusion of the electrolyte, which can reach the platinum layer and thus increase the measured current. This is supposed to lead to diffusion with an apparent diffusion coefficient that is smaller than that in solution ($D_{O,por}<D_O$). Thus, the problem has two unknown parameters, $D_{O,por}$ and Z_{por} and only one experimental information, the diffusion plateau current (taken equal to 17 nA here), the shape of the stationary voltammogram being hardly influenced by $D_{O,por}$ and Z_{por}. Therefore, several

combinations of ($D_{O,por}$, Z_{por}) may lead to a correct match with the measured current. These parameters combinations have been evaluated for the geometric parameters of the considered probe. Results are presented in Figure 5. The case of a completely removed silicon oxide corresponds to the combinations ($D_{O,por}$=D_O, Z_{por}=6.25b) as previously discussed. Figure 4.5 demonstrates that a strong decrease in $D_{O,por}$ is expected when Z_{por} increases (one has to take care of logarithmic scale of vertical axis). Thus, for a Z_{por} larger than 12, a particularly small diffusion coefficient (0.008D_O) into the silicon oxide is observed.

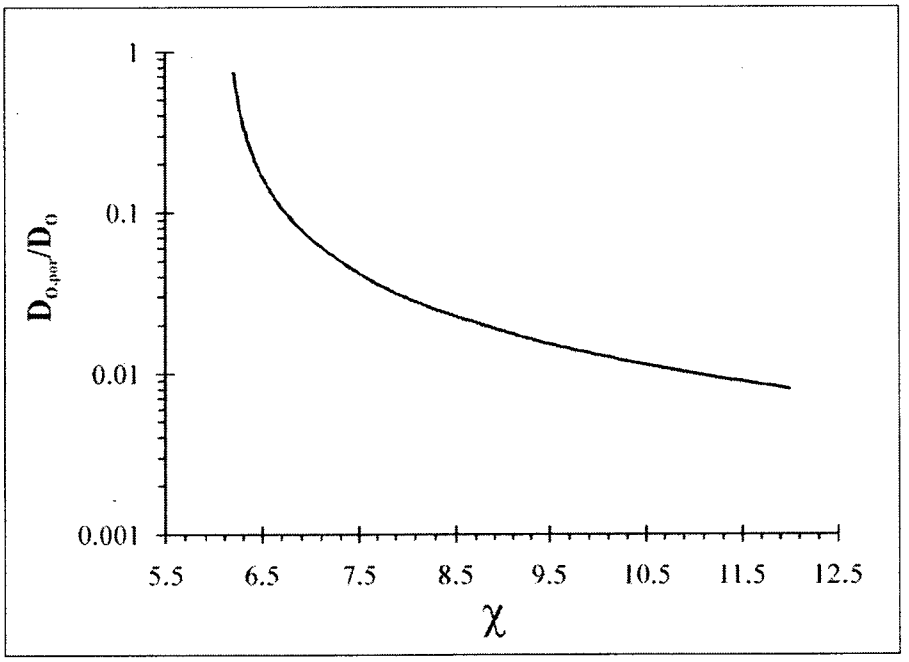

Figure 4.5. Numerical simulation of a series of ($D_{o,por}/D_O$, Z_{por}/b) points given a steady-state current of 17 nA. This curves leads to the determination of the length of the micropipet tip over which the focused ion beam procedure affecs the silicon oxide layer insulating properties.

4.7 Conclusion

In the present work, we proposed a new way to fabricate platinum ring microelectrodes that could be used as new SECM probes. These probes were made from platinum-coated laser-pulled pure pipets, insulated with silicon oxide. The ring surface was exposed by focused ion beam milling. The advantage of this procedure is that all materials can be evaporated thermally or by E-beam in one step. This implies that the platinum and silicon oxide can be deposited sequentially during a single step, without breaking the vacuum.

A higher current than that expected was observed during cyclic voltammetry characterisation. It was concluded that an edge was created upon the exposure of the platinum ring by focused ion beam. This was however not perfectly consistent with the SEM imaging. A more realistic model was to assume that the insulating properties of silicon oxide were weakened during the FIB procedure rather then having the formation of a purely conductive edge at the tip beginning of the microelectrode. Another hypothesis is currently under investigation. The focused ion beam procedure involves Ga^+ ions, which can adsorb on the microelectrode tip surface. Therefore, the high current observed during cyclic voltammetry measurement is not necessarily due to platinum exposure, but rather to Ga^+ desorption. This suggests that perhaps a more appropriate technique, such as precision scissors, could be used to expose the platinum ring. Also, a finishing treatment with polymerisable resins during E beam lithography process might be an alternative. Despite this problem, this work opens the way to the fabrication of

pure platinum ring microelectrodes that are suitable for SECM probes in a more simpler way than currently available, which involves fewer preparation and design steps.

Chapter 5. Conclusion

The overall goal of this thesis was to develop models capable of mimicking membrane bound electrochemical reactions. To do so, specially a designed redox liposome was designed and studied by scanning electrochemical microscopy experiments. In the literature, two types of redox liposomes are presented, e.g. liposomes containing redox active units within their internal void and surface-modified liposomes mostly with quinone derivatives. In order to meet our ongoing SECM studies an organometallic redox surface-modified liposome was designed. Consequently, the first objective was to modify a phospholipid headgroup with a redox active tether. This was done through PLD-catalyzed transphosphatidylation reaction between 1,2-distearoyl-*sn*-glycero-3-phosphocholine (DSPC) and primary alcohol ferrocene derivatives. DSPC headgroup was first modified with ferrocenemethanol. The results showed that the synthesised redox DSPC is unstable. The presence of water in the reaction medium combined to the fact that $-OCH_2Fc$ is a good leaving group makes a S_N2 and/or hydrolysis reaction more than possible. This secondary reaction resulted in the reaction of the desired product with water to form phosphatidic acid and the corresponding alcohol. However, ^{31}P NMR analysis demonstrated that indeed the DSP-OCH_2Fc was synthesised. In order to overcome the stability issue, the same headgroup modification was performed using this time ferrocene-ethanol as the primary alcohol. The addition of a carbon between the phosphorus atom and the ferrocene function should lead to the synthesis of a stable redox modified DSPC. This was confirmed by MS and ^{31}P NMR analysis. Moreover, the solid-state ^{31}P NMR was preferred over the liquid NMR because it allowed reaction mixture quantification while preventing sample degradation due to solvent.

Infrared results proved that the ferrocene tether is covalently bond to the phospholipid headgroup and that the choline group is no longer attached to it. Finally, cyclic voltammetry experiments demonstrated that this novel organometallic phospholipid is redox active, which indicates that the resulting liposome will probably be as well.

The second objective was to assemble the synthesised redox phospholipid into redox liposomes and study them electrochemically through scanning electrochemical microscopy experiments. Redox liposomes were conceived by double emulsion technique using two emulsions made from a DSPC, redox modified DSPC, (DSP-OCH_2CH_2Fc) and 1,2-distearoyl-*sn*-glycero-3-phospho-(1'-*rac*-glycerol) (DSPG) mixture. In order to immobilise liposomes, their internal void were filled with sucrose. Once added to the electrolyte solution used in SECM studies, they will sediment at the bottom of the electrochemical cell. This is possible because the electrolyte solution is made from glucose. The difference between sucrose and glucose densities allows that phenomenon. This immobilisation technique was preferred over others, such as avidin-biotin linkage, because it is simpler and does not require any extra steps during the liposome formation. Once immobilise, liposomes are ready for electrochemical studies. This is done by approaching a microelectrode close to the redox liposome surface. The electrode positioning was performed with approach curve experiments combined with optical microscopy. Once the microelectrode was positioned close to the surface of a unique redox liposome, chronoamperometry measurements were performed. By applying a potential predetermined by cyclic voltammetry, it was possible to activate the liposome surface and therefore modulate its response to an electrochemical disturbance. These

preliminary results suggest that further SECM studies would profile the mechanism associated with membrane surface reactions.

The final objective of this thesis was to develop a novel ring micropipet that suits better our SECM needs. This type of SECM sensor can be used to perform injection studies on liposomes, resulting in the extraction of kinetic parameters that would be difficult to obtain by other means. The microrings presented in the literature are usually made of gold or platinum/titanium alloy and are isolated using electrophoretic paints or non-conductive polymers. Here, we proposed a simplified five steps protocol to fabricate pure platinum ring micropipets isolated with a silicon oxide layer. The ring surface was exposed by focus ion beam milling. SEM images indicated that the proposed protocol was adequate to fabricate reproducible 10 μm diameter ring microelectrodes. However, validation of the experimental cyclic voltammetry results with numerical simulations demonstrated that the exposure of the platinum ring by focus ion beam weakens silicon oxide insulating properties. Thus, the lateral diffusion of the electroactive species enhances the measurement current and thus modifies the electrochemical behaviour of the micropipet. This drawback limits for now the use of the microring as a local sensor.

5.1 Future work

The work performed and presented in this thesis is the ground work that will enable future studies on our group. The first thing to do is to complete the microring pipets. While keeping the original protocol, that is to say pure platinum coating followed by silicon oxide insulation, the ring exposure step has to be modify or improve if one

wants to use this ring microelectrode as a local probe. To avoid weakening the insulating properties of silicon oxide layer, the use of precision scissors can be an alternative to the focus ion beam method for ring exposure. Another alternative is to add a treatment by use of resins during the E beam lithography process perhaps between each layer or right on top of the silicon oxide layer. To verify these protocol modifications, SEM imaging and cyclic voltammetry experiment will be performed once more. After completing and determining the size of the micropipets through SECM approach curve experiments and fitting to given analytical expressions, the effect of injection dynamics on the observed electrochemical response has to be validate both experimentally and using numerical simulations.

Also, the electrochemical studies of the proposed biomimetic models must be completed. As such, ^{1}H NMR analysis of the ferrocene-ethanol surface-modified phospholipid must be realized to complete the characterisation of the new redox phospholipid. Approach curve experiments on the previous liposomes are still needed as well as their validation by numerical simulations that take into consideration biological substrates. The extracted kinetics from numerical simulations will be characteristic of a surface bound reaction. It would also be interesting to perform similar experiments with variants of the proposed liposomes. For example, passive diffusion can be studied using liposomes containing redox active units within its internal void. It would be remarkable if the results could be compare to those obtain from the study of a surface-modified redox liposome containing electroactive units within its internal void as well. Redox active units that may or may not react with the liposome surface could be use during the experiments. Also, it would be interesting to design a redox active liposome similar to the

one studied in this work using a longer or a larger ferrocene derivative, as for example ferrocenepropanol. Norman and Badia[79] presented recently a AFM study of a redox active ferrocenylundecanethiolate self-assembled monolayer ($FcC_{11}SAu$ SAM) on gold. Oxidation of the ferrocene headgroup with perchlorate electrolyte demonstrated steric constraints in the close-packed $FcC_{11}SAu$ system and an efficient coupling between the chemisorbed $FcC_{11}S$-monolayer and the pure gold surface. The monolayer volume increases due to complexation of perchlorate ions to the surface immobilized ferroceniums. Thus, ferrocenium-bearing alkylthiolates reoriente upon each other rather than to individual anion pairing events. By using a ferrocenepropanol surface-modified redox active liposome, similar events, such as ion pairing and tether sensitivity to their environment (and/or to their nearest neighboor), can be studied as well. In short, many liposome combinations are possible now that an organometallic redox active liposome is available. It is important to mention that regardless of the type of liposome studied or the type of mechanism mimicked, numerical simulations taking into account a biological substrate are essential to better understand and characterise the transport mechanism.

Furthermore, the liposome system has to be complexify by including transmembrane transport proteins that can add and interfere with the electrochemical bound reaction to understand and simulate transport phenomena. An example of such transmembrane transport protein is the multidrug resistant protein (MRP), particularly the MRP1 an ATP-binding cassette transporter C (ABCC). MRP1 confers to the cell a resistance to hydrophobic compounds that are PGP substrates and to non-anionic organic compounds, like anthracyclines. It can transport glutathione (GSH), glucuronate and sulphate conjugates of organic anions. MRP1 can also export compounds just as they are,

without them being conjugated with GSH. Therefore, assisted-diffusion of electroactive, such as ferrocene derivatives, can be mimicked by imbedding MRP1 into liposome membranes (design of a proteoliposome). The study of this mechanism is important to better understand the cellular resistance mechanism and eventually test the efficiency of MRP inhibitors.

Finally, once the behaviour of transport mechanisms understood and assess by using the appropriate biomimetic models, it would be interesting to compare these results with those obtained using living cells. Once more, validation through numerical simulations is crucial.

References

1. Szakacs, G.; Paterson, J. K.; Ludwig, J. A.; Booth-Genthe, C.; Gottesman, M. M. *Nat. Rev. Drug Discovery.* **5** (3), 219-234 **(2006)**.

2. Filipits, M. *Drug Discovery Today: Disease Mechanisms* **1**(2), 229-234 **(2004)**.

3. Mauzeroll, J.; Bard, A. J. *Proc. Nat. Acad. Sci. U.S.A.*, **101** (21), 7862-7867 **(2004)**.

4. Mauzeroll, J.; Bard, A. J.; Owhadian, O.; Monks, T. J. *Proc. Nat. Acad. Sci. U.S.A.*, **101** (51), 17582-17587 **(2004)**.

5. Bard, A. J.; Li, X.; Zhan, W. *Biosens. Bioelectron.*, **22** (4), 461-472 **(2006)**.

6. Longobardi, F.; Cosma, P.; Milano, F.; Agostiano, A.; Mauzeroll, J.; Bard, A. J. *Anal. Chem.*, **78** (14), 5046-5051 **(2006)**.

7. Mauzeroll, J.; Buda, M.; Bard, A. J.; Prieto, F.; Rueda, M. *Langmuir.* **18** (24), 9453-9461 **(2002)**.

8. Monné, J.; Diez, Y.; Puy, J.; Galceran, J.; Nelson, A. *Langmuir.* **23** (21), 10581-10588 **(2007)**.

9. Nelson, A. *Biophys. J.*, **80** (6), 2694-2703 **(2001)**.

10. Cannes, C.; Kanoufi, F.; Bard, A. J. *J. Electroanl. Chem.*, **547** (1), 83-91 **(2003)**.

11. Lee, L. Y. S.; Sutherland, T. C.; Rucareanu, S.; Lennox, R. B. *Langmuir.* **22** (9), 4438-4444 **(2006)**.

12. Mouritsen, O. G. *Life - As a matter of fat. The emerging science of lipidomics.* **(2005)** Springer-Verlag Berlin Heidelberg: Germany. 276 p.

13. Lorin, A.; Flore, C.; Thomas, A.; Brasseur, R. *Biotechnol. Argon. Soc. Environ.*, **8** (3), 163-176 (**2004**).

14. Bangham, A. D.; Standish, M. M.; Watkins, J. C. *J. Mol. Biol.*, **13**, 238-252 (**1965**).

15. Pilot, T.; Goethals, M.; Vanloo, B.; Talussot, C.; Brasseur, R.; Vandekerckhove, J.; Rosseneu, M.; Lins, L. *J. Biol. Chem.*, **271**, 28757-28765 (**1996**).

16. Li, C.; Deng, Y. *J. Pharm. Sci.*, **93** (6), 1403-1414 (**2004**).

17. Szoka, F. J.; Papahadjopoulos, D. *Proc. Nat. Acad. Sci. U.S.A.*, **75** (9), 4194-4198 (**1978**).

18. Ramadan, W. M. A. *Mansoura J. Pharm. Sci.*, **24** (1), 87-90 (**2008**).

19. Otake, K.; Shimomura, T.; Goto, T.; Imura, T.; Furuya, T.; Yoda, S.; Takebayashi, Y.; Sakai, H.; Abe, M. *Langmuir.* **22** (6), 2543-25502543 (**2006**).

20. Torchilin, V. P.; Weiissig, V. *Liposomes: practical approach.* (**2003**) 2nd Edition, Oxford University Press: England: Oxford.

21. Angelova, M. I.; Dimitrov, D. S. *Faraday Discuss.*, **81**, 303-311 (**1986**).

22. Rodriguez, N.; Pincet, F.; Cribier, S. *Colloids Surf. B.* **42** (2), 125-130 (**2005**).

23. Koeller, K. M.; Wong, C.-H. *Nature.* **409**, 232-240 (**2001**).

24. Puskas, J. e.; Sen, M. Y.; Seo, K. S. *J. Polym. Sci., Part A: Polym. Chem.*, **47**, 2959-2976 (**2009**).

25. Dong, C.; Su-jia, S. *Eur. J. Lipid Sci. Technol.*, **110** (1), 48-51 (**2008**).

26. Bruzik, K. S.; Tsai, M.-D. *Methods Enzymol.*, **197**, 258-269 (**1991**).

27. Bossi, L.; D'Arrigo, P.; Pedrocchi-Fantoni, G.; Mele, A.; Sevi, S.; Leiros, I. *J. Mol. Catal. B: Enzym.*, **11** (4-6), 433-438 (**2001**).

28. Brown, H. A.; Henage, L. G.; Preininger, A. M.; Xiang, Y.; Exton, J. H., Biochemical analysis of phospholipase D. In *Methods in Enzymology*. (2007) Elsevier Inc.: Vol. 434, pp 49-87.

29. Guo, B. Z.; Xu, G.; Cao, Y. G.; Holbrook, C. C.; Lynch, R. E. *Planta*. **223**, 512-520 (**2006**).

30. Heller, M.; Mozes, N.; Peri, I.; Maes, E. *Biochim. Biophys. Acta*. **369** (3), 397-410 (**1974**).

31. Leiros, I.; Hough, E.; D'Arrigo, P.; Carrea, G.; Pedrocchi-Fantoni, G.; Secundo, F.; Servi, S. *Acta Crystallogr. Sect. D*. **56** (4), 466-468 (**2000**).

32. Shimbo, K.; Yano, H.; Miyamoto, Y. *Agric. Biol Chem.*, **54** (5), 1189-1193 (**1990**).

33. Yang, S. F.; Freer, S.; Benson, A. A. *J. Biol. Chem.*, **242** (3), 477-484 (**1967**).

34. Yu, C.-H.; Liu, S.-Y.; Panagia, V. *Mol. Cell. Biochem.*, **157** (1-2), 101-105 (**1996**).

35. Nakazawa, Y.; Sato, H.; Uchino, M.; Takano, K. *Protein J.*, **25** (3), 212-223 (**2006**).

36. Tzur, R.; Shapiro, B. *Biochim. Biophys. Acta*. **280**, 290-296 (**1972**).

37. Rich, J. O.; Khmelnitsky, Y. L. *Biotechnol. Bioeng.*, **72** (3), 374-377 (**2001**).

38. Rouessac, F.; Rouessac, A. *Analyse chimique. Méthodes et techniques instrumentales modernes*. **(2000)** 5th, Dunod: Paris. 430 p.

39. Mendham, J.; Denney, R. C.; Barnes, J. D.; Thomas, M. *Analyse chimique quantitative De Vogel*. **(2006)** 6th, De Boeck Université: Bruxelle. 889 p.

40. Andrews, E. R. *Phil. Trans. R. Soc. Lond. A*. **299** (1452), 505-520 **(1981)**.

41. Seelig, J. *Biochim. Biophys. Acta*. **515**, 105-140 **(1978)**.

42. Seelig, J.; Seelig, A. *Q. Rev. Biophys.*, **13**, 19-61 **(1980)**.

43. Amatore, C., Electrochemistry at ultramicroelectrodes (Chapter 4). In *Physical electrochmistry principles, methods and applications*. (1995) Rubinstein, I., Marcel Decker: New York, pp 131-207.

44. Bard, A. J.; Faulkner, L. R. *Electrochemical methods: fundamentals and applications*. **(2001)** 2nd Edition, Jonh Wiley & Sons Inc.: New Jersey. 833 p.

45. Clegg, A. D.; Rees, N. V.; Klymenko, O. V.; Coles, B. A.; Compton, R. G. *J. Electroanl. Chem.*, **580** (1), 78-86 **(2005)**.

46. Marcus, R. A., Electron transfer reactions in chemistry: theory an experiment. In *Nobel Price Lecture*, Noyes Laboratory of Chemical Physics, California Institute of Technology, 1992.

47. Bard, A. J.; Mirkin, M. V. *Scanning electrochemical microscopy*. **(2001)** Marcel Decker Inc.: USA: New York. 950 p.

48. Sun, P.; Laforge, F. O.; Mirkin, M. V. *Phys. Chem. Chem. Phys.*, **9** (7), 802-823 **(2007)**.

49. Kwak, J.; Bard, A. J. *Anal. Chem.*, **61** (11), 1221-1227 (**1989**).

50. Forster, R. J.; Keyes, T. E., Behavior of ultramicroelectrodes (Section 6.1). In *Handbook of electrochemistry*. (2007) Zoski, C. G., Elsevier Science: England: Oxford, pp 155-171.

51. Zoski, C. G. *Handbook of electrochemistry*. (**2007**) Elsevier's Science and Technology: 935 p.

52. Zoski, C. G. *Electroanal.*, **14** (15-16), 1041-1051 (**2002**).

53. Zhang, B.; Zhang, Y.; White, H. S. *Anal. Chem.*, **76** (21), 6229-6238 (**2004**).

54. Zhang, B.; Zhang, Y.; White, H. S. *Anal. Chem.*, **78** (2), 477-483 (**2006**).

55. Lee, S.; Zhang, Y.; White, H. S.; Harrell, C. C.; Martin, C. R. *Anal. Chem.*, **76** (20), 6108-6115 (**2004**).

56. Fan, F.-R. F.; Fernandez, J.; Liu, B.; Mauzeroll, J.; Zoski, C. G., Platinum and gold Inlaid disks 5 um diameter (section 6.3.3) in UME fabrication/characterization basis (section 6.3). In *The Handbook of Electrochemistry*. (2007) Zoski, C. G., Elsevier Science: England: Oxford, pp 189-197.

57. Lee, H. Y.; Jung, H. S.; Fujikawa, K.; Park, J. W.; Kim, J. M.; Yukimasa, T.; Sugihara, H.; Kawai, T. *Biosens. Bioelectron.*, **21** (5), 833-838 (**2005**).

58. Roy, R. C.; Das, D. K.; Das, B. *Indian J. Chem.*, **46A** (8), 1252-1256 (**2007**).

59. Zhan, W.; Bard, A. J. *Anal. Chem.*, **78** (3), 726-733 (**2006**).

60. Jewell, C. M.; Hays, M. E.; Kondo, Y.; Abbott, N. L.; Lynn, D. M. *Bioconjugate Chem.*, **19** (11), 2120-2128 (**2008**).

61. Alakoskela, J.-M. I.; Kinnunen, P. K. J. *Biophys. J.* **80** (1), 294-304 (**2001**).

62. Kakharenko, O. K.; Trusova, V. M.; Gorbenko, G. P. *J. Biol. Phys. Chem.*, **8** (2), 43-48 (**2008**).

63. Bothun, G. D.; Rabideau, A. E.; Stoner, M. A. *J. Phys. Chem. B.* **113** (22), 7725-7728 (**2009**).

64. Hock, S. M. D. *Histochem.*, **52** (2), 97-103 (**1977**).

65. Wang, P.; Schuster, M.; Wang, Y. F.; Wong, C.-H. *J. Am. Chem. Soc.*, **115** (23), 10487-10491 (**1993**).

66. Liu, M. D.; Patterson, D. H.; Jones, C. R.; Leidner, C. R. *J. Phys. Chem.*, **95** (4), 1858-1865 (**1991**).

67. Leidner, C. R.; Liu, M. D. *J. Am. Chem. Soc.*, **111** (17), 6859-6860 (**1989**).

68. Skowronek, M.; Jemiota-Rzeminska, M.; Kruk, J.; Strzalka, K. *Biochim. Biophys. Acta.* **1280** (1), 115-119 (**1996**).

69. Nijhuis, C. A.; Sinha, J. K.; Wittstock, G.; Huskens, J.; Ravoo, B. J.; Reinhoudt, D. N. *Langmuir.* **22**, 9770-9775 (**2006**).

70. Thévenot, C.; Daussant, J.; Kas, J.; Valentova, O. *Trends Anal. Chem.*, **12** (6), 266-271 (**1993**).

71. Sajdok, J.; Jandus, J.; Valentova, O.; Novotna, Z.; Kas, J.; Daussant, J. *Anal. Chim. Acta.* **315** (1-2), 109-112 (**1995**).

72. Khmelnitsky, Y. L.; Welch, S. H.; D. S. Clark; Dordick, J. S. *J. Am. Chem. Soc.*, **116** (6), 2647-2648 (**1994**).

73. Sotirhos, N.; Herslöf, B.; Kenne, L. *J. Lipid Res.*, **27** (7), 386-392 (**1986**).

74. Collet, O. *Europhys. Lett.*, **53** (1), 93-99 (**2001**).

75. Schomburg, D., BRENDA the comprehensive enzyme information system. TU Braunschweig Department of Bioinformatics.

76. Jemiota-Rzeminska, M.; Latowski, D.; Strzalka, K. *Chem. Phys. Lipids* **110** (1), 85-94 (**2001**).

77. Ong, W.; Yang, Y.; Cruciano, A. C.; McCarley, R. L. *J. Am. Chem. Soc.*, **130** (44), 14739-14744 (**2008**).

78. Correia-Ledo, D.; Mauzeroll, J. *ECS Transactions*. **19** (33), 1-10 (**2009**).

79. Norman, L. L.; Badia, A. *J. Am. Chem. Soc.*, **131** (9), 2328-2337 (**2009**).

80. Kim, S.; Martin, G. M. *Biochim. Biophys. Acta*. **646** (1), 1-9 (**1981**).

81. Laloy, E.; Vuillemard, J.-C.; Ackermann, H.-W.; Robin, O. *Biotechnol. Tech.*, **8** (10), 717-722 (**1994**).

82. Pinheiro, T. J.; Watts, A. *Biochemistry*. **33** (9), 2459-2467 (**1994**).

83. Sani, M.-A.; Dufourc, E. J.; Gröbner, G. *Biochim. Biophys. Acta*. **1788**, 623-631 (**2009**).

84. Cougnon, C.; Bauer-Espindola, K.; Fabre, D. S.; Mauzeroll, J. *Anal. Chem.*, **81**, 3654-3659 (**2009**).

85. Smith, I. C.; Ekiel, I. H., Chapter 15: Phosphorus-31 NMR of phospholipids in membranes. In *Phosphorus-31 NMR, principales and applications.* (1984) Gorenstein, D. G., Academic Press, Inc.: London, pp 447-475.

86. Schmidt-Rohr, K.; Spiess, H. W. *Multidimensional solid-state NMR and polymers.* **(1994)** Academic Press: Toronto, Canada.

87. Popenoe, D. D.; Deinhammer, R. S.; Porter, M. D. *Langmuir.* **8** (10), 2521-2530 **(1992)**.

88. Davis, W. L.; Shago, R. F.; Langner, E. H. G.; Swarts, J. C. *Polyhedron.* **24**, 1611-1616 **(2005)**.

89. Ludden, M. J. W.; Sinha, J. K.; Wittstock, G.; Reinhoudt, D. N.; Huskens, J. *Org. Biomol. Chem.*, **6**, 1553–1557 **(2008)**.

90. Correia-Ledo, D.; Arnold, A.; Mauzeroll, J. *J. Am. Chem. Soc. Comm.*, Submitted **(2010)**.

91. Brookes, B. A.; Gavaghan, D. J.; Compton, R. G. *J. Phys. Chem. B.* **106** (18), 4886-4896 **(2002)**.

92. Cornut, R.; Mayoral, M.; Fabre, D.; Mauzeroll, J. *J. Electrochem. Soc.*, **157** (6), in press **(2010)**.

93. Senthamarai, R.; Rajendran, L. *Eletrochim. Acta.* **53** (10), 3566-3578 **(2008)**.

94. Rajendran, L. *Electrochim. Acta.* **51** (21), 4439-4446 **(2006)**.

95. Tallman, D. E. *Anal. Chem.*, **66** (4), 557-565 **(1994)**.

96. Walsh, D. A.; Fernandez, J. L.; Mauzeroll, J.; Bard, A. J. *Anal. Chem.*, **77** (16), 5182-5188 (**2005**).

97. Lee, Y.; Amemiya, S.; Bard, A. J. *Anal. Chem.*, **73** (10), 2261-2267 (**2001**).

98. Amemiya, S.; Bard, A. J. *Anal. Chem.*, **72** (20), 4940-4948 (**2000**).

99. Nashimoto, Y.; Takahashi, Y.; Yamakawa, T.; Torisawa, Y.; Yasukawa, T.; Ito-Sasaki, T.; Yokoo, M.; Abe, H.; Shiku, H.; Kambara, H.; Matsue, T. *Anal. Chem.*, **79** (17), 6823-6830 (**2007**).

100. Slevin, C. J.; Gray, N. J.; Macpherson, J. V.; Webb, M. A.; Unwin, P. R. *Electrochem. Comm.*, **1** (7), 282-288 (**1999**).

101. Zu, Y.; Ding, Z.; Zhou, J.; Lee, Y.; Bard, A. J. *Anal. Chem.*, **73** (10), 2153-2156 (**2001**).

102. Lee, Y.; Bard, A. J. *Anal. Chem.*, **74** (15), 3626-3633 (**2002**).

103. Lee, Y.; Ding, Z.; Bard, A. J. *Anal. Chem.*, **74** (15), 3634-3643 (**2002**).

104. Chen, S.; Kucernak, A. *J. Phys. Chem. B.* **106** (36), 9396-9404 (**2002**).

105. Watkins, J. J.; Chen, J.; Whyte, H. S.; Abruna, H. D.; Maisonhaute, E.; Amatore, C. *Anal. Chem.*, **75** (16), 3962-3971 (**2003**).

106. Takahashi, Y.; Hirano, Y.; Yasukawa, T.; Shiku, H.; Yamada, H.; Matsue, T. *Langmuir.* **22** (25), 10299-10306 (**2006**).

107. Arrigan, D. W. M. *Analyst.* **129** (12), 1157-1165 (**2004**).

108. Sun, P.; Zhang, Z.; Guo, J.; Shao, Y. *Anal. Chem.*, **73** (21), 5346-5351 (**2001**).

109. Woo, D.-H.; Kang, H.; S.-M. *Anal. Chem.*, **75** (23), 6732-6736 (**2003**).

110. Cornut, R.; Mayoral, M.; Fabre, D.; Mauzeroll, J. *J. Electrochem. Soc.*, **157** (6), **(2010)**.

111. Xiong, H.; Guo, J.; Amemiya, S. *Anal. Chem.*, **79** (7), 2735-2744 **(2007)**.